NOTICE

The quality of this microform is heavily dependent upon the quality of the original thesis submitted for microfilming. Every effort has been made to ensure the highest quality of reproduction possible.

If pages are missing, contact the university which granted the degree.

Some pages may have indistinct print especially if the original pages were typed with a poor typewriter ribbon or if the university sent us an inferior photocopy.

Reproduction in full or in part of this microform is governed by the Canadian Copyright Act, R.S.C. 1970, c. C-30, and subsequent amendments.

AVIS

La qualité de cette microforme dépend grandement de la qualité de la thèse soumise au microfilmage. Nous avons tout fait pour assurer une qualité supérieure de reproduction.

S'il manque des pages, veuillez communiquer avec l'université qui a conféré le grade.

La qualité d'impression de certaines pages peut laisser à désirer, surtout si les pages originales ont été dactylographiées à l'aide d'un ruban usé ou si l'université nous a fait parvenir une photocopie de qualité inférieure.

La reproduction, même partielle, de cette microforme est soumise à la Loi canadienne sur le droit d'auteur, SRC 1970, c. C-30, et ses amendements subséquents.

Canada

Wavelength Dependent, Solvent Dependent and Transient Absorption Behavior in Photochemical Substitution Reactions of $W(CO)_5L$ (L = pyridine, piperidine, CO)

Carol Moralejo

A Thesis

in

The Department

of

Chemistry and Biochemistry

Presented in Partial Fulfillment of the Requirements
for the Degree of Doctor of Philosophy at
Concordia University
Montreal, Quebec, Canada

August. 1989

Abstract

Wavelength Dependent, Solvent Dependent and Transient Absorption Behavior in Photochemical Substitution Reactions of $W(CO)_5L$ (L = CO, pyridine, piperidine)

Carol Moralejo, Ph.D.
Concordia University, 1989

$W(CO)_5L$ (L = CO, pyridine, piperidine) undergoes photochemical replacement of L by solvent. If the solvent is a poor ligand, $W(CO)_5S$ can be rapidly converted to an alkene or alcohol complex to render the primary product observable. For both pyridine and piperidine complexes, the quantum yields for photochemical substitution increase with decreasing excitation energy across the region of LF singlet absorption. Quantum yields in the triplet region are smaller. There appears to be a distinct singlet pathway. Photochemical substitution from CT states in $W(CO)_5$pyr are due to efficient internal conversion to the reactive LF states. The photosubstitution quantum yields are solvent dependent. In mixed chlorinated alkane/alkene solvents, the quantum yields increase in the order $CH_2Cl_2 < CHCl_3 < CCl_4$. In the alcohols, the quantum yields are similar for propanol, butanol and octanol. Methanol yields are significantly lower.

Transient absorption spectroscopy reveals that the solvo intermediate, $W(CO)_5S$, is formed from $W(CO)_5L$ (L = pyridine, piperidine) in less than 10 picoseconds under 355 nm irradiation. Formation of $W(CO)_5S$ from $W(CO)_6$ is slower. In neat 1-hexene, growth of a $W(CO)_5$(alkyl) intermediate from $W(CO)_6$ similar to the one observed for this complex in cyclohexane occurs between 0 and 50 ps. For $W(CO)_6$, rearrangement from the alkyl intermediate to the stable $W(CO)_5$(1-hexene) product is observed between 50 ps and 10 ns. Low temperature studies indicate

that the barrier to rearrangment is approximately 1 kcal/mole.

Triplet reactivity can be understood from spectroscopic results in the structure of the vibrationally equilibrated triplet. Singlet reactivity is interpretable using Hollebone's octapole rule. Competitive vibrational relaxation to the ground state may account for quantum yields less than unity. The differences in rates of vibrational relaxation may explain the solvent dependence. Simultaneous formation of transients with trigonal bipyramidal (TBP) and square pyramidal (SP) geometries can occur on very short time scales (<< 50 ps). Rearrangement of the TBP species to the more stable SP species occurs on a time scale of approximately 600-700 ps.

To my Parents

ACKNOWLEDGEMENTS

My sincerest thanks to my supervisor, Dr. C.H. Langford, for both his continued guidance and generous contribution of his time throughout this entire project.

I would also like to extend my thanks to Dr. P.H. Bird for his kind assistance with the X-ray crystal structure and Dr. D.K. Sharma for his assistance with the picosecond experiments.

I also thank NSERC and FCAR for their financial support.

TABLE OF CONTENTS

	Page
1. Introduction	
1.1. History of the Metal Carbonyls	1
1.2. Objectives of the Research	2
1.3. Review	
1.3.1. Geometric Structure	3
1.3.2. Vibrational Spectroscopy	6
1.3.3. Luminescence Spectroscopy	7
1.3.4. Transient Absorption Spectroscopy	8
1.3.5. Solvatochromic Behavior of Metal Carbonyls	11
1.4. Review of $M(CO)_6$ and Related Photochemistry	
1.4.1. Ligand Field Photochemistry	14
1.4.2. Charge-transfer Photochemistry	18
1.5. Role of the Solvent	22
1.5.1. The Cage Effect	24
1.5.2. Solvent Dynamics	27
1.5.3. Donor and Acceptor Number of Solvents	29
1.5.4. Solvent Polarity	31
2. Experimental	
2.1. Materials	33
2.2. Preparation of the Complexes	
2.2.1. $W(CO)_5$pyridine	34
2.2.2. $W(CO)_5$piperidine	35
2.2.3. Potassium Ferrioxalate	36
2.3. Irradiation Procedures	36
2.4. Light Absorption Measurements	38
2.5. Analysis of Data	
2.5.1. $W(CO)_5$(product)	39
2.5.2. Fe^{2+}	41
2.5.3. Quantum Yield Determinations	43
2.6. Picosecond Flash Photolysis	44
2.7. X-Ray Crystallography of $W(CO)_5$piperidine	52

Page

2.8. Electronic Spectral Band Deconvolution 52

3. Results

3.1. Electronic Spectra 53

3.2. Wavelength Dependent Behavior 62

3.3. MLCT Reactivity 73

3.4. Solvent Dependence 81

3.5. Picosecond Spectroscopy 93

3.6. X-Ray Crystallography 119

4. Theory and Discussion

4.1. Bonding in $W(CO)_5L$
4.1.1. $W(CO)_6$ 122
4.1.2. $W(CO)_5L$ 124

4.2. Photoreactivity
4.2.1. Relationship between Reactivity and Spectroscopy 126

4.3. Triplet Reactivity 134

4.4. MLCT Reactivity and Solvent Dependence 137

4.5. Polymerization of 1-hexene 145

4.6. Transient Absorption Spectroscopy 145

Conclusion 154

References 156

Appendix A 162

Appendix B 166

Appendix C 168

Appendix D 170

LIST OF FIGURES

Page

Chapter 1

1.1. A) $W(CO)_6$, B) Bonding Interactions between a metal and CO 4
1.2. A) $W(CO)_5$pyridine, B) $W(CO)_5$piperidine 5
1.3. State diagram indicating lowering of MLCT energy upon substitution of pyr by 4-Y-Pyr 19

Chapter 2

2.1. Optical trains for 313, 365, 436, 457 and 488 nm irradiation 37
2.2. Schematic representation of the picosecond flash photolysis experimental apparatus 45

Chapter 3

3.1. Electronic spectra of $W(CO)_6$ in cyclohexane 54
3.2. Tanabe-Sugano diagram for a d^6 complex in an octahedral field 55
3.3. Energy level diagram showing correlation between LF states in O_h and C_{4v} symmetries 56
3.4. Electronic spectra of $W(CO)_5L$ in isooctane 57
3.5. Electronic spectra of $W(CO)_5$pyr in methanol and octanol 59
3.6. Electronic spectra of $W(CO)_5$pyr in isooctane/1-hexene, benzene/1-hexene and dichloromethane/1-hexene 60
3.7. Correlations between Reichardt's polarity scale and MLCT energies for $W(CO)_5$pyr in several solvents 61
3.8. Correlations between Reichardt's polarity scale and MLCT energies for $W(CO)_5$pyr in different groups of solvents 63
3.9. Electronic spectral changes for $W(CO)_5$pyr in isooctane/1-hexene under 457.5 nm irradiation 66
3.10. Electronic spectral changes for $W(CO)_5$pip in isooctane/1-hexene under 436 nm irradiation 67
3.11. Electronic spectral changes for $W(CO)_5$pyr in isooctane/1-hexene under 365 nm irradiation 68
3.12. Electronic spectral changes for $W(CO)_5$pip in isooctane/1-hexene under 365 nm irradiation 69
3.13. Electronic spectral changes for $W(CO)_5$pip in isooctane/1-hexene under 313 nm irradiation 71
3.14. Electronic spectral changes for $W(CO)_5$pyr in dichloromethane/1-hexene under 436 nm irradiation 77
3.15. Electronic spectral changes for $W(CO)_5$pip in dichloromethane/1-hexene under 436 nm irradiation 78
3.16. Electronic spectra of $W(CO)_5$pyr in $CHCl_3$/1-hex and CCl4/1-hex 82
3.17. Electronic spectral changes for $W(CO)_6$ in octanol under 365 nm irradiation 84

Page

3.18. Electronic spectral changes for $W(CO)_5$pyr in butanol under 365 nm irradiation 85
3.19. Electronic spectral changes for $W(CO)_5$pip in butanol under 365 nm irradiation 86
3.20. Electronic spectral changes for $W(CO)_5$pyr in $CHCl_3$/hex under 436 nm irradiation 88
3.21. Electronic spectral changes for $W(CO)_5$pip in $CHCl_3$/hex under 436 nm irradiation 89
3.22. Transient absorption spectra of $W(CO)_6$ in perfluoromethylcyclohexane 94
3.23. Transient absorption spectra of W(CO)6 in cyclohexane 95
3.24. Transient absorption spectra of $W(CO)_5$pyr in cyclohexane 96
3.25. Transient absorption spectra of $W(CO)_5$pip in cyclohexane 97
3.26. Transient absorption spectra of $W(CO)_6$ in 1-hexene 100
3.27. Transient absorption spectra of $W(CO)_5$pyr in 1-hexene 101
3.28. Transient absorption spectra of $W(CO)_5$pip in 1-hexene 102
3.29. Transient absorption spectra of $W(CO)_6$ in 1-hexene between 50 ps and 5 ns at 23° C 104
3.30. Transient absorption spectra of $W(CO)_6$ in 1-hexene between 200 ps and 5 ns at -10° C 105
3.31. Transient absorption spectra of $W(CO)_6$ in methanol 107
3.32. Transient absorption spectra of $W(CO)_6$ in butanol 108
3.33. Transient absorption spectra of $W(CO)_6$ in octanol 109
3.34. Transient absorption spectra of $W(CO)_5$pyr in methanol 110
3.35. Transient absorption spectra of $W(CO)_5$pyr in butanol 111
3.36. Transient absorption spectra of $W(CO)_5$pyr in octanol 112
3.37. Transient absorption spectra of $W(CO)_5$pip in methanol 113
3.38. Transient absorption spectra of $W(CO)_5$pip in butanol 114
3.39. Transient absorption spectra of $W(CO)_5$pip in octanol 115
3.40. Transient absorption spectra of $W(CO)_5$pyr in CCl_4/cyclohexane 120
3.41. ORTEP diagram of $W(CO)_5$pip 121

Chapter 4

4.1. Simple diagram indicating vector directions for σ and π bonds of an octahedral complex 123
4.2. Molecular orbital diagram for an octahedral complex 125
4.3. Molecular orbital diagram for a C_{4v} complex 127
4.4. Splitting of orbitals from octahedral symmetry to C_{4v} 129
4.5. Simple diagram indicating t_{1u} asymmetric and buckle stretch modes 133
4.6. Deconvoluted spectral bands for $W(CO)_5$pyr in CCl_4/1-hex and $W(CO)_5$pip in isooctane 139
4.7. Deconvoluted spectral bands for $W(CO)_5$pyr and $W(CO)_5$pip in CH_2Cl_2/1-hex 140
4.8. Deconvoluted spectral bands for $W(CO)_5$pyr and $W(CO)_5$pip in methanol 141

Page

4.9. Deconvoluted spectral bands for $W(CO)_5$pyr and $W(CO)_5$pip in octanol 142

4.10. Diagram of a trigonal bipyramid and square pyramid structures 151

LIST OF TABLES

	Page
Chapter 1.	
1.1. Relaxation Times of Selected Alcohols	23
Chapter 2.	
2.1. List of Reagents	33
Chapter 3.	
3.1. Molar Extinction Coefficients of $W(CO)_5$(pyridine)	64
3.2. Molar Extinction Coefficients of $W(CO)_5$(piperidine)	65
3.3. Photosubstitution Quantum Yields for $W(CO)_5L$ in isooctane/1-hexene	72
3.4. Effect of Concentration of Initial Reactant on photosubstitution quantum yields for $W(CO)_5$pyr in isooctane/1-hexene	74
3.5. Effect of Concentration of Initial Reactant on photosubstitution quantum yields for $W(CO)_5$pip in isooctane/1-hexene	75
3.6. Photosubstitution Quantum Yields for $W(CO)_5L$in benzene/1-hexene	79
3.7. Photosubstitution Quantum Yields for $W(CO)_5L$ in dichloromethane/1-hexene	80
3.8. Photosubstitution Quantum Yields for $W(CO)_5L$ in alcohols	87
3.9. Photosubstitution Quantum Yields for $W(CO)_5L$ in chlorinated alkanes	91
3.10. Photosubstitution Quantum Yields for $W(CO)_5L$ in 1-hexene and mixed isooctane/1-hexene solutions	92
3.11. Calculated Molar Extinction Coefficients of Transients from picosecond spectroscopy of $W(CO)_5L$ in cyclohexane at 50 ps	99
3.12. Calculated Molar Extinction Coefficients of Transients from picosecond spectroscopy of $W(CO)_5L$ in 1-hexene at 50 ps	99
3.13. Molar Extinction Coefficients of $W(CO)_5$ (alcohol) from steady state photolysis of $W(CO)_5L$	117
3.14. Calculated Alkyl Transient Percentages for $W(CO)_5L$ at 450.2 nm	118
3.15. Bond Lengths in the ground electronic spectra of $W(CO)_5L$	118

1. INTRODUCTION

1.1. History of the Metal Carbonyls (1).

The discovery of the first transition metal interaction with carbon monoxide was made in 1890 by L. Mond (2) who observed that valves made of nickel in reaction vessels used for the production of sodium carbonate corroded severely during many of the reactions. Extensive experimentation revealed that nickel could react slowly with carbon monoxide at temperatures of about 100°C to produce a mixture of gases containing greater than 30% of $Ni(CO)_4$. Other experiments which attempted to produce similar compounds with cobalt, iron, copper and platinum failed until 1891 when iron pentacarbonyl, $Fe(CO)_5$, was successfully synthesized simultaneously by L. Mond and F. Quinke in England (3) and M. Berthelot in France (4). The first photochemical reaction of a metal carbonyl was observed in 1903, the formation of diiron enneacarbonyl, $Fe_2(CO)_9$ from $Fe(CO)_5$ in sunlight (5). Between 1910 and 1940, the carbonyls of cobalt, molybdenum, chromium, tungsten, ruthenium and iridium were also synthesized. The preparation of these compounds with the general formula $M_X(CO)_Y$ was generally straightforward. The major criteria were the use of high pressures of carbon monoxide, reaction temperatures of 100°C or higher, and the presence of a reducing agent since most syntheses began with a metal in a high oxidation state and the stable metal carbonyls required a metal with an oxidation state of 0 or $\pm$ 1. These metal carbonyls were observed to be extremely stable and this stability is due to the high tendency to achieve an inert-gas configuration around the central metal. In these, and other, organometallics, the stable configuration requires 18 electrons and the compounds will form in such a way as to obtain this configuration.

1.2. Objectives of the Research

This research project was divided into four related areas. The first area involved the reexamination, by an independent method, of the wavelength dependent behavior of the photochemical substitution of L in $W(CO)_5L$ (L = pyridine, piperidine) by an alkene upon irradiation into the LF singlet state and an extension of these studies into the LF triplet states. Second, the reactivity of the MLCT state towards photosubstitution as a function of separation of MLCT and LF states was studied. $W(CO)_5$pyridine possesses a d --->π^* (pyridine) MLCT state which is higher in energy than the corresponding LF singlet states. The MLCT and LF states are mixed in non-polar solvents and can be resolved in polar solvents. $W(CO)_5$piperidine does not possess a corresponding MLCT state. Photosubstitution quantum yields were compared between these two compounds in solvents which resolved the MLCT and LF states in the pyridine complex to determine if dissociative reactivity was affected in the presence of a mixed MLCT-LF state or if a separate reactive pathway exists from the MLCT state. Third, the solvent dependence of the photochemical substitution of L by a suitable ligand upon LF singlet excitation was studied in several different solvents for the pyridine and piperidine complexes. Finally, the transient absorption behavior for $W(CO)_5L$ (L = CO, pyridine, piperidine) in alkane, alkene and alcohol solvents was examined.

1.3. Review

1.3.1. Geometric Structure.

X-ray and electron diffraction studies have confirmed the octahedral geometry of $W(CO)_6$ (Figure 1.1a) in solid and vapor phases (6-8). Interatomic distances for the W-C bond are measured to be 2.06 $\pm$ 0.04 Å (6). The electronic configuration of the free W atom is $5d^4 6s^2$ and the valence orbitals available for bonding are the 5d, 6s and 6p orbitals. The bonding between carbon and oxygen in carbon monoxide consists of a filled σ orbital and two filled π orbitals which are localized between the carbon and oxygen. There are two lone pairs of electrons localized on the carbon and oxygen atoms which are directed away from the molecule, and two π-antibonding orbitals which are empty in the ground state and directed away from the CO internuclear region. The bonding π orbitals have large O atomic orbital coefficients and the anti-bonding π^* orbitals have large C atomic orbital coefficients. The dz^2 orbital of the metal bonds in a σ fashion with the carbon sp-hybridized lone pair and the dxz and dyz orbitals interact with the π^*x and π^*y orbitals respectively (Figure 1.1b). The electron density donated by the CO ligands is delocalized from the metal into the empty π^* orbitals of the CO. This increases the attractive potential to the metal resulting in a highly stable complex with a strong d-orbital σ bond, strong CO π acidity, and as a result of the latter, a metal of low formal charge.

Substitution of a CO in $W(CO)_6$ by a pyridine or piperidine molecule reduces the symmetry of the complex from octahedral to C_{4v}. Both pyridine and piperidine are bonded to the W metal via the lone pair of the nitrogen atom (Figures 1.2a, 1.2b). Bonding between the metal and the CO ligands is the same as described for $W(CO)_6$. Pyridine has low-lying π-orbitals which can accept electron density. Piperidine has no π orbitals. X-ray data show that the plane of the

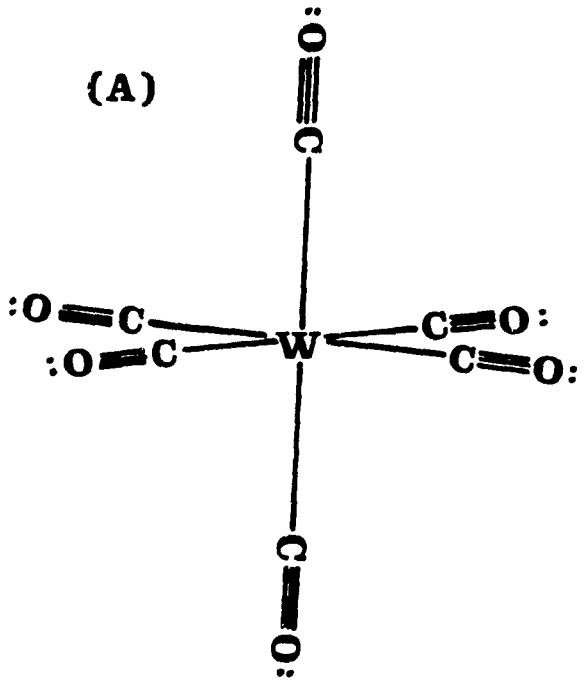

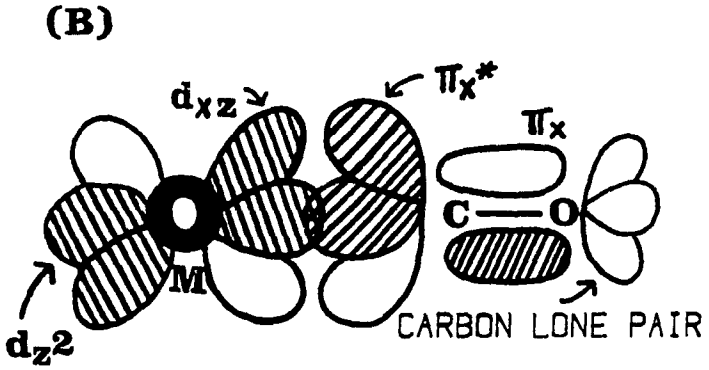

FIGURE 1.1. (A) $W(CO)_6$, (B) BONDING INTERACTIONS BETWEEN A METAL AND CO
(ref 48 for (B)

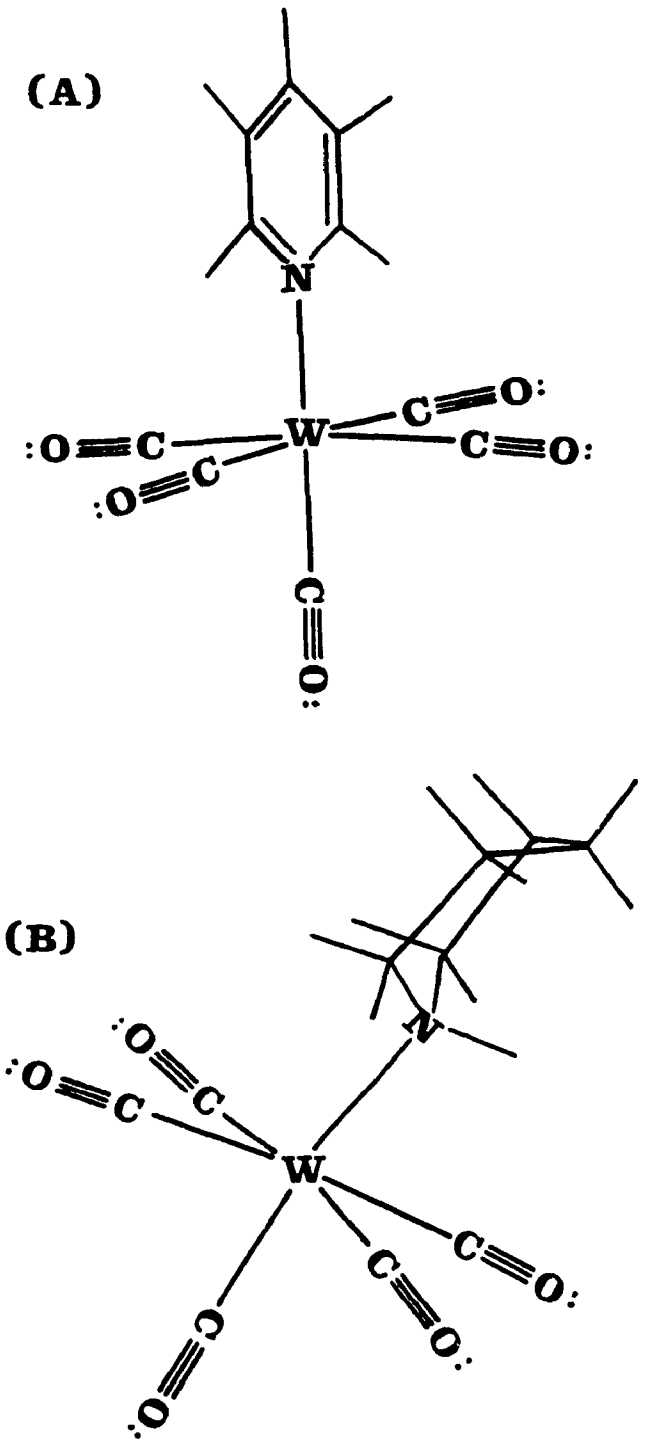

FIGURE 1.2. GEOMETRIC STRUCTURES OF (A) $W(CO)_5$PYRIDINE AND (B) $W(CO)_5$PIPERIDINE

pyridine ring almost bisects the equatorial C-W-C bond (9). The W-N bond length is 2.26 ± .01 Å, the cis W-C bonds are 2.04 ± .02 Å and the W-C bond length trans to the pyridine ligand is 2.00 ± .01 Å in the $W(CO)_5$pyridine molecule (9). The $W(CO)_5$piperidine structure will be reported in this thesis.

1.3.2. Vibrational Spectroscopy

The infrared absorption spectra for $M(CO)_6$, (M = Cr,Mo,W) have been recorded in the solid state (10). Metal-carbon and carbon-oxygen force constants have been calculated. The order of the metal-carbon force constants is observed to be $F_{WC} > F_{CrC} > F_{MoC}$. The M-C force constants for the W-C bonds have been calculated to be 2.148 mdyn/Å. The MCO force constants decrease in the same order as the M-C force constants. The CO stretching frequencies for $W(CO)_6$ as a solid adsorbed upon a CsBr window at 120K are 2124 cm^{-1} (A_{1g}), 2019 cm^{-1} (E_g), and 1998 cm^{-1} (T_{1u}). The T_{1u} W-C stretching frequency is reported at 373 cm^{-1} (10). The CO force constants have been calculated to be 17.695 mdyn/Å (10). For $W(CO)_5$pyridine in isooctane, the CO stretching frequencies are 2073 cm^{-1} (A_1^2), 1934 cm^{-1} (E) and 1921 cm^{-1} (A_1^1) (11). The W-C stretching frequencies are 428 cm^{-1} (A_1), 403 cm^{-1} (A_1) and 368.5 cm^{-1} (E) (11). The strongest W-C stretch is the E mode which corresponds to the stretch of the equatorial carbonyls. The axial and equatorial CO force constants have been calculated to be 15.14 and 15.77 mdyn/Å, respectively (11). For $W(CO)_5$piperidine in isooctane, the CO stretching frequencies are 2072.5 cm^{-1} (A_1^2), 1930 cm^{-1} (E) and 1919 cm^{-1} (A_1^1). The W-C stretching frequencies are very similar to those of $W(CO)_5$pyr: 429 cm^{-1} (A_1), 403 cm^{-1} (A_1) and 371 cm^{-1} (E) (11). The axial and equatorial force constants have been calculated to be 15.12 and 15.73 mdyn/Å, respectively (11). Since the carbonyl stretching frequencies are lower for the monosubstituted complexes than they are

for the hexacarbonyl, more extensive metal-to-carbonyl π-bonding and stronger metal-carbonyl bonds are expected. Comparison of the W-C bond lengths indicate (7,9) this to be true. The values obtained for the CO force constants of the pyridine complex do not differ significantly from those obtained for the piperidine complex. This suggests that there is no appreciable π-bonding between tungsten and the pyridine (11). IR and Raman frequencies from 3000 - 195 cm^{-1} are reported for all three complexes in Appendix A.

1.3.3. Luminescence spectroscopy

Radiative decay has been reported at 77K for $W(CO)_5L$ complexes where L is a ketone, ether, amine or pyridine (12-14). No emission has been detected for these complexes at room temperature. The emission maxima for these complexes is found to lie between 510 and 543 nm and emission lifetimes are in the range of 6.5 x 10^{-7} to 2.6 x 10^{-5} sec (12). The wavelength of maximum excitation for these complexes is 400 nm which is associated with the LF $^1A_1$ ---> ^1E transition. There is little or no structure observed for the band maxima and some overlap between the emission and absorption bands exists. $W(CO)_6$ does not emit at any temperature but emission at 533 nm has been reported for $W(CO)_5$ in low temperature methylcyclohexane glass (77K) provided the trapped CO generated upon excitation of $W(CO)_6$ is removed (13). The lack of emission before removal of trapped CO is believed to be due to prompt regeneration of $W(CO)_6$ in the low temperature glass. The emitting state for these complexes is assigned as the ^3E --> $^1A_1$ transition whose spin forbidden character is relaxed in the presence of the heavy W atom. No emission from the corresponding Cr or Mo complexes has been reported.

Several $W(CO)_5L$ complexes, where L = acetylpyridine, 4-benzoyl-pyridine, 4-

cyanopyridine, and 4-formylpyridine emit at room temperatures as well as low temperatures from their lowest lying energy states which are MLCT in character (15). In these complexes, emission lifetimes increase and emission maxima decrease as the electron-withdrawing effect of L increases. Emission band maxima are found between 15.4 and 18.8 x 10^3 cm^{-1}. Solvent dependence for luminescence of these compounds show that emissions are of higher yield and longer lifetimes for non-polar solvents compared to polar solvents. An increased rate of nonradiative decay from the excited state of $W(CO)_5L$ is believed to be responsible for differences between polar and non-polar solvents. Emissions from these complexes are quenched by anthracenes with triplet energies less than 18 x 10^3 cm^{-1}. This has been attributed to the existence of two low-lying MLCT states, a quenchable state at 18.5 $\pm$ .4 x 10^3 cm^{-1} and an emitting state at 19.6 $\pm$ .4 x 10^3 cm^{-1} (15).

1.3.4. Transient Absorption Spectroscopy

Much effort has been focused during the last decade on the identification and characterization of coordinatively unsaturated metal carbonyl species in solid, liquid and gas phases. Laser flash photolysis in all three phases has provided evidence for the existence of an intermediate pentacarbonyl species, $M(CO)_5$, from $M(CO)_6$ (M = Cr,Mo,W) which can interact with a variety of relatively inert species to form $M(CO)_5S$ (16-21). The loss of more than one CO to form $M(CO)_n$ (n = 2-4) has also been documented in inert matrices (22).

Early studies of these complexes using nanosecond flash photolysis (5-20 ns pulses) have shown that in alkane solvents, such as cyclohexane, photogeneration of the $Cr(CO)_5S$ species, where S is a solvent molecule, occurs in less than 50 ns with an absorbance maximum at 503 $\pm$ 5 nm and a lifetime of several hundred microseconds (23). $M(CO)_6$ (M = Cr,Mo,W) photolyzed in fluorinated solvents

such as argon-flushed perfluoromethylcyclohexane (C_7F_{14}), which are presumed to be more inert solvents than cyclohexane, reveals the existence of a short-lived transient at 620, 460, and 475 nm for Cr, Mo and W, respectively (17,24). These transients, which are formed within 5 ns, have been assigned as the naked $M(CO)_5$ species because of the very weak interactions with the perfluoromethylcyclohexane solvent and the close similarity between the free $M(CO)_5$ species observed in low temperature Ne matrices (20). A second transient with a maximum absorbance at ~ 485 nm is observed to grow as the 620 nm transient decays. This second transient is assigned as the $Cr_2(CO)_{11}$ species formed by coordination of $Cr(CO)_5$ to $Cr(CO)_6$ via the carbonyl oxygen of the $Cr(CO)_6$ (25). In CO-flushed C_7H_{14} solutions of $Cr(CO)_6$, the transient at 480 nm, assigned as the $Cr_2(CO)_{11}$ species, is observed to decay at two different rates. The decay shows a strong transient with a lifetime of 450 ns and a weaker long-lived transient with a lifetime > 1 μs. The short-lived transient decay has been assigned as the reaction between $Cr_2(CO)_{11}$ and CO to give 2 $Cr(CO)_6$ and the long-lived transient has been assigned as an impurity complex (24). In mixed cyclohexane-perfluoromethylcyclohexane solutions, $M(CO)_5$ reacts with cyclohexane. Transients are at 503 nm for Cr and 415 nm for W. These transient absorptions are in agreement with those reported for these complexes in cyclohexane solutions (23,25).

Nanosecond photolysis (12 ns pulses) of $Cr(CO)_6$ alone in the gas phase or in the presence of He gas has revealed the presence of three transients with absorption maxima at 620, 500 and 410 nm, corresponding rise times of $\leq$ 20 ns for the 620 nm transient and 100-500 ns for the 500 and 410 nm transients. Corresponding lifetimes are 100-500 ns, 100 μs, and > 1 msec, respectively (26). The 620 nm transient has been assigned as the free $Cr(CO)_5$, the 500 nm transient has been assigned as the $Cr(CO)_5$-(CO)$Cr(CO)_5$ species, and the 410 transient has

been tentatively assigned as $Cr_2(CO)_{10}$ or $Cr_2(CO)_9$. In the presence of other species, Q, photolysis of $Cr(CO)_6$ forms $Cr(CO)_5Q$, where Q is N_2, NH_3, methanol, acetone, ethylene or silane with corresponding absorption maxima at $\lambda < 400$ nm, 445, 460, 438 and $\lambda < 400$ nm for both ethylene and silane (19,26).

Most of the time-resolved experiments which focus on the study of unsubstituted metal carbonyls use UV-visible spectroscopy to identify the limited number of transients formed. Little information about the structural properties of the absorbing molecules is gained. In the case of substituted metal carbonyls, UV-Vis spectroscopy is limited because the larger number of possible transients which can be formed have few observable differences in their UV-Vis spectra. The technique of IR resolved flash photolysis has been used to identify different species based on obvious differences in CO vibrational frequencies (27,28). Flash photolysis of $M(CO)_6$, (M = Cr,Mo,W), using a 5 μs flash in CO-saturated cyclohexane, and thermal reaction of the solvated primary photoproduct in acetone, benzene and methanol have been studied (27). This IR technique confirms the presence of a short-lived intermediate at 1962 cm^{-1} corresponding to the frequency of $Cr(CO)_5S$. As this species decays, a second transient with two maxima at 1916 and 1950 cm^{-1} grows. This second transient is associated with $Cr(CO)_5X$, where X is a contaminant, possibly moisture. For solutions of $Cr(CO)_6$ in mixtures of acetone, benzene or methanol and cyclohexane, the band at 1962 cm^{-1} is not observed and the lifetimes and intensities of the transients at 1950 and 1916 cm^{-1} are increased signficantly. Because they decrease by first order kinetics with the rate constant decreasing with increasing [L], it is concluded that in the presence of L, the transients are the various $Cr(CO)_5L$ species (27). Results for both $Mo(CO)_6$ and $W(CO)_6$ are comparable. This technique has been used to investigate the transient absorption spectroscopy of derivatives of $W(CO)_5PPh_3$ in an argon matrix at low

temperature (28). 367 nm irradiation (10-15 ns pulse) confirms the presence of two photoproducts which are photochemically interconvertible. These transients have been assigned as the trans and cis-isomers of $W(CO)_4(PPh_3)$ weakly coordinated to Ar. A parallel assignment is made for the cis and trans isomers produced by photolysis of $LMo(CO)_5$ (L = tri(cyclohexyl)phosphine) in a methylcyclohexane/isopentane glass at 77K (29). IR time-resolved studies of $W(CO)_6$ in n-heptane at room temperature confirm the formation of a $W(CO)_5S$ transient, where S is n-heptane, within 10 ns.

355 nm excitation of $Cr(CO)_6$ in cyclohexane and benzene using a 25 picosecond laser pulse generates transients which are observed within 25 picoseconds and absorb at 497 and 470 nm, respectively (30). These transients do not decay within the maximum probe delay limit of 3 ns and they are assigned as the $Cr(CO)_5$-solvent species observed in the same two solvents on longer time scales. The very short time scale suggests that no activation barrier inhibits the formation of the $M(CO)_5$ species.

Finally, the study of the rise time of $Cr(CO)_5$ in cyclohexane at .2 ps time intervals using a .8 ps laser pulse has shown that the formation of $Cr(CO)_5$ (cyclohexane) occurs within the instrument response time (.8 ps) (31). The transient absorption which is at 505 nm does not decay within the maximum delay limit of several nanonseconds. Corresponding information on the Mo and W species has not been reported.

1.3.5. Solvatochromic Behavior of Metal Carbonyls

Solvatochromism is a term used to describe a positive (lower energy) or negative (higher energy) shift of the electronic transitions of any number of compounds in a given solvent. Many transition metal complexes have been found

to display solvatochromic properties and in these complexes, solvatochromism is seen most often in polar organic solvents where charge transfer bands are extremely solvent sensitive (32-38). The degree of solvatochromism, in many cases, is found to have some correlation with the degree of solvent polarity.

The solvatochromic behavior observed for group VIB metal carbonyl complexes involves the MLCT transitions which exhibit negative solvatochromism (shifts to higher energy) in more polar solvents. The MLCT absorption bands of (μ-L)$[Mo(CO)_4]_2$ complexes(μ-L = 2,2'-bipyrimidine (bpym);2,5-bis(2-pyridyl)pyrazine (dppz);3,6-bis(2-pyridyl)-1,2,4,5-tetrazine (dptz); and azo-2,2'-bipyridine (abpy)) (32), $Mo(CO)_{4-x}(PR_3)_x$ complexes (R = an alkyl group (33)), $M(CO)_4L$ (M = Cr,Mo,W; L = 2,2'-bipyridine, 1,10-phenanthroline or a derivative amine (34)), $W(CO)_5L$ (L = pyridine or a substituted pyridine) (14,35), and $(CO)_5W$-(pyz)$W(CO)_5$ (pyz = pyrazine)(36) all exhibit negative solvatochromism with shifts of band maxima up to 50 kcal/mole.

There are two general explanations given for the solvatochromism observed for the charge-transfer transitions of metal complexes in polar solvents (32,37). The first involves changes in polarity which arise because of the presence of a greater charge transfer between metal and ligand in the excited state of the complex compared to that found in the ground state. The solvent arranges itself so that its dipole can interact with the ground state dipole of the complex. Generally, the dipole of the CT excited state is different from the ground state dipole, in direction or magnitude. When the solute undergoes a Franck-Condon transition the solvent is no longer oriented as it was prior to excitation and depending on the nature of the solvent and the dipole change, the solute excited state may be stabilized or destabilized. The energy of the transition thus depends on the solvent and usually its polarity. Theoretically, if the molecule is symmetric and has no permanent

dipole then the change in energy may be small or negligible but if the transition moment of the CT state is parallel to the ground state dipole and a significant change occurs upon excitation then a large solvent effect can be observed. When the CT transition is in opposition to the ground state dipole the spectral shifts will be to higher energy (negative solvatochromism) as the solvent becomes more polar. This type of behavior is generally observed with transitions of the MLCT type. If the CT transition shifts its charge in the same direction as the ground state dipole then the spectral shift will be to lower energy in more polar solvents. This behavior can be observed with transitions of the LMCT type.

In complexes which possess no permanent dipole moment, an alternative explanation for the observation of significant spectral changes induced for CT transitions in polar solvents involves the polarizability of the complex. The charge distribution and polarizability of both solute and solvent molecules are sensitive to each other. Interactions such as hydrogen-bonding or other donor-acceptor interactions can result in large energy changes for the solvated molecule if the solvent changes. In these complexes, the polarizability α which is the proportionality constant between the induced moment μ_{ind} and an inducing electric field E determines the magnitude of the charge within a molecule (32). CT complexes such as $M(CO)_4$(bidiazine) (bidiazine = 3,3'-bipyridazine, 2'2- and 4'4-bipyrimidine, 2,2-bipyrazine; M= Cr,Mo,W) which have no permanent dipole moment experience polarizability due to σ-donation and π back-bonding (38). The 4'4-bipyrimidine and 3'3-bipyridazine complexes exert stronger back-bonding toward the d^6 metal fragments and exhibit greater sensitivity of their MLCT bands toward the solvent change than 2'2-bipyrimidine and 2'2-bipyrazine. For all of these complexes, the geometry, composition and nodal properties of the π^* level are comparable and so the degree of solvatochromism depends solely on the amount of

back donation. The polarizability will be large for MLCT transitions in the ground state because the charge shift occurs from the usually negative polarized low-valent metal center to the positively polarized ligand, lowering the polarizability of the MLCT excited state. Therefore, when the polarizability of the ground state is greater than the polarizability of the excited state negative solvatochromism will be observed.

1.4. Review of $M(CO)_6$ and Related Photochemistry

1.4.1. Ligand Field Photochemistry

The photochemistry of the group VIB metal hexacarbonyls, $M(CO)_6$ (M = Cr,Mo,W), has been studied extensively during the past two decades (37). The primary event upon irradiation of these complexes in low temperature matrices (20,39,40), solution (24,27,41,42), and in the gas phase (19,43) is efficient loss of CO to give $M(CO)_5$ (eq. 1.1).

$$M(CO)_6 \xrightarrow{h\upsilon} M(CO)_5 + CO \qquad (1.1)$$

If a suitable ligand is available, prompt replacement of the expelled CO is easily achieved. Synthesis of a wide variety of monosubstituted derivatives is often accomplished by photochemical replacement of CO by a weakly coordinated solvent followed by thermal substitution of the solvent ligand with the desired ligand (44). An example is the preparation of $W(CO)_5$pyridine (eq. 1.2):

$$W(CO)_6 + THF \xrightarrow{h\upsilon} W(CO)_5THF \xrightarrow[pyr]{\Delta} W(CO)_5pyridine + THF \qquad (1.2)$$

The photochemistry of $M(CO)_6$, (M = Cr,W) suggests that rapid internal conversion and efficient prompt intersystem crossing occurs with all substitutional reactivity originating in the LF triplet (41,42). The evidence includes the following points. The quantum yield for photosubstitution of CO by pyridine for $Cr(CO)_6$ in cyclohexane is 0.67 ± 0.02, independent of concentration and wavelength of irradiation (41,42). Similar behavior is observed for $W(CO)_6$ in cyclohexane or benzene. Photosubstitution of CO by pyridine is 0.72 ± 0.04, independent of wavelength of irradiation (42). Benzophenone-sensitized photosubstitution of CO by pyridine in both hexacarbonyls gives yields comparable to those obtained upon direct irradiation; $0.68 \pm .04$ for $Cr(CO)_6$ and $0.71 \pm .07$ for $W(CO)_6$ (42).

These compounds do not phosphoresce even at low temperatures suggesting that the substitution yield < 1.0 is due to competition with radiationless decay. The excited states of the metal hexacarbonyls are very short-lived since quenching studies fail to alter the photosubstitution yields.

As well as substitution of CO by an olefin, UV irradiation of $M(CO)_6$ (M = Cr,Mo,W) in the presence of excess olefins results in cis-trans isomerization and 1,3-hydrogen shifts of the olefin (45). Olefin isomerization depends on the metal in the order W > Mo >> Cr, and in these systems, thermal as well as photochemical pathways are important.

Steady-state photolysis of monosubstituted $W(CO)_5L$ complexes, where L is a nitrogen donor, an alkene, or a phosphorous donor has revealed that both loss of L and loss of CO occur depending on the wavelength of irradiation (46-51)(eq. 1.3 and 1.4).

$$W(CO)_5L \xrightarrow[L']{h\upsilon} W(CO)_5L' + L \qquad (1.3)$$

$$W(CO)_5L \xrightarrow[L]{h\upsilon} W(CO)_4L_2 + CO \qquad (1.4)$$

Loss of L remains the predominant reaction for complexes with nitrogen donors or alkenes. Both L and CO loss are comparable for phosphorus donor ligands (46). For $W(CO)_5L$ (L = pyridine, trans-2- and trans-4-styrylpyridine (47), piperidine (48)), Wrighton et al have reported an increase in substitution quantum yields with decrease of excitation energy in the LF singlet region from 254 to 436 nm. The quantum yields for photosubstitution of pyridine by 1-pentene for $W(CO)_5$pyridine in isooctane/1-pentene increases from 0.34 $\pm$ .03 at 254 nm to 0.63 $\pm$ .06 at 436 nm in contrast to 0.05 $\pm$ .005 at 313 nm to 0.16 $\pm$ .016 at 436 nm for photosubstitution of t-4-styrylpyridine by 1-pentene. Quantum yields for substitution of L for phosphorous compounds is ~ 0.3 $\pm$ .03 (46).

In addition to photosubstitution reactions involving loss of L, loss of a second CO from $W(CO)_5$pyridine to yield cis-$W(CO)_4$(pyridine)$_2$ occurs with low efficiency in the presence of excess pyridine at high energy (.04 at 254 nm (47)). Cis-trans isomerization of c-4 and c-2-styrylpyridine occurs with relatively high efficiency upon irradiation of $W(CO)_5L$ (L = t-2- or t-4-styrylpyridine (47)). Quantum yields increase from 0.21 $\pm$ .02 at 254 to 0.49 $\pm$ .05 at 436 nm for $W(CO)_5$t-4-styrylpyridine. Irradiation into the lowest LF band of $W(CO)_5L$ where L is a substituted pyridine, not already described, gives substitution yields which are > 0.5 (14).

UV irradiation (254, 313 nm) of $W(CO)_5$(alkene) (alkene = C_2H_4,C_3H_6,1-C_5H_{10}) in methylcyclohexane at low temperatures (77K) yields both alkene and CO loss (49). Alkene loss occurs more readily (~ 2 times) at 313 nm than at 254 nm and

the most massive alkene tends to be the most labile. Loss of alkene yields $W(CO)_5$ while loss of CO yields $W(CO)_4$(alkene). Loss of CO from $W(CO)_5$(pentene) to form $W(CO)_4(pentene)_2$ has been reported to be fairly efficient with quantum yields of $0.31 \pm .05$ and $0.44 \pm .05$ at 313 and 365 nm, respectively (45). In many cases, disubstituted products are observed to have the cis orientation for $M(CO)_5L$ complexes, where L is an N donor. In cases where L is a phosphorus donor, equal amounts of cis and trans disubstituted products are observed (46). This is believed to be due to the loss of a CO which is bound to the metal in an equatorial position. Photochemical reactions of compounds such as $Mo(CO)_5NHC_5H_{10}$ with ^{13}CO produce $Mo(CO)_4(^{13}CO)NHC_5H_{10}$ with the labeled CO in the equatorial position (50). This is also observed for $M(CO)_4[PC_6H_{11})_3]_2$ (51). Exceptions are found for $W(CO)_4[P(C_6H_{11})_3]_2$ and $Cr(CO)_4[P(C_6H_5)_3]_2$ which form the trans product. Coordinatively unsaturated intermediates of the type $M(CO)_5$ or $M(CO)_4L$ may undergo rapid thermal rearrangements in their ground state before being scavenged by an incoming ligand and definite assignment of CO loss based on ^{13}CO replacement can not be made. Quantum efficiencies for CO substitution in these complexes are generally found to be lower for complexes which contain nitrogen donors compared to those complexes which have phosphorus donor ligands (46).

Other groups of d^6 complexes which display photosubstitution behavior upon LF irradiation include the Rh(III) and Co(III) amine complexes (52-56). The lowest energy excited state for $M(NH_3)_6^{3+}$ (M = Co,Rh) is assigned as the $^1A_{1g}$ ----> $^1T_{1g}$ transition (52). $Ir(NH_3)_6^{3+}$ shows a long wavelength tail assigned to the $^1A_{1g}$ ---> $^3T_{1g}$ transition (53). $Co(NH_3)_6^{3+}$ shows contrasting behavior to that of Rh or Ir complexes. LF excitation for the Co(III) complexes gives photosubstitution quantum yields for aquation that are approximately ten times smaller and show a

wavelength dependence with increasing quantum yields upon higher energy excitation (.0054 at 365 nm and .00052 at 460 nm) (54). While the substitution behavior of Rh and Ir is wavelength independent (.075 for Rh and .08 for Ir) (55,56) indicating that photosubstitution occurs from the thermally equilibrated lowest energy excited state (LEES), the behavior from the Co(III) complexes suggests that excited states other than the LEES are largely responsible for the observed photosubstitution behavior (52).

In addition to the hexammine complexes, quantum yields for substitution of Cl by H_2O in $Co(NH_3)_5Cl^{2+}$ and cis-$Co(en)_2Cl$ are higher upon ligand field singlet irradiation than they are upon ligand field triplet irradiation (57,58). In addition, wavelength dependence is observed upon LF singlet irradiation with increasing photosubstitution occurring with increasing excitation energy (58). Transient absorption spectroscopy of these complexes reveals that the triplet has a short lifetime on the order of 50-150 ps. The difference from Rh and Ir complexes arises from these short lifetimes. The analysis of detailed kinetics (58) suggests that the triplet reactivities are similar for Rh(III) and Cr(III) complexes.

1.4.2. Charge-transfer Photochemistry

Several mononuclear metal carbonyls, including complexes of the general formula, $W(CO)_5L$ where L is an oxygen or a nitrogen donor, have low-lying metal-to-ligand charge transfer (MLCT) excited states (14,37). As L becomes more electron withdrawing, the CT state lowers in energy (Figure 1.3), compared to the LF $^1A_1$ ---> ^3E state, and in many complexes, the CT state becomes the lowest lying energy state. Analagous complexes are the d^6, low spin, C_{4v} $Ru(NH_3)_5X^{2+}$ (X = a substituted pyridine) complexes where the lowest energy transition has been assigned as the Ru ---> X CT transition (59). Irradiation into the lowest energy

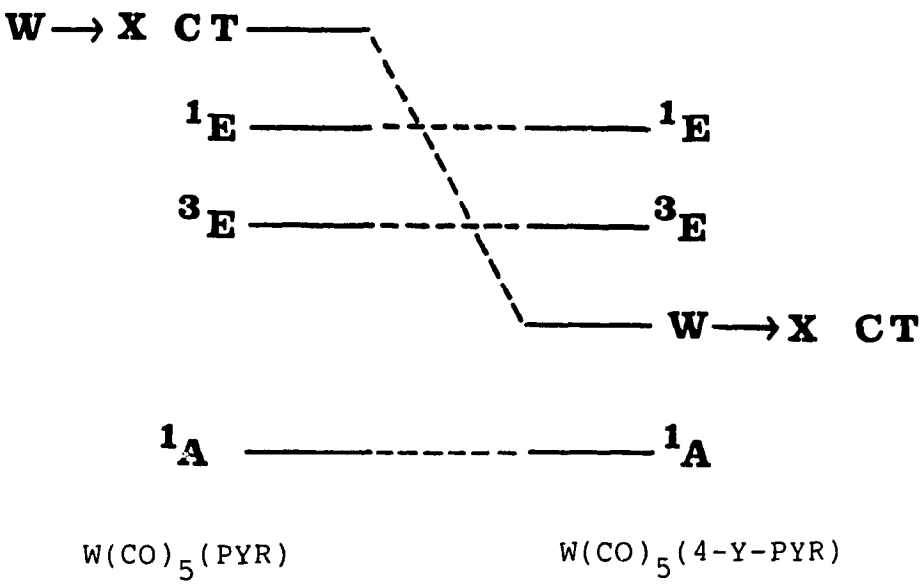

FIGURE 1.3. STATE DIAGRAM INDICATING LOWERING OF MLCT ENERGY UPON SUBSTITUTION OF PYR BY 4-Y-PYR (Y= CYANO, ACETYL, BENZOYL, FORMYL) (REF 14)

band of $Ru(NH_3)_5X^{2+}$ in H_2O reveals comparable photoaquation of both the NH_3 and the X ligands (~ 0.043 $\pm$ .001) (60) but this photoreactivity is believed to be due to some LF character of the lowest excited state rather than to a reactive MLCT state. This conclusion has been supported by studies of the photochemical reactivity upon low energy CT irradiation of $Ru(NH_3)_5$(4-formylpyridine)$^{2+}$ which has very inefficient substitution (61). Experimental studies of the photoreactivity of $W(CO)_4L$ (L = 1,10-phenanthroline and related compounds) which have a lowest lying W ---> L CT transition show that while CO substitution occurs upon the higher energy LF excitation, no detectable CO substitution is observed upon irradiation into the MLCT bands of these complexes (62). For complexes of the type, $W(CO)_5X$, where X is a substituted pyridine, the nature of the lowest electronic state can be altered by varying the substituents on the pyridine. For $W(CO)_5X$ (X = 4-benzoylpyridine, 4-cyanopyridine, 4-acetylpyridine, 4-formylpyridine) (14), the W ---> pyridyl CT transition is assigned as the lowest energy transition which shifts to lower energy as the substituents on the pyridine become more electron-withdrawing. Corresponding LF bands in these complexes are not affected.

Compared to LF irradiation for these complexes, the photosubstitution of X upon irradiation into the MLCT bands is very inefficient. Quantum yields are approximately 0.02 $\pm$ .002 upon irradiation into the lowest energy band which is MLCT in character (14). This is in contrast to the quantum yield of $\geq$ 0.50 for irradiation into a lowest energy band which is LF in character (14,37). Efficient dissociative loss of CO from these low-lying MLCT states is also not observed and the conclusion is that depopulation of π-d orbitals which are π-bonding with respect to the W-CO interaction does not result in CO labilization within the lifetime of the excited state. Since MLCT irradiation also does not result in signficant substitution

of X, it is believed that the MLCT state is not as reactive as the corresponding LF state. Solvent and temperature dependence studies of the photochemical reactivity of these complexes upon MLCT irradiation show that changing the polarity of the solvent so as to shift the energy of the MLCT states does not significantly alter the substitution yields (37). The yields increase with increasing temperature in all the solvents studied and good Arrhenius behavior is observed for the temperature studies corresponding to an apparent activation energy of 7.6 $\pm$ 1 kcal/mole. The photosubstitution reactivity of $W(CO)_5$(4-cyanopyridine) can be quenched with anthracene. The Stern-Volmer plot of [quencher] vs Φ^o/Φ is linear and the slope corresponds to a bimolecular rate constant of 4 x 10^9 $M^{-1}s^{-1}$ which is approximately the diffusion-controlled limit. The activation energies calculated for these complexes correspond to the differences between MLCT and LF states implying that chemical reaction occurs from the higher-lying LF state which is in thermal equilibrium with the emitting MLCT state (37).

The MLCT photodissociation of low-spin, d^6 FeN_4XY complexes, where N_4 = bis(dimethylglyoximate) or bis(napthoquinone dioximate) and X or Y = CO, PBu_3, ~ $P(OBu)_3$, BzNC or MeIm, proceeds through a dissociative state (63). As the π-acceptor strength of the axial ligand decreases in the order CO >> BzNC ~ $P(OBu)_3$ > PBu_3 > MeIm, the quantum yields decrease. In these complexes, irradiation in the presence of X or Y results in the formation of FeN_4X_2 or FeN_4Y_2 products, respectively, and in the presence of a different incoming ligand Z, FeN_4XZ and FeN_4YZ products can be formed. The lowest energy band in the electronic spectra of these complexes is assigned as the $d\pi$ ---> oxime π^* transition and irradiation into this band results in the loss of the X or Y ligand with quantum yields ranging from 3 x 10^{-4} to 0.05 depending on the complex and the entering ligand.

1.5. Role of the Solvent

The study of the chemical behavior of a given complex in condensed phases, as compared to the gas phase, can become complicated due to the fact that the complex under investigation is in constant intimate contact with its surrounding solvent neighbors. In these systems, it becomes necessary to understand the interaction between solute and solvent molecules before a complete picture of the solute behavior can be obtained. In circumstances where the effects of different solvent environments on the solute behavior are studied, it can be difficult to interpret the results because the problem of altering solvent parameters other than the one desired exists.

In our experiments, we have investigated solvent influence on the photochemical substitution reactions of monosubstituted tungsten carbonyls by comparing both steady state photolysis and picosecond spectroscopy of these compounds in different solvents. Two series of related solvents were used. The first group of solvents was a series of straight chain alcohols: methanol, propanol, butanol and octanol. These were used to investigate possible dynamical effects since longtitudinal relaxation times are available for these solvents (Table 1.1). The second series of solvents was the chlorinated solvents dichloromethane, chloroform, and carbon tetrachloride. These solvents were studied to determine how differences in vibrational energy transfer could affect the photosubstitution quantum yields. The alcohols were used as neat solvents since they are suitable ligands which can bind easily to $W(CO)_5$. The chlorinated solvents, which are unsuitable ligands, were mixed with 1-hexene in a 2:1 v/v ratio. In order to interpret the results of these studies, it is necessary to review the different solvent parameters which may be important in these reactions.

Table 1.1. Relaxation Times of the Alcohols.

Solvent	Longtitudinal Relaxation Times (23°C)[a,b] (ps)	Dielectric Relaxation Time (ps)[a,b]
Methanol	3.3	68
Propanol	39.0	408
Butanol	72.0	624
Octanol	319.0	1597

a) values taken from references 80,81
b) ps refers to picoseconds

1.5.1. The Cage Effect

One of the earliest recognized interactions between solute and solvent molecules is known as the "cage effect" (64). In liquid media, solute molecules are constantly surrounded by solvent molecules. The number of solvent molecules is generally many times the number of solute molecules. Constant motions between solute and solvent molecules allow for the movement of the solute through the solvent molecules at a finite rate. In order for a reaction to occur, the interacting species must make contact with each other. This contact is limited by the rate of diffusion of the molecules towards each other through the solvent. This diffusion rate has been approximated to be inversely proportional to the bulk shear viscosity of the solvent (65).

When a solute molecule absorbs a photon of light, it is elevated to some excited state in which the atoms of the molecule vibrate at a highly increased rate. If enough kinetic energy is available, the molecule may dissociate and the dissociated fragment will move a given distance away from the remaining fragment and retain a given amount of the kinetic energy. This excess energy is lost upon multiple collisions with the surrounding molecules and the distance between the fragmented molecules may be at most only a few molecular diameters. The surrounding solvent keeps any pair of partners which collide together because as they rebound from their collision, surrounding solvent molecules deflect them back toward each other. If a solvent molecule has not made its way between the two separated fragments, recombination to form the original molecule becomes probable. This is termed primary or geminate recombination. The probability that fragmented species will recombine is inversely proportional to the rate of diffusional separation. The recombination rate can depend on the viscosity of the solvent and the wavelength of irradiation. Theoretically, recombination becomes

less probable with increased excess energy since the distance between the molecular fragments is increased significantly. Secondary recombination, where two fragments are separated by one solvent molecule, can also occur at a reduced probability.

The cage effect has been studied by several groups (66-75). The most extensive investigation involves the bimolecular reaction of I_2 in different solvents. In the 1950's, Noyes and his co-workers (66,67) investigated the geminate recombination yield as a function of wavelength and solvent viscosity . They found that the photodissociation quantum yield decreased with increasing wavelength (ie decreasing excess energy) and increasing solvent viscosity. Subsequent experimental studies have focused on short time scale aspects of I_2 photodissociation. Using picosecond spectroscopy, Chuang et al noted (68) that the observed time for decrease in the signal associated with the dissociated I atoms was 100 picoseconds. This was interpreted as the characteristic time scale for primary recombination. Molecular dynamics simulations placed the primary recombination of I atoms at $\leq$ 10 ps (69,70). The 100 ps time scale was later interpreted by several groups (71-73) to be due to vibrational relaxation of the recombined I_2 molecules since it was only possible to monitor the I_2 molecules in their unreactive ground state.

Most recently, the recombination dynamics of iodine in inert solvents using picosecond flash photolysis has supported earlier molecular dynamics simulations that predicted geminate recombination would occur in under 15 picoseconds (74,75). Once geminate recombination has taken place, vibrational and electronic energy relaxation occurs at a much reduced rate. This relaxation accounts for the 100 ps decay observed in the transient absorption spectra. The time scale for vibrational relaxation depends on the solvent and is longest in chlorinated solvents

as compared to the alkanes. The rate of vibrational relaxation increases in the order $CCl_4 < CHCl_3 < CH_2Cl_2$ requiring approximately 200 ps for the entire process in CCl_4. Vibrational relaxation in the hexanes requires approximately 60 ps. The differences in vibrational relaxation times for I_2 in different solvents may be due to one of two mechanisms for energy transfer or a combination of both. The two mechanisms are vibrational-translational (VT) energy transfer and vibrational-vibrational (VV) energy transfer. In solvents such as xenon where only VT transfer is possible, the typical relaxation time is about 1 ns. The faster (60-200 ps) relaxation in the chlorinated solvents may be due to a combination of VV and VT transfer. Vibrational-rotational (VR) energy transfer may also be involved. VT energy transfer for I_2 is predicted to be efficient from upper vibrational levels and inefficient at lower levels. In CCl_4, the v_2 structural bending mode of CCl_4 at 217 cm^{-1} is near resonant with the 214 cm^{-1} vibrational frequency of I_2 low in its well. The lowest frequency modes for CH_2Cl_2 and $CHCl_3$ are 261 and 285 cm^{-1}, respectively. Resonance between vibrational levels can significantly enhance the probability of energy transfer. However, the differences between the lowest vibrational modes of I_2 and the chlorinated solvents suggest that the rate of vibrational relaxation should increase in the order $CH_2Cl_2 < CHCl_3 < CCl_4$. VV transfer alone, therefore, cannot account for the opposite trend observed. It has been speculated that for I_2 in CCl_4, relaxation within the first 50 ps is due to pure VT transfer. After 40-50 ps, the population has arrived in the neighborhood of important VV energy transfer probability. The VV mechanisms carries the population down into the F-C region. This speculation has yet to be confirmed experimentally.

1.5.2. Solvent Dynamics (76)

The solvent induces changes in the potential energy barrier and free energy of reaction (77). If the reaction rates are faster than solvent fluctuations then details about the motion and structure of the surrounding solvent become important in understanding these roles. Picosecond and subpicosecond studies have played a role in understanding these phenomena.

In non-equilibrium phenomena, the solvent is treated as a dielectric continuum where the solvent is modeled as a structureless fluid with a frequency-dependent constant, $\varepsilon(\omega)$. expressed as (78):

$$\varepsilon(\omega) = \varepsilon_0 + \frac{\varepsilon_0 - \varepsilon_\infty}{1 + i\omega\tau_D} \tag{1.5}$$

where ε_∞ and ε_o are high-frequency and zero-frequency dielectric constants, respectively, and τ_D is the Debye relaxation time. Some solvents show that $\varepsilon(\omega)$ is well described by eq 1.5 but many others, such as the alcohols, are more complex and are generally described by (79):

$$\varepsilon(\omega) = \varepsilon_0 + \frac{\varepsilon_{10} - \varepsilon_{1\infty}}{1 + i\omega\tau_{D1}} + \frac{\varepsilon_{20} - \varepsilon_{2\infty}}{1 + i\omega\tau_{D2}} + \frac{\varepsilon_{30} - \varepsilon_{3\infty}}{1 + i\omega\tau_{D3}} \tag{1.6}$$

where τ_{D1},τ_{D2} and τ_{D3} are associated with rotations which break hydrogen bonds, monomer rotation and rotation of the terminal C-OH groups, respectively (80). A second relaxation time, the longtitudinal relaxation time τ_L, is usually invoked to gauge dynamic solvent effects. It depends slightly on the nature of the perturbation and the value of ε (81,82) and for a point charge is related to τ_D by $\tau_L = (\varepsilon_\infty / \varepsilon_o)\tau_D$

(82). In polar solvents, $\varepsilon_o >> \varepsilon_\infty$ and $\tau_L << \tau_D$.

The importance of the longtitudinal relaxation time, τ_L, in solvent dynamics has been discussed by Kosower and co-workers (81) who observed that the intramolecular charge-transfer rates of several molecules in alcohols are well correlated with τ_L^{-1}. Simon and his co-workers (83) have studied the time-dependent Stokes shift of the emission from the twisted intramolecular charge-transfer (TICT) state of several aminophenyl sulfones. They observed that the rate of intramolecular charge transfer for these molecules is significantly faster than τ_L. Simon and his co-workers have also examined the photodissociation of $Cr(CO)_6$ in methanol (31) and pentanol (84) using picosecond spectroscopy in order to study the role of solvent dynamics on such a system. Using a .8 ps laser pulse and .2 ps time steps, they observed that the rise time for the formation of the $Cr(CO)_5$(MeOH) transient was 2.5 ps which was slower than the .8 ps rise time for the formation of $Cr(CO)_5$(cyclohexane) (31). The delay in the rise time for the methanol species is believed to correspond to the time required for the local solvent to reorganize and coordinate to the ground state of the $Cr(CO)_5$ fragment. Whereas cyclohexane coordination occurs on a time scale fast enough to compete with vibrational relaxation of the excited $Cr(CO)_5$ species, methanol coordination does not. Therefore cyclohexane coordinates to an excited state $Cr(CO)_5$ molecule while methanol coordinates to a ground state $Cr(CO)_5$ species. The Debye relaxation time for methanol is ~ 50 ps and dynamics on this time scale would be expected for formation of $Cr(CO)_5$(MeOH) if breaking of the solvent hydrogen bonds to free a methanol was required (31). The conclusion is that only a small change in the local solvent environment was necessary in this case for solvent coordination to occur (31).

Picosecond flash photolysis of $Cr(CO)_6$ in pentanol (84) reveals the presence of two transients at 460 and 520 nm. These transients correspond to observed transients for $Cr(CO)_5$(MeOH) and $Cr(CO)_5$(cyclohexane), respectively. An instantaneous rise of the 460 nm absorption occurs immediately after excitation with a .8 ps laser pulse and is followed by a slow increase in absorption for the next 800 ps. The absorption signal monitored at 520 nm also rises instantaneously followed by a decay in the signal to approximately 30% of the initial signal. The absorptions at both wavelengths become constant for delay times greater than 1 ns. Based on the observations for $Cr(CO)_6$ in pentanol, it is believed that greater than 50% of the photofragments are initially coordinated by the hydroxyl group of the alcohol (84). After 1 ns, rearrangement of the $Cr(CO)_5$(alkyl) species to the more stable $Cr(CO)_5$(hydroxyl) species has occurred. This could occur because in long-chain alcohols $Cr(CO)_6$ could be preferentially solvated by the hydroxyl end and the local solvent structure around the photoexcited $Cr(CO)_6$ could affect which CO is eliminated (84).

1.5.3. Donor and Acceptor number of Solvents (85,86)

Solvents can be divided into donor or acceptor solvents depending on their specific chemical properties. A donor solvent will react with acidic molecules and ions while an acceptor solvent will react with basic compounds. Metal ions which generally are electron pair acceptors react with donor molecules to produce solvated metal cations. Anions which are Lewis bases interact with acceptor solvents. In solution, competition between solvents and other donor ligands for interaction with acceptor molecules depends on the donor strength of each of the competing species. The donor strength has been determined experimentally relative to the specific reference antimony pentachloride, $SbCl_5$, which has been used to determine the

donor number (basicity or donor ability) of several different solvents. The donor number is defined as the negative molar enthalpy value for the reaction of a donor, D, with the Lewis acid $SbCl_5$ as a reference acceptor in a 10^{-3} M solution of dichloroethane (86):

$$B + SbCl_5 \text{ ----> } B\text{-->}SbCl_5 \quad DN_{SbCl5} \equiv - \Delta H_{D.}SbCl_5 \qquad (1.7)$$

The donor number represents the total amount of interaction with an acceptor molecule including dipole-dipole or dipole-ion contribution and the binding effect caused by the availability of the free electron pair. The acceptor number characterizes the acceptor or electrophilic properties of a solvent. It is deduced from the ^{31}P NMR chemical shift of triethylphosphine oxide in different solvents (87).

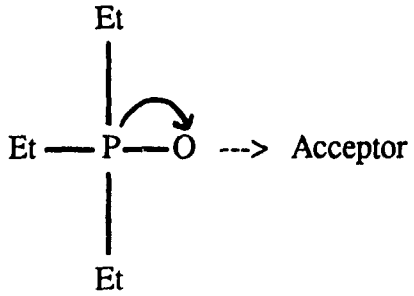

induced bond polarization — coordinate bond

The acceptor number is a dimensionless number which is related to the relative

chemical shift of ^{31}P in Et_3PO in the specific solvent using hexane as one reference and the adduct Et_3PO-$SbCl_5$ in 1,2-dichloroethane as a second reference. Acceptor numbers of 0 and 100 have been assigned, respectively (87,88):

$$AN \equiv \frac{\delta_{corr} \cdot 100}{\delta_{corr}\,(Et_3PO{\cdot}SbCl_5)} = \delta_{corr} \cdot 2.348 \qquad (1.8)$$

where δ_{corr} represents the chemical shift values corrected for the difference in volume susceptibilities between hexane and the respective solvents.

1.5.4. Solvent Polarity (89,90)

Dielectric constants and dipole moments are often used as empirical parameters of solvent polarity. The dielectric constant describes the change in the electric field intensity which occurs between the plates of a condenser when it is removed from a vacuum and placed in a solvent. A permanent asymmetric distribution of the charges in a molecule describes the permanent dipole moment. It is measured by the orientation polarization of the molecule in an applied field. These two parameters do not sufficiently describe the "polarity" of a solvent since other interactions including inductive, directional, specific hydrogen bond, electron pair and acceptor, and solvophobic interactions must be taken into account. The molar transition energy, E_T, from the visible spectrum of pyridinium N-phenol betaines in different solvents give empirical measures of solvent polarity and provides an over-all solvation ability of the solvent (91). These energies have been calculated from the following equation (1.9) (90):

$$E_T[\text{kcal/mole}] = 2.859 \times 10^{-3} \times \tilde{\nu}\ (\text{cm}^{-1}) \qquad (1.9)$$

where $\tilde{\nu}$ represents the frequency of the hypsochromic shift of the longest absorption of the dye pyridiniophenolate from diphenyl ether to water.

Correlations have been observed to exist between E_T values and the energies of the MLCT bands of different complexes which display solvatochromism in different solvents (92-96). This has been observed for $M(CO)_4$(diimine)(M = Cr,Mo,W) (92), cis-$M(CN)_2L_2$(M = Fe,Ru)(93), $(OC)_5W(pyz)W(CO)_5$(94), $M(bpy)X_2$ (M = Pd,Pt;X = Cl,Br,I)(95) and $W(CO)_4L$ (M = Cr,Mo,W), L = 2,2'-bipyridine, 1,10-phenanthroline, 1,4-diazabutadiene (96). For $M(CO)_4$(diimine) complexes, for example, the best least squares fits of E_{MLCT} vs E_T occurs by separately plotting groups of solvents such as chlorinated solvents, alcohols, aliphatic solvents, and aromatic solvents (92). In these complexes, the results indicate that the position of the MLCT absorption depends on the type of solvent and the solvent polarity.

2. EXPERIMENTAL

2.1 Materials

Commercially available materials were used in all synthetic and analytical procedures. A list of the reagents used, their grade and supplier is given in Table 2.1.

Table 2.1. List of Reagents.

Compound	Grade	Supplier
Aluminum Oxide	reagent	J.T. Baker
Benzene	spectrophotometric	Caledon
Butanol	99%+, anhydrous	Aldrich
Carbon Tetrachloride	spectrophotometric	Aldrich
Chloroform	spectrophotometric	Caledon
Dichloromethane	spectrophotometric	Anachemia
Ethanol	99%	Anachemia
1-Hexene	99+%	Aldrich
Methanol	99%+, anhydrous	Aldrich
Octanol	99%+, anhydrous	Aldrich
1,10-phenanthroline	99+%	Aldrich
Piperidine	reagent	Aldrich
Propanol	99%+, anhydrous	Aldrich
Pyridine	reagent	Aldrich
Tetrahydrofuran	reagent	Aldrich
2,2,4-Trimethylpentane	spectrophotometric	Aldrich
$W(CO)_6$	99%	Aldrich

Tetrahydrofuran was dried over potassium metal before use. All other reagents were used without further purification. The aluminum oxide was neutralized by preparing a slurry in .1N NaOH and adjusting the pH to between 6.5 and 7.5 by the addition of .1N HCl. The alumina was drained and placed in a 100°C oven for at least 24 hours. The purity of all synthesized products was established by comparison with published UV-Vis spectra.

2.2 Preparation of the Complexes.

2.2.1. $W(CO)_5$pyridine.

A modification of the method described by Strohmeier (44) was used. 30 ml of tetrahydrofuran (THF) was mixed with .65 g of $W(CO)_6$ in a 100 ml pyrex three-necked round bottom flask. 5 ml of pyridine was added and the solution exposed to fluorescent lab light ($\lambda > 350$ nm) for a period of 72 hours. Stirring was continuous by means of a magnetic stirring bar and stirring unit. Prepurified nitrogen was passed through a THF bubbler before passing through the reaction mixture to minimize evaporation of the solvent and to remove the displaced CO. The reaction was monitored for remaining $W(CO)_6$ by thin-layer chromatography (TLC) on alumina plates. The developing solvent was 2,2,4-trimethylpentane (isooctane). When no further $W(CO)_6$ remained in the reaction mixture, the reaction was stopped. The yellow solution was filtered to separate it from a white residue which coated the sides of the flask and was present in the solution. The residue was washed with THF to remove all traces of the product. The filtrate was evaporated by means of rotary evaporation. The residue was dissolved in benzene and approximately 1-2 g of alumina was added to the solution. The benzene was allowed to evaporate overnight to encourage the product to adsorb onto the alumina. All procedures were carried out with the product exposed to as little light

as possible. The dried alumina containing the product was added to a column of alumina in benzene. The height of the column was adjusted so that the alumina containing the product was at most 1/20th the height of the entire column. Benzene was used to elute the product and ethanol was used to elute the excess pyridine. This procedure was repeated twice to ensure removal of the excess pyridine. The benzene was removed by evaporation and the yellow crystals were recrystallized once from isooctane/benzene (1:1). The yield was greater than 70%.

2.2.2. $W(CO)_5$piperidine

The procedure described for the preparation of $W(CO)_5$pyridine was used for the preparation of $W(CO)_5$piperidine. 30 ml of THF was mixed with .65 g of $W(CO)_6$ and 5 ml of piperidine. Due to a greater light absorption by $W(CO)_5$-piperidine, as compared to $W(CO)_5$pyridine, not all the $W(CO)_6$ reacted. The reaction was stopped when the TLC analysis showed no further change in the concentration of the $W(CO)_6$. The product was adsorbed onto neutral alumina as described previously. This plug of alumina was added to a column of alumina in isooctane. Approximately 500 - 1000 ml of isooctane was needed to elute the unreacted $W(CO)_6$. The eluent was monitored for $W(CO)_6$ by UV spectroscopy. When no further $W(CO)_6$ appeared in the eluent, benzene was used to elute the product and ethanol used to elute the excess piperidine. The latter part of the procedure was repeated twice to ensure removal of the excess piperidine. The yellow crystals were recrystallized once from isooctane/benzene (1:1). The yield was greater than 70%.

2.2.3. Potassium Ferrioxalate ($K_3Fe(C_2O_4)\cdot 3H_2O$)

Potassium ferrioxalate was prepared according to the procedure described by Calvert and Pitts (97). 1 volume of 1.5M $K_2C_2O_4$ solution was mixed with 3 volumes of a 1.5M $FeCl_3$ solution. The green crystals of $K_3Fe(C_2O_4)_3 3H_2O$ were allowed to precipitate out overnight. They were recrystallized 3 times from warm water and dried in a 40°C oven. The yield was 15 g.

2.3. Irradiation Procedures.

Samples were irradiated in a cylindrical fused quartz cell with optically flat windows (Hellma, 1 cm pathlength, 19 mm diameter, volume 2.8 ml). A PRA Model # 3402 medium pressure Xenon arc lamp (150 W), coupled with the appropriate interference filters, was used for photolysis at 313, 365, and 436 ($\pm$ 10) nm. An argon ion laser (Spectra-Physics, 4W) was used for photolysis at 457.9 nm and 488.0 nm. The laser beam was expanded to the diameter of the photolysis cell by passing it through a plano-convex lens. A block diagram of both optical trains is given in Figure 2.1.

All steady-state reactions were monitored by UV-visible absorption spectroscopy using a microprocessor-controlled Hewlett Packard Model #8452A diode array spectrophotometer. The resolution was $\pm$ 2 nm. Photolysis and spectrocopic analysis were carried out using the same cell. Samples in mixed alkane/alkene solvents were degassed by passing solvent saturated prepurified N_2 through the sample for 5-30 minutes. Alcohols were anhydrous and sealed in bottles under N_2. Syringes were used to extract the solvents and to introduce samples into the photolysis cell. No other special precautions were taken. Each sample was irradiated for successive time intervals, and a full spectrum taken after each irradiation. Solutions were hand mixed at several intervals during each

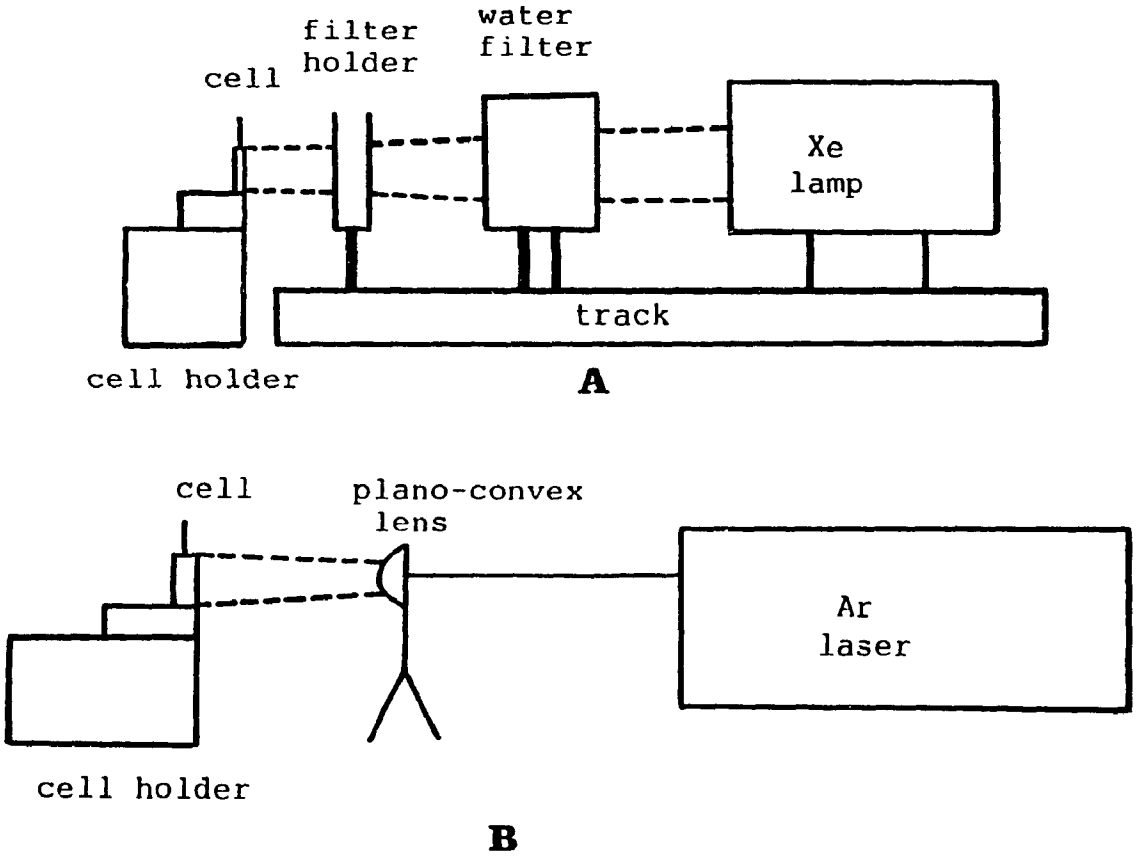

Figure 2.1. Optical trains for (A) 313, 365, and 436 nm irradiations, (B) 457.5 and 488 nm irradiation.

irradiation run and prior to analysis. This was done after blocking the light. Solution concentrations ranged from 1.5×10^{-4} to 1×10^{-3} M. $W(CO)_5$pyridine did not undergo any thermal reactions in the mixed alkane/alkene solvents. A white precipitate appeared in highly concentrated (> 1×10^{-3} M) solutions of $W(CO)_5$piperidine in mixed alkane/alkene solvents after several days. Both compounds undergo thermal substitution reactions in the alcohols within 12 hours. In all cases where thermal reactions occurred, the rates of these reactions were observed to be very slow (< .01%) compared to the photochemical reactions and therefore quantum yields needed no corrections for these products.

2.4. Light Absorption Measurements

The amount of light absorbed by the $W(CO)_5L$ reactants in all steady-state reactions was determined based on the light absorbed by the well-known potassium ferrioxalate chemical actinometer (98).

For irradiations at 313 and 365 nm, the absorptivity of the actinometer for concentrations of $\geq$ .006 M was 100%. The number of photons/second entering the photolysis cell through the 313 or 365 nm filter was easily determined. Solutions of $W(CO)_5$pyridine were made sufficiently concentrated so that the absorptivities over the band width of the filters were greater than 98% for these two wavelengths. Solutions of $W(CO)_5$piperidine in the mixed alkane/alkene solvents were only made sufficiently concentrated to raise the average absorptivity over the filter range to 85% ($\pm$ 6%). This was to ensure that the absorbance at the maximum monitoring wavelength remained < 2. Concentrations of $W(CO)_5$piperidine in the alcohols could be made somewhat higher but were limited due to the increase of absorbances of the product beyond 2 at the monitoring wavelength (λ = 426 nm). The average absorptivity was used to calculate the number of photons absorbed by

these systems. For irradiations at 436 nm, the absorbances of reactant and actinometer were matched as closely as possible by matching the integrated areas over the filter range. This procedure worked best when optically dilute solutions were used to minimize the absorption differences between actinometer and reactant. For irradiations at 457.5 and 488.0 nm, the absorbance of actinometer and reactant were matched to within one percent.

In all cases, the same photolysis cell was used for irradiation of the reactant and actinometer. Both were mixed in the same manner and irradiated for the same time intervals. Changes in the absorptivities of the reactants with increasing irradiation time were taken into account in the calculations. For less than 10% conversion, the absorptivities of either actinometer or $W(CO)_5L$ rarely changed by more than 5%. Several actinometer readings were obtained during each day of experiments and the average value was taken. The average deviations was usually $\pm$ 5%. The average number of photons/sec entering the cell through the 313 and 365 nm filters was 6.5 x 10^{14}/sec and 3.8 x 10^{15}/sec ($\pm$ 5%), respectively. The average power emitted by the laser at 457.5 and 488.0 nm was 10 mW/cm^2 and 100 mW/cm^2, respectively.

2.5. Analysis of Data.

2.5.1. $W(CO)_5L'$ (L' = 1-hexene, alcohol)

For solutions of $W(CO)_5L$ in S/1-hexene (2:1) (S = isooctane, benzene, dichloromethane, chloroform, CCl_4), the decrease of the absorbance of the reactant was monitored as a function of time of irradiation. The wavelength of analysis was chosen to be 382 nm (L = pyridine) or 404 nm (L = piperidine) if concentrations of these reactants were sufficiently low to ensure that the absorbances of these peaks

were less than 2. For solutions with concentrations high enough to increase the absorbances of these peaks to values greater than 2, 412 nm was chosen as the wavelength of analysis. These wavelengths were chosen because absorbance differences between reactant and product were large. In all alkane/alkene solvents, except CCl_4, irradiation of both compounds at wavelengths $\geq$ 436 nm produced no loss of isosbestic points in their absorption spectra up to 100 % conversion. The molar extinction coefficient at the wavelength of analysis of the product was determined by converting the reactant to 100% product using irradiation wavelengths $\geq$ 436 nm. The molar extinction coefficient of the product in CCl_4 was estimated based on its value in other similar solvents. For irradiations of $W(CO)_5L$ in the alcohols, the increase in the product absorbance at 426 nm was monitored. Irradiation of both compounds at 365 nm produced no loss of isosbestic points in their absorption spectra up to 100% conversion. The molar extinction coefficient at the wavelength of analysis of the product was determined by converting the reactant to 100% product using 365 nm as the irradiation wavelength. The molar extinction coefficient of the reactant in all solvents was simply determined at zero irradiation time. The molar extinction coefficients determined for alkane and alcohol solvents were used to correct for reactant or product absorption. For 313, 436, 457.5 and 488.0 nm, data of less than 10% conversion was used for calculation of product formation. For 365 nm, data of less than 15% conversion was used. The amount of product formed was calculated based on these absorbance changes. The calculations used to determine the number of molecules formed are given below.

A. Alkane/alkene solvents (by decrease of reactant)

$$A^t_{react} = A^t_{TOT} - [((A_0 - A^t_{TOT})/(\varepsilon_{react} - \varepsilon_{prod})) \times \varepsilon[_{prod}] \quad (2.1)$$

$$n_{prod} \text{ (at time t)} = (A_0 - A^t_{react})/A_0 \times [W(CO)_5L] \times V \times A \quad (2.2)$$

B. Alcohols (by increase of product)

$$A^t_{prod} = ((A_0 - A^t_{TOT})/(\varepsilon_{react} - \varepsilon_{prod}) \times \varepsilon_{prod}) \quad (2.3)$$

$$n_{prod} \text{ (at time t)} = A^t_{prod}/ A \times [W(CO)_5L] \times V \times A_{100} \quad (2.4)$$

A^t_{TOT} = total absorbance at time t

A_0 = total absorbance at time 0 = reactant only

$\varepsilon_{prod/react}$ = molar extinction coefficient of product or reactant

$A^t_{prod/react}$ = corrected absorbance of product or reactant only

$[W(CO)_5L]$ = initial concentration of reactant (moles/l)

V = volume of cell (2.8 ml)

A = Avogradro's number of 6.023×10^{23} molecules/mole

A_{100} = absorbance of product at 100% conversion

n_{prod} = number of molecules of $W(CO)_5$(1-hexene) or $W(CO)_5$(alcohol)

2.5.2. Fe^{2+}

Exposure of tris(oxalato)ferrate (III) to light between 254 and 514 nm reduces the Fe(3+) to Fe(2+) according to the following reaction:

$$[Fe^{III}(C_2O_4)_3]^{-3} \xrightarrow{h\upsilon} [Fe^{II}(C_2O_4)_2]^{-2} + 2CO_2 \quad (2.5)$$

The number of moles of Fe(2+) produced during the irradiation of potassium ferrioxalate was determined as follows: an aliquot of the actinometer (2.8 ml) was irradiated for a given amount of time. The irradiated volume was transferred and the cell rinsed into a 25 ml volumetric flask containing 6 ml of developer solution (.05% 1,10-phenanthroline/.25 M sodium acetate/.1 N H_2SO_4). The solution was diluted to the mark with doubly deionized water. The absorbance of the red solution was taken at 510 nm. The entire procedure was carried out only in the presence of red safety lights. The [Fe(2+)] was calculated as:

$$n(Fe(2+))/sec = (V_1V_3(6.023 \times 10^{20}))/(V_2\ \varepsilon(Fe(2+)\ t\ l) \qquad (2.6)$$

where n(Fe(2+))/sec = number of molecules of Fe(2+) produced/sec of irradiation

V_1 = volume of aliquot irradiated (2.8 ml)

V_2 = volume of aliquot complexed (2.8 ml)

V_3 = total volume (25 ml)

6.023×10^{20} = Avogadro's number of molecules/mole/ml

ε(Fe(2+) = molar extinction coefficient of Fe(2+)-phenanthroline at 510 nm (1.11×10^4 $lmole^{-1}cm^{-1}$)

t = time (seconds)

l = path length of cell (1 cm)

The number of photons/sec entering the photolysis cell through the 313 and 365 nm filters is given by:

$$I_a = n(Fe(2+))/\Phi_{Fe(2+)}I_f t \qquad (2.7)$$

where I_a = number of photons/sec

$\Phi_{(Fe(2+)}$ = quantum yield for formation of Fe(2+)(1.24 at 313 nm; 1.21 at 365 nm) (97,98)

I_f = fraction of light absorbed at 313 and 365 nm(1.00)

t = time, in seconds

2.5.3. Quantum yield determinations.

The determination of quantum yields for the photosubstitution of $W(CO)_5L$ (L = pyridine, piperidine) was carried out using the following calculations:

A. For 313 and 365 nm:

$$I_{abs}\ (W(CO)_5L) = (I_f(W(CO)_5L) \times I_{abs}\ (\text{actinometer}) \qquad (2.8)$$

I_{abs} = number of photons/sec absorbed

I_f = fraction of light absorbed : (L = pyridine) $\geq$ .98

(L = piperidine) $\geq$ .85

(ferrioxalate) = 1.00

$$\Phi(\text{prod}) = n_{prod}/I_{abs}(W(CO)_5L) \qquad (2.9)$$

B. For 436, 457.5, 488.0 nm:

Since the fraction of light absorbed by both the reactant and actinometer was $\leq$ 25% and matched, quantum yields were determined as follows:

$$\Phi(\text{prod}) = \Phi(Fe(2+) \times n_{prod})/\ n_{Fe(2+)} \qquad (2.10)$$

Φ(prod) = quantum yield for photosubstitution of $W(CO)_5L$

Φ(Fe(2+) = quantum yield for Fe(2+) formation at 436 nm

(1.01) (97,98), 457.9 nm (0.85) and 488.0 nm (0.85)(99)

n_{prod} = number of molecules of product produced for a given time

$n_{Fe(2+)}$ = number of molecules of Fe^{2+} produced for a given time

2.6. Picosecond Flash Photolysis.

All picosecond flash photolysis experiments were conducted in the Canadian Centre for Picosecond Laser Spectroscopy at Concordia University. The system uses a mode-locked Nd/YAG laser (Quantel YG 402G) with a 2.5 mJ, 355 nm, 30 ps pulse for excitation and a 425-675 nm probe pulse for detection. An OMA (Optical Multichannel Analyzer) is used for data collection. A block diagram of the system used is given in Figure 2.2 (100).

The mode-locked Nd/YAG laser has a cavity length of 1.1 m and passive mode-locking is achieved by the use of the dye Q-switch I (Kodak, 9470). A periodic train of ~ 12 picosecond (10^{12} sec) light pulses is emitted by the laser with a fundamental output wavelength of 1064 nm. An appropriate pulse is selected from the pulse train by a PF 302 pulse selector which contains two cross-polarizers and a birefringent crystal of deuterated potassium dihydrogen phosphate (KD*P) driven by an electronic circuit. The pulse is selected in the following manner. The pulse train enters a Glan-air polarizer which removes the minor vertical component of the light. It then enters the KD*P crystal which changes the polarization of one of the pulses. This pulse exits the pulse selector via a second Glan-air cross-polarizer. The selected pulse is first amplified by a Quantel SF 410-07(7 x 115 mm) Nd/YAG rod and again by an SF 410-09 (9.35 x 114 mm) Nd/YAG rod. The amplified pulse passes through a second harmonic generator cell of KD*P which

Figure 2.2. Schematic representation of the picosecond flash photolysis experimental apparatus.

1. Laser: a) head
   b) mode-locking cell
   c) mirror
2. Beam Expander
3. Glan-air Polarizers
4. Pulse Selector
5. Amplifier
6. Second Harmonic Crystal
7. Third Harmonic Crystal
8. Delay Ramp
9. Continuum Cell
10. Energy Detector
11. Energy Meter
12. Sample Cell
13. Double Monochromator
14. Photodiode Array Detector
15. Multichannel Analyzer
16. Computer

DM. Dichroic Mirror

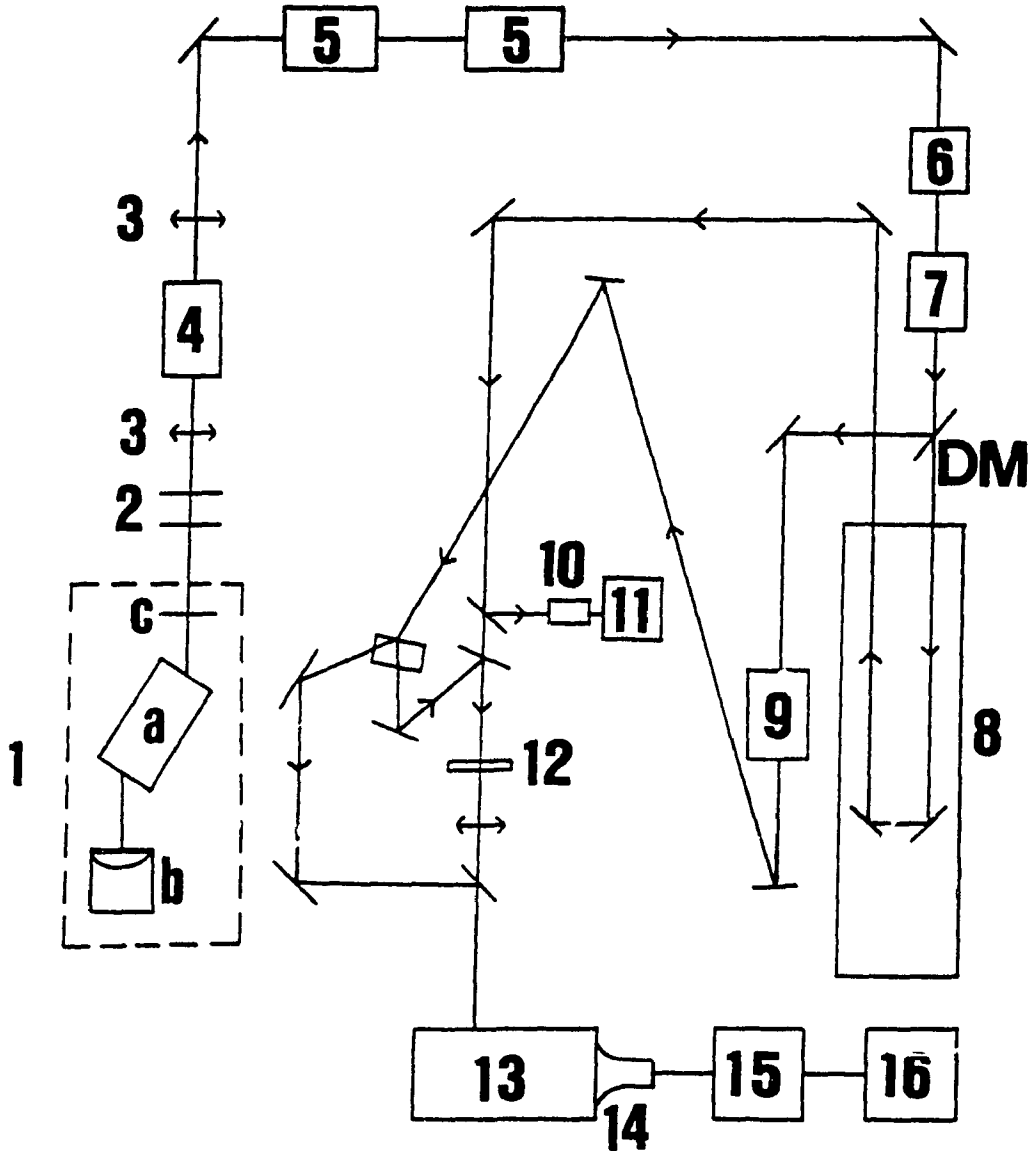
5
5
6
3
7
4
3
DM
2
10
11
c
a
1
9
8
12
b
13
15
16
14

doubles the fundamental frequency of 1064 nm to 532 nm. The energy of the 532 nm pulse is approximately 20% (~ 20 mJ) of the energy of the initial pulse. Combination of the 1064 and 532 nm pulses by a third harmonic generator of KD*P gives a pulse of 355 nm light and 2-3 mJ of power. The different wavelengths are separated by dichroic mirrors. The second or third harmonic pulse which acts as the pump pulse is passed along a delay line which can vary the time of the arrival of the pump pulse compared to the probe pulse from between 0 ps and 10 ns.

The probe pulse is generated by the focusing of the 1064 nm pulse into a solution of dilute phosphoric acid which produces a white light (continuum) due to self-phase modulation extending from approximately 400-700 nm and having the same pulse width as the laser pulse. The probe continuum is split into a reading pulse (I) which enters the sample cell and a reference pulse (I_o) which passes beside the cell. The absorbance of the sample is taken with and without excitation. The absorbance of the sample taken without excitation corresponds to the ground state absorption. The absorbance of the sample taken after excitation corresponds to the excited state absorption. An average of 9-12 excited state absorptions and 3-4 ground state absorptions are taken for each experiment at each time delay.

The detection system consists of a silicon enhanced photodiode array which detects the reading and reference pulses after they have passed through a double monochromator. Two arrays corresponding to I_o and I and consisting of 250 photodiodes, each capable of detecting a different wavelength, are read by a multichannel analyzer. The signals are sent to a microcomputer, stored on a diskette, and used later by a minicomputer (PDP-11) to calculate the absorbance at each wavelength.

A sample shot may be rejected during the experimental stage or later during the

calculation stage. During the experimental stage, a shot may be rejected for the following reasons: 1) there is a double train of pulses created in the oscillator; 2) the pump pulse energy may be too high or too low; 3) saturation of the photodiodes by one of the probe beams may occur; or 4) an unsatisfactory continuum pulse may be generated. During the calculation stage, a shot may be rejected because of an unacceptable level of noise. The absorbance of each shot is calculated by the computer using the formula $a = I_o/I$. The noise is calculated by:

$$N_i = \frac{\Sigma_k(a_{ik} - a_k)^2}{a_k} \qquad (2.11)$$

where N_i is the noise for the curve, $a_{i,k}$ is the absorbance of the shot at wavelength k, and a_k is the average absorbance value at the same wavelength for all the shots on a specific state. An average value for the excited state and ground state absorptions is also calculated by the computer. The noise values calculated in these experiments were generally between 1 and 7. Any shot whose noise value was above 7 generally was rejected. The absorbance change for every wavelength is calculated by the computer by subtracting the ground state absorbance from the excited state absorbance. The absorbance change (ΔA) vs wavelength (425 - 675 nm) is reported for the picosecond experiments. All spectra were normalized with respect to energy.

Sources of error must be taken into account when interpreting the spectra. Noise ratios at 425-440 nm and 635-675 nm can be a major source of error. This problem arises because the number of counts in these regions are low due to the bell shape of the continuum curve. In our experiments, the peaks or tails of the peaks for the transients formed in the alkane or alcohol solvents fall within the 425

- 460 nm region and it is necessary to be cautious when interpreting qualitative or quantitative information in this region. In particular, it is difficult to determine if the shape of the spectra represents a true peak at approximately 440 nm or the tail of the peak which is farther to the blue. Since noise is not considered to be a significant problem at 475 nm, the transient peak observed can be considered to be a true peak. The second source of error involves the appearance of a "DC shift" at time delays of 10 ns. This "DC shift" appears as a significant absorbance (~ .1 absorbance unit) at all the wavelengths. This shift is believed to be due to scattering of the probe beam by ultrasonic waves as the beam passes through the cell. In our systems, this DC shift may be caused by the formation of a precipitate. The DC shift is not always evident in the spectra of $W(CO)_6$ at 10 ns. Similar shifts are visible in the spectra of both $W(CO)_5$pip and $W(CO)_5$pyr at these time delays.

Molar extinction coefficients at 450 and 475 nm for the transients at 50 ps were calculated using the ΔA values and the quantum yield for photosubstitution determined for each complex under 365 nm steady state irradiation. Quantum yields for steady state irradiation of these complexes in isooctane/1-hexene and 1-hexene were used to determine molar extinction coefficients of $W(CO)_5L$ (L = pyr, pip) in cyclohexane and 1-hexene, respectively. The quantum yield used for photosubstitution of $W(CO)_6$ by a suitable ligand was taken from reported literature values (42). The extinction coefficients were calculated in the following manner:

1. $\Delta A(t) = A_{ex}(t) - A_{gr}(t)$ (2.12)

$$A_{ex}(t) = \Delta A(t) + A_{gr}(t) = A_{trans}(t) \quad (2.13)$$

$$A_{gr}(t) = [conc]_{grd} \times \varepsilon_{grd} \times b \quad (2.14)$$

where $A_{ex}(t)$ = absorbance of the transient at time t

$[conc]_{grd}$ = concentration of unreacted species = $[conc]_0$ - $[conc]_{trans}$

ε_{grd} = molar extinction coefficient of reactant determined from UV-Vis spectroscopy

b = pathlength of cell (.2 cm)

$\Phi(365)$ = the quantum yield for photosubstitution in the specific solvent under 365 nm irradiation

2. $$\varepsilon_{trans} = A_{trans}/((b)[conc]_{trans}) \quad (2.15)$$

where ε_{trans} = the molar extinction coefficient of the transient

b = the path length of the cell = 2 mm

$[conc]_{trans}$ = concentration of the transient at time t

3. $[conc]_{trans}$:

a) volume of solution irradiated:

$$\pi r^2 x l = 3.5 \times 10^{-3} \text{ ml} \quad (2.16)$$

where r = laser beam radius = .075 cm

l = path length of cell = .2 cm

b) # of photons per pulse:

$$E_1/E_2 \qquad (2.17)$$

where E_1 = energy of laser per pulse in joules

E_2 = energy of one photon at 355 nm = hc/λ

c) $[conc]_{trans}$ depends on the total number of molecules in the volume irradiated. The number of molecules irradiated depends on the number of photons absorbed.

If the number of molecules in the volume irradiated < the number of photons absorbed then:

$$[conc]_{trans} = \Phi(365 \text{ nm}) \times [conc]_0. \qquad (2.18)$$

If the number of molecules in the volume irradiated > the number of photons absorbed then the number of molecules reacted = the number of photons absorbed x Φ(365 nm) and :

$$[conc]_{trans} = \frac{\text{number of molecules reacted}}{6.023 \times 10^{23} \text{ molecules/mole} \times 3.5 \times 10^{-6} \text{ l}} \qquad (2.19)$$

2.7. X-Ray Crystallography for $W(CO)_5$piperidine.

The X-ray crystal structure determination was performed on a crystal which was .2 x .5 x .1 mm. The crystals of $W(CO)_5$piperidine were grown by slow evaporation (2 weeks) in benzene/isooctane (1:1 v/v). The diffractometer used was a Picker Facs-I which collected 1865 independent reflections on a room-temperature crystal. The tungsten atom and the piperidine molecule are located on general sites. The crystallographic independent unit consists of 1 molecule. The pertinent crystal data are given in Appendix B. Lorentz polarization and general absorption corrections were applied. The structure was solved via the heavy atom method on Fourier maps and difference Fourier maps. Hydrogen atom positions were not calculated. Anisotropic and isotropic thermal parameters were used for all nonhydrogen atoms. All atomic scattering factors and anomalous dispersion corrections were from the International Table for X-ray Crystallography. All calculations were performed on a Concordia departmental PDP8A computer. The R factor converged to .0278.

2.8. Electronic Spectral Band Deconvolution

The electronic spectra of $W(CO)_5L$ (L = pyr, pip) in all solvents used in this study were deconvoluted using a Gaussian band least squares minimization routine (101) employing a Marquardt algorithm (102). The program allows the band positions to be fixed and the best Gaussian fits for the MLCT, ^1A and ^1E bands were determined when the positions of the ^3E band maxima were initially fixed. The fixed position of the ^3E bands depended on the solvent.

3.RESULTS

3.1. Electronic spectra.

The UV-Vis absorption spectra of $W(CO)_6$, $W(CO)_5$pyridine and $W(CO)_5$-piperidine in alkane solvents display characteristics which have been well documented (12,13,49,103,104). For $W(CO)_6$ in cyclohexane (Figure 3.1), the lowest energy absorption band at ~ 28,570 cm^{-1} (350 nm) is assigned as the spin-forbidden $^1A_{1g}$ --> $^3T_{1g}$ transition (103,104). The first LF singlet transition, $^1A_{1g}$ ---> $^1T_{1g}$, predicted by the Tanabe-Sugano diagram of a d^6 complex in an octahedral field (Figure 3.2), is observed at 32,258 cm^{-1} (310 nm) as a shoulder on the more intense M ---> π^* CO charge-transfer absorption at 34,485 cm^{-1} (290 nm). A higher energy absorption band observed as a shoulder at 37,037 cm^{-1} (270 nm) is assigned as the second LF $^1A_{1g}$ ---> $^1T_{2g}$ transition. The highest absorption observed at ~ 43,000 cm^{-1} (233 nm) is assigned as the second component of the M ---> π^* CO charge-transfer transition.

Substitution of a CO in $W(CO)_6$ by a pyridine or piperidine molecule reduces the symmetry of the complex from octahedral to C_{4v}. Reduction of the symmetry results in a splitting of the T_{1g} and T_{2g} states as seen in Figure 3.3. The electronic spectra of $W(CO)_5$pyridine and $W(CO)_5$piperidine exhibit similar features in alkane solvents (Figures 3.4a and 3.4b). In isooctane, each compound exhibits a low energy band, near 22,625 cm^{-1} (442 nm) which has been previously assigned as a LF $^1A_1$ ---> ^3E transition and which appears as a shoulder on the more intense LF ^1A ---> ^1E transition centred near 26,180 cm^{-1} (382 nm) for pyridine and 24,350 cm^{-1} (404 nm) for piperidine (12,13,49). Higher energy transitions have not been definitively assigned. The asymmetry of the band observed for piperidine at ~ 26,180 cm^{-1} (382 nm) has been attributed to a possible contribution from the spin-forbidden $^1A_1$ ---> $^3A_2$ transition (105). Transitions in the piperidine complex at 31,045 cm^{-1} (322 nm) and 34,485 cm^{-1} (290 nm) have been attributed to two

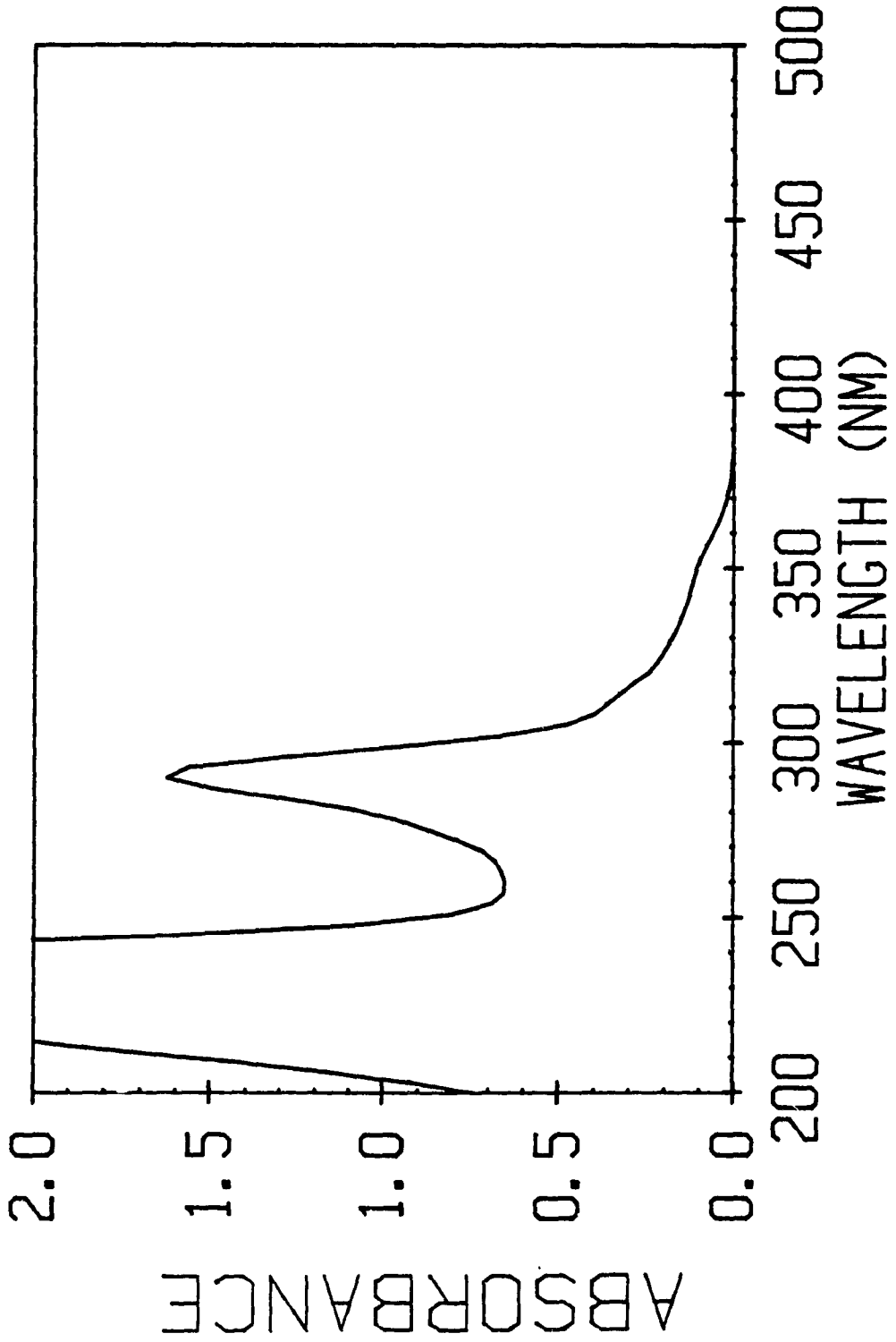

Figure 3.1. Electronic spectrum of W(CO)6 in cyclohexane. The concentration is 1 x 10^{-4} M.

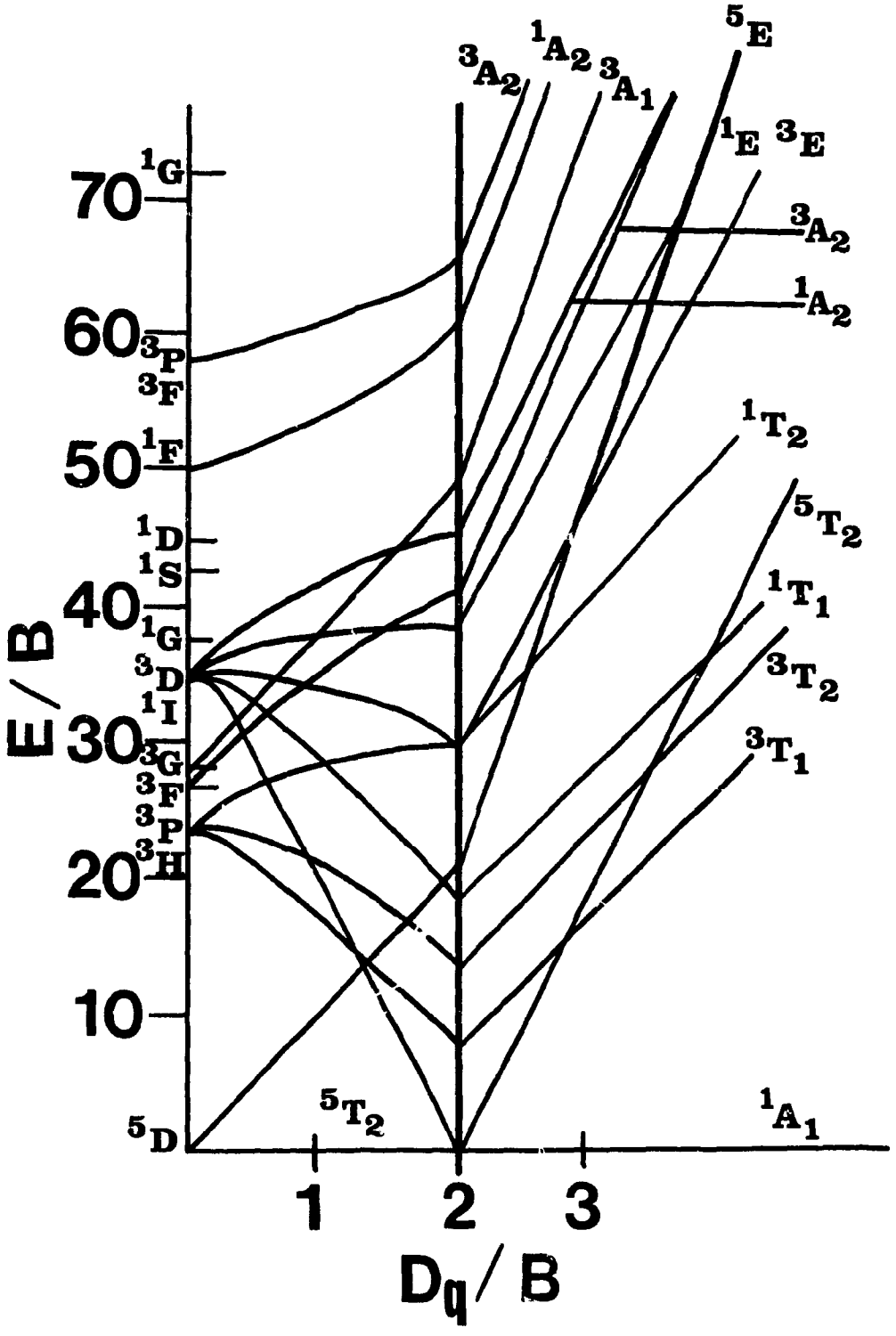

Figure 3.2. Tanabe-Sugano diagram of a d^6 complex in an octahedral (O_h) field.

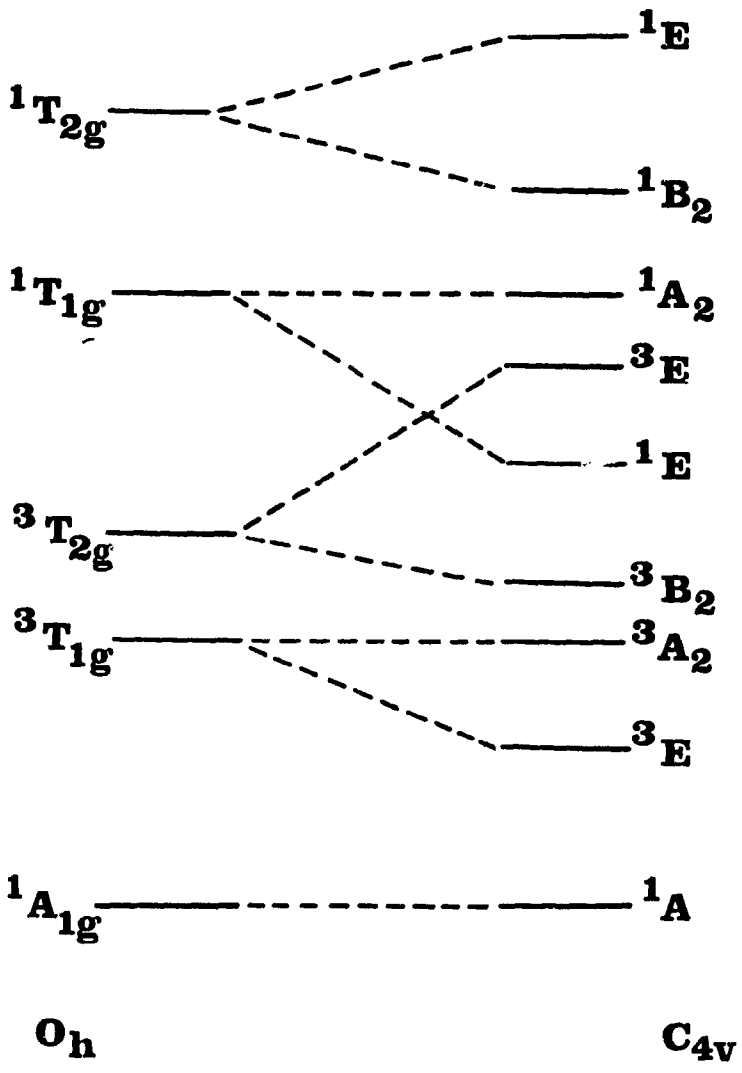

Figure 3.3. Energy level diagram showing correlation between ligand field states in octahedral (O_h) and C_{4V} symmetries

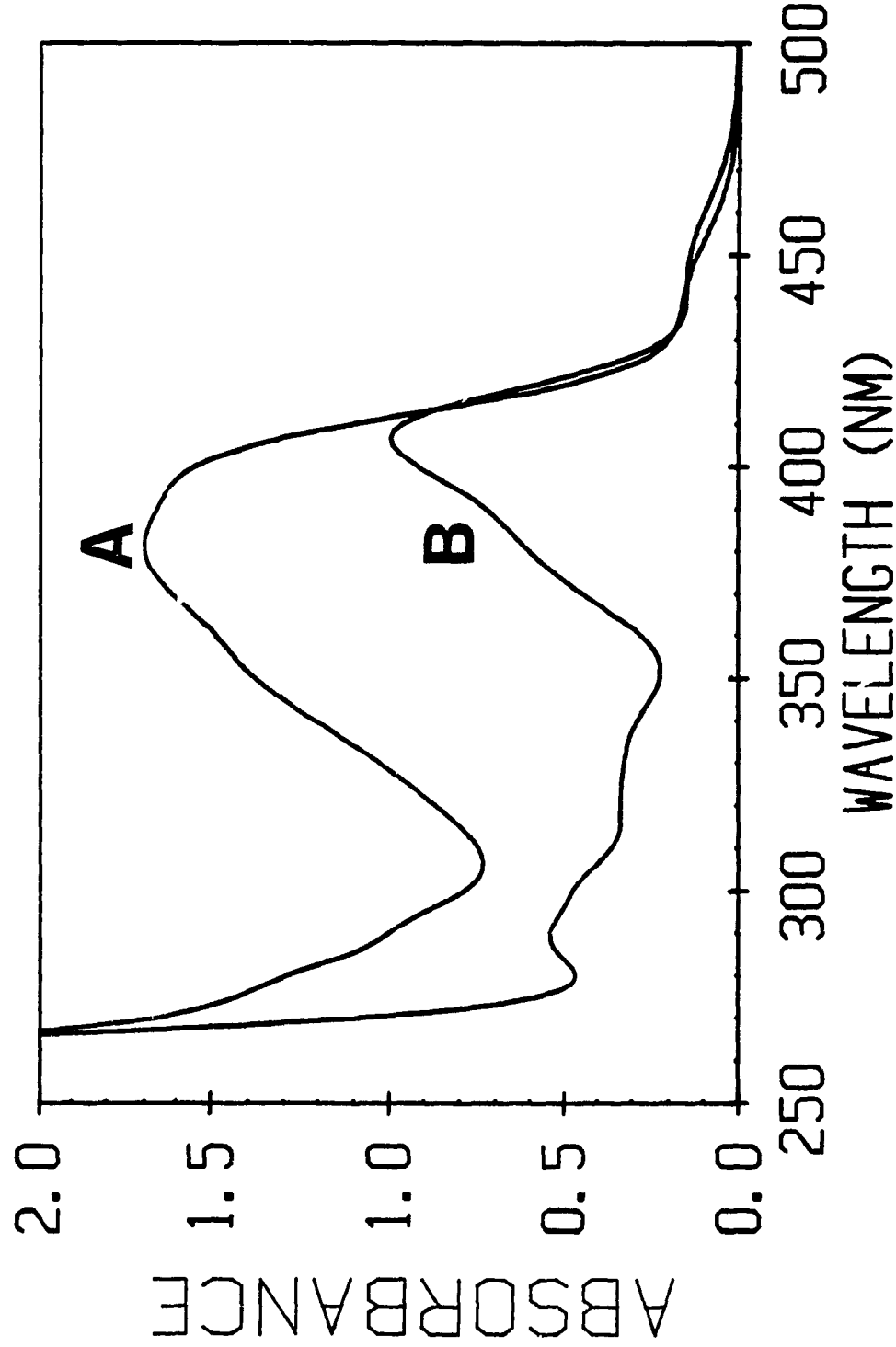

Figure 3.4. Electronic spectra of (A) $W(CO)_5$pyridine in isooctane, and (B) $W(CO)_5$piperidine in isooctane. The concentration is 2.8×10^{-4} M.

components of the orbitally forbidden, spin-allowed $^1A_1$ ---> $^1A_2$ transition (105). These transitions are not observed in the pyridine complex. The intense absorption at ~ 37,040 cm^{-1} (270 nm) observed for both complexes, by analogy to the MLCT assignment for $W(CO)_6$ (103,104), is probably the W ---> π^* CO CT transition.

The electronic spectra of $W(CO)_5$pyridine and $W(CO)_5$piperidine can be altered depending on the solvents. In solvents, which are essentially non-polar, such as isooctane/1-hexene (2:1 v/v), CCl_4/1-hexene (2:1 v/v) or 1-hexene, a decrease in the molar extinction coefficients of all transitions is observed compared to neat alkane solvents. For $W(CO)_5$pyridine in polar solvents, such as the n-alcohols, the asymmetry of the band observed near 28,570 cm^{-1} (350 nm) in non-polar solvents splits to reveal an apparent absorption band which blue shifts and is resolved from the LF singlet-singlet band in these more polar media (Figures 3.5 and 3.6). This is also observed for benzene/1-hexene and dichloromethane/1-hexene (2:1) solutions (Figure 3.6). This behavior is not observed for the piperidine complex in the polar solvents and since pyridine has available π^*-orbitals whereas piperidine does not, this band may be assigned as a W ---> pyridine CT transition (14). Resolution of the CT and LF bands in the pyridine complex further reveals another transition at ~ 370 nm indicated by the asymmetry of the LF band. The degree to which the MLCT band in the pyridine shifts to higher energy in more polar solvents exhibits some correlation to the polarity of the solvent. A correlation (r = .91) is observed between the energies of the MLCT band and Reichardt's E_T polarity scale (90) (Figure 3.7). The MLCT energies plotted are those observed for this complex in alkane, mixed alkane/1-hexene and pure alcohol solvents. For the purposes of this correlation, isooctane and 1-hexene, for which no E_T values have been reported, are assumed to have a polarities equal to that of hexane. The E_T values are those of the pure solvent. The best correlations arise when these values are plotted in

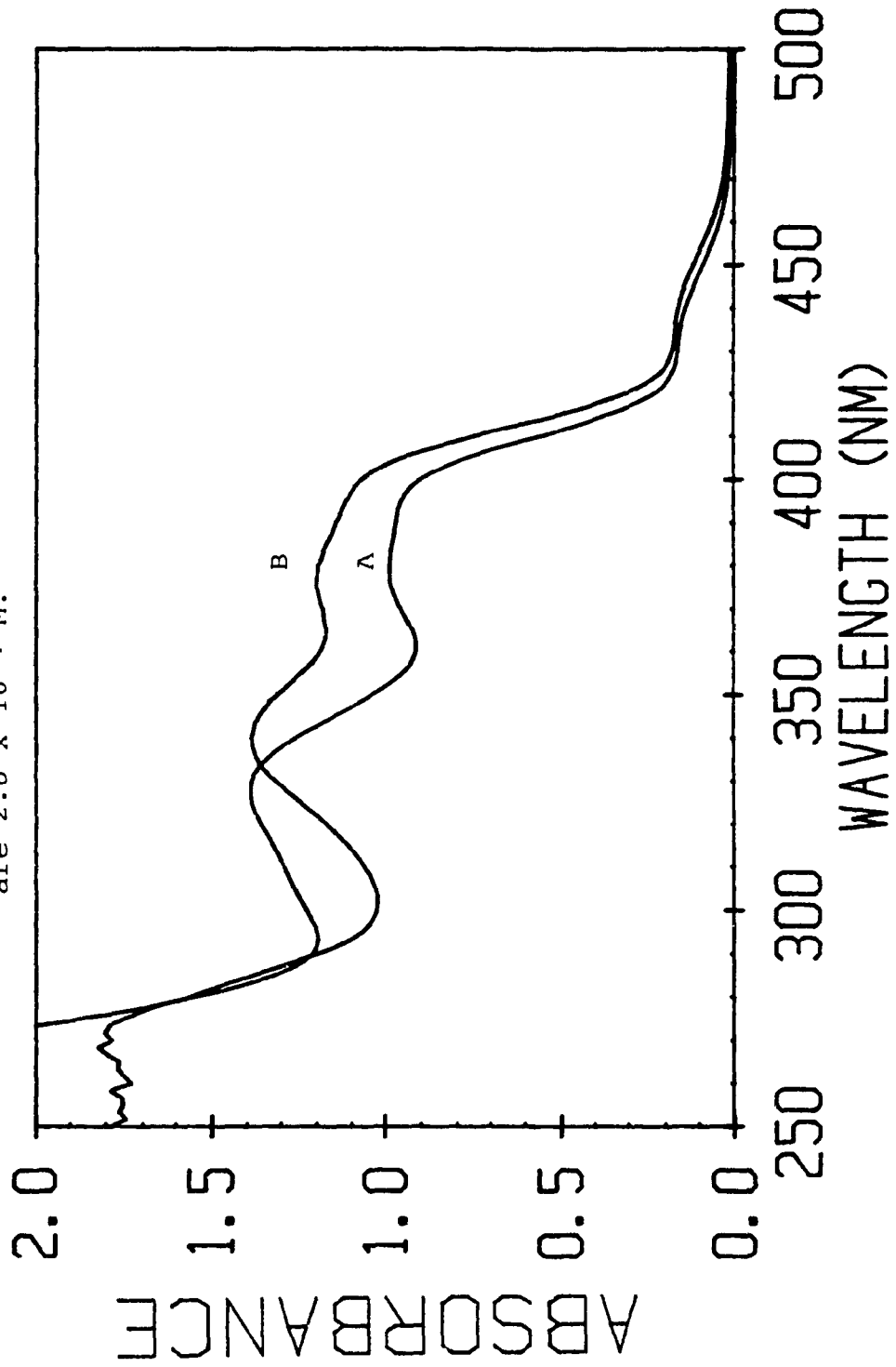

Figure 3.5. Electronic spectra of $W(CO)_5$pyridine in (A) methanol, and (B) octanol. Concentrations are 2.8×10^{-4} M.

Figure 3.6. Electronic spectra of $W(CO)_5$pyridine in (A) isooctane/1-hexene, (B) Benzene/1-hexene and (C) dichloromethane/1-hexene. Concentrations are 2.8×10^{-4} M.

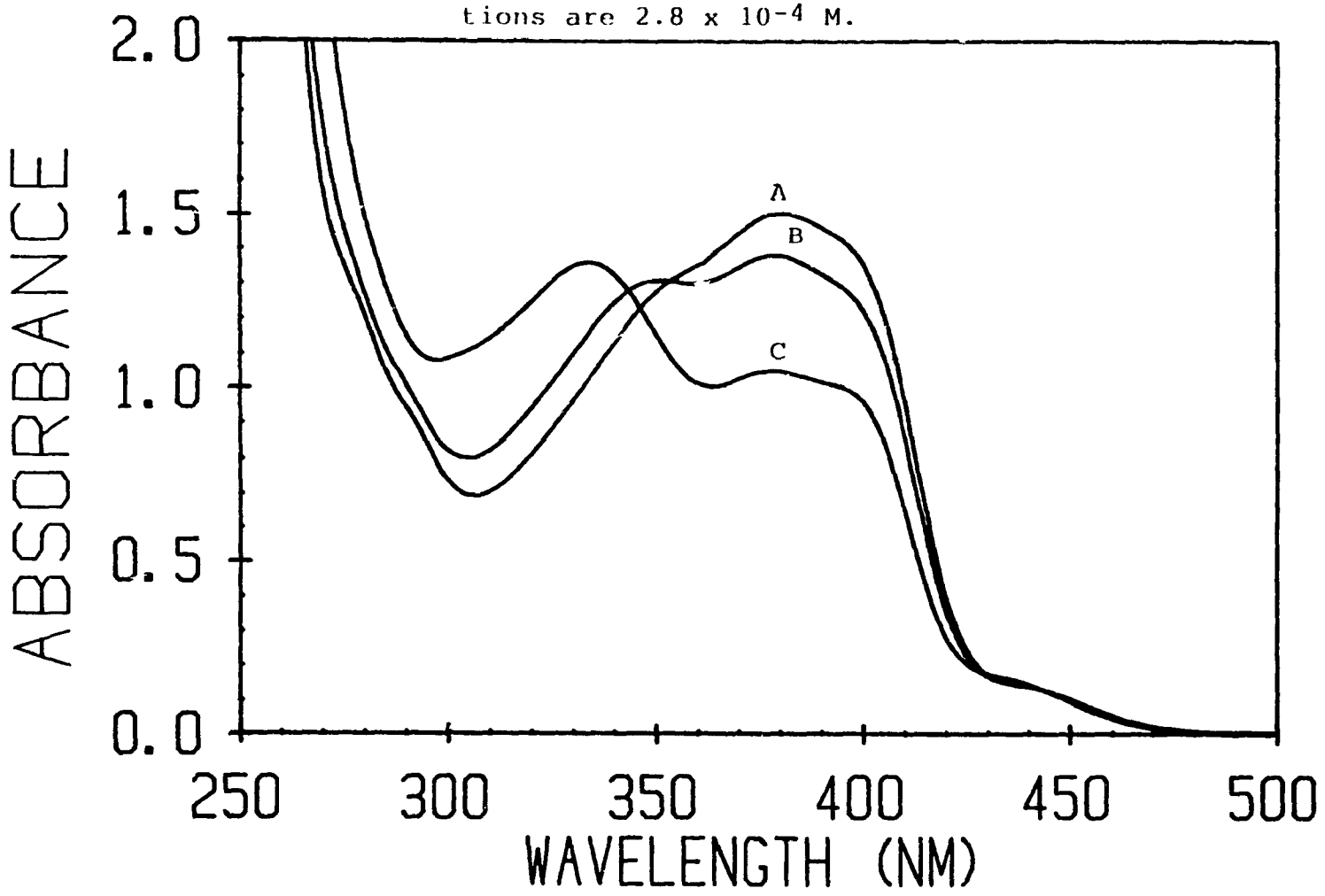

Figure 3.7. Correlations between Reichardt's polarity scale and the energies of the MLCT transitions for $W(CO)_5$pyridine in several solvents.

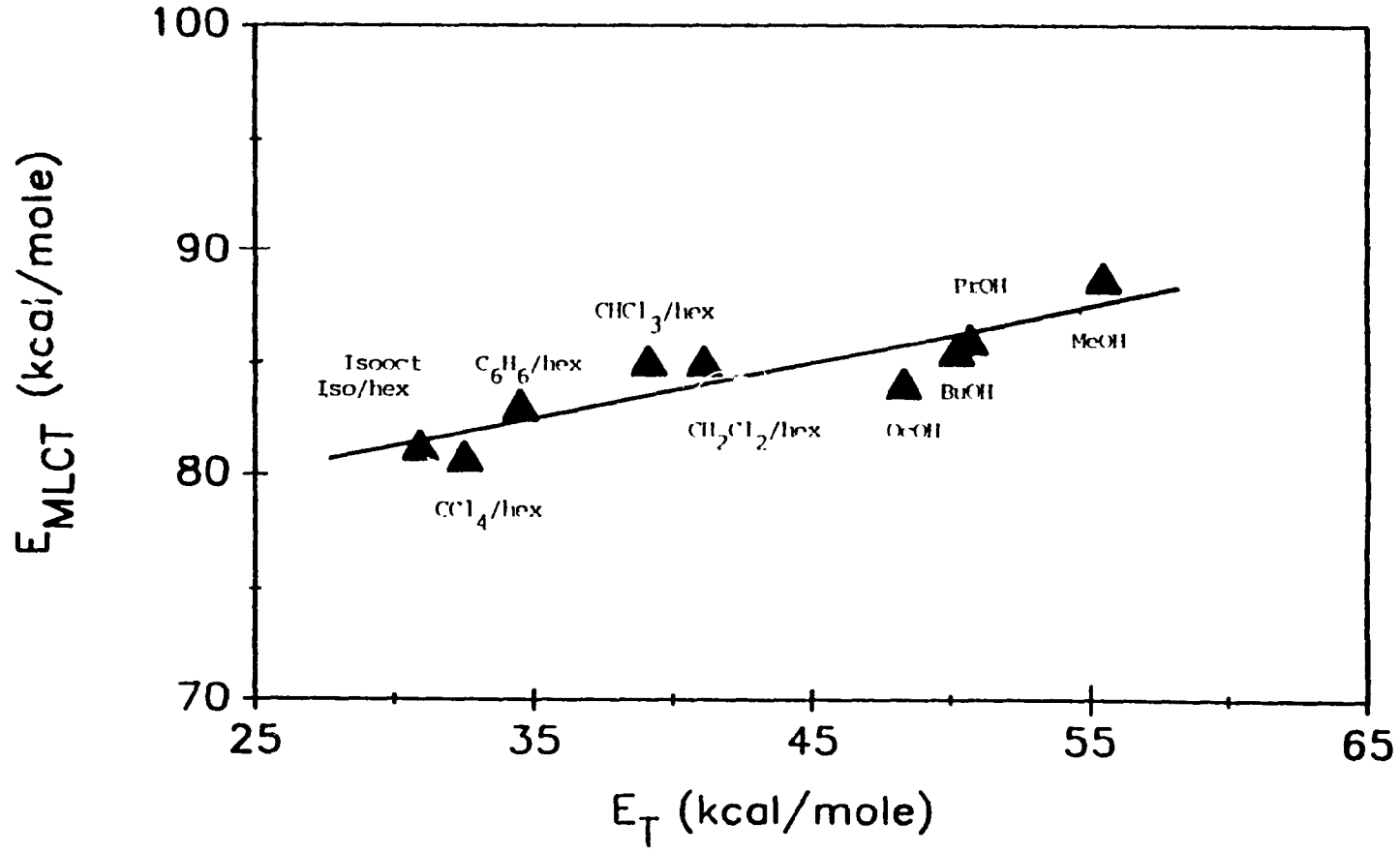

groups of solvents (Figure 3.8). The significance of these correlations must be viewed with some reservations since they are based on a small number of values. The molar extinction coefficients for peak absorbances of both complexes in different solvents are given in Table 3.1 and 3.2.

3.2. Wavelength dependent behavior

Irradiation of $W(CO)_5L$ (L = pyridine, piperidine) in isooctane/1-hexene (2:1 v/v) leads to efficient replacement of L by 1-hexene at all wavelengths studied. The electronic spectra of the product is identical to that reported for $W(CO)_5$(1-pentene)(48) which supports the conclusion that $W(CO)_5$(1-hexene) is the product. No secondary photolysis is observed to occur under $\geq$ 436 nm irradiation of either complex. At these wavelengths, $W(CO)_5$(1-hexene) is the sole product. This is indicated by the observation of a clean isosbestic point at ~ 320 nm for $W(CO)_5$-(pyridine) and 360 nm for $W(CO)_5$(piperidine) from zero to 100% conversion (Figures 3.9 and 3.10). Irradiation of both compounds at 365 nm leads to the appearance of a white precipitate after 85% conversion (Figures 3.11 and 3.12) with subsequent loss of the isosbestic point. Spectral changes upon early irradiation of $W(CO)_5$(pyridine) at 313 nm are identical to those observed upon $\geq$ 365 nm irradiation. Precipitation and loss of the isosbestic point are observed after about 30% irradiation. The precipitate causes light scattering and leads to the loss of isosbesticity. When the precipitate is removed from the solution, the isosbestic point is regained. The precipitate is formed in both aerated and deaerated solutions. The precipitate is believed to be a polymeric species of 1-hexene catalyzed by the tungsten complex. A possible mechanism will be presented later. Irradiation of $W(CO)_5$piperidine at 313 nm reveals the prompt formation of a product whose spectrum differs in the 430-500 nm region compared to that of $W(CO)_5$(1-hexene).

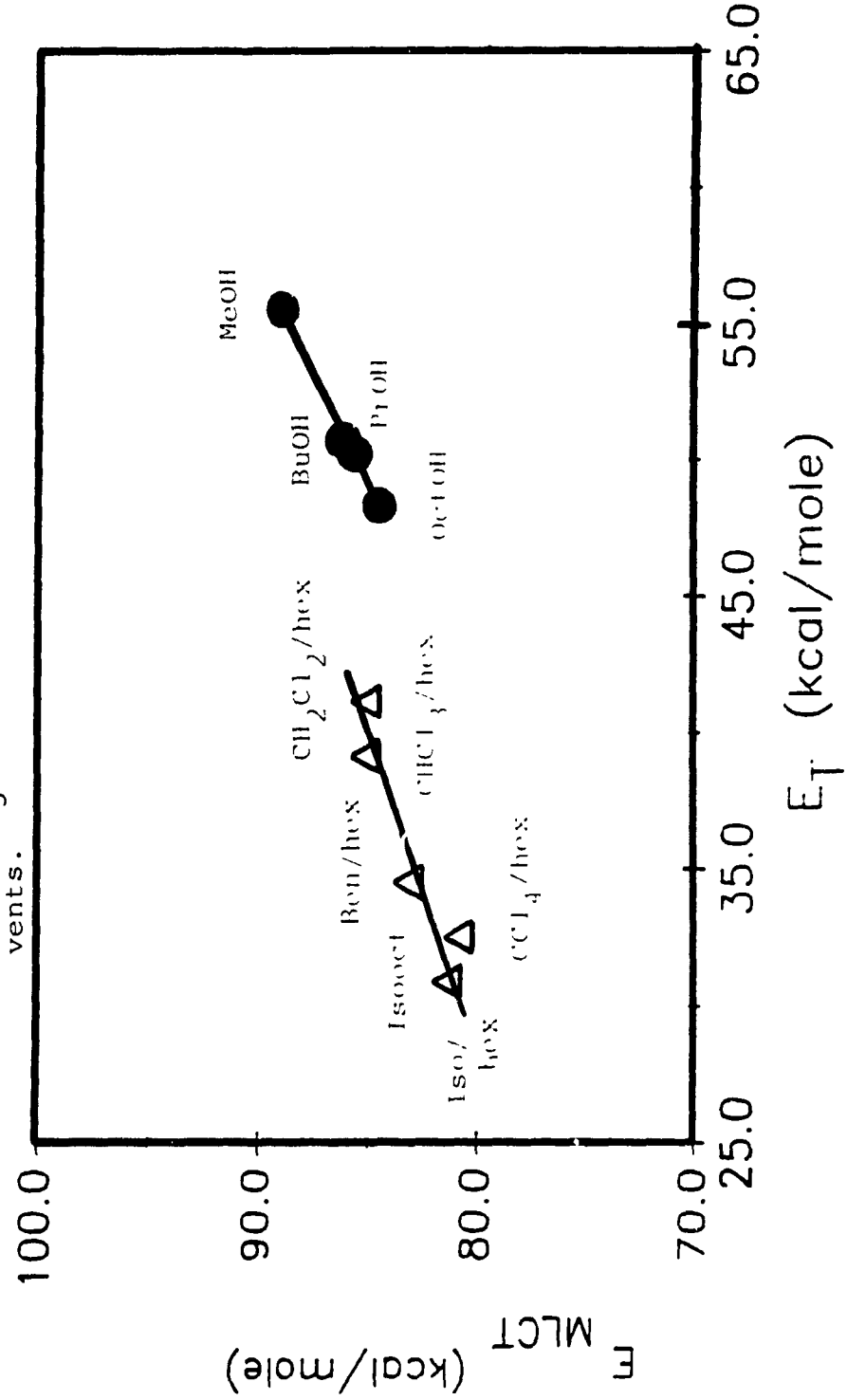

Figure 3.8. Correlations between Reichardt's polarity scale and the energies of the MLCT transitions of $W(CO)_5$pyridine in different groups of solvents.

Table 3.1. Molar Extinction Coefficients of $W(CO)_5$pyridine ($l\ mole^{-1}\ cm^{-1}$)[a]

Solvent	Wavelength (± 2 nm)				
	344	382	412[b]	426[c]	442
Isooctane	5150	7000			660
1-hexene	5145	5860			570
Isooctane/1-hex (2:1)	5250	6630	3575		580
Benzene/1-hex (2:1)	6010	5490	2835		605
Dichloromethane/1-hex (2:1)	7200	5995	2360		565
Chloroform/1-hex (2:1)	5960	5490			640
Carbon tet/1-hex (2:1)	4275	5320			552
Methanol	4040	3435		640	420
n-Propanol	5080	4150		740	550
n-Butanol	5170	4255		820	550
n-Octanol	5295	4620		840	620

a) extinction coefficients are ± 10%
b,c) these extinction coefficients represent wavelengths of analysis rather than absorption peaks

Table 3.2. Molar Extinction Coefficients of $W(CO)_5$piperidine ($l\ mole^{-1}\ cm^{-1}$)[a]

Solvent	Wavelength[a] (± 2 nm)			
	404	412[b]	426[c]	442
Isooctane	3900			560
1-hexene	3725			574
Isooctane/1-hex (2:1)	3630	3180		550
Benzene/1-hex (2:1)	3510	2950		570
Dichloromethane/1-hex (2:1)	3300	2670		580
Chloroform/1-hex (2:1)	3750			575
Carbon Tet/1-hex (2:1)	3820			585
Methanol	2930		605	460
n-Propanol	3220		670	505
n-Butanol	3285		670	510
n-Octanol	3395		720	535

a) extinction coefficients are ± 10%
b,c) these extinction coefficients represent wavelengths of analysis rather than absorption peaks

Figure 3.9. Electronic spectral changes for $W(CO)_5$pyr in isooctane/ 1-hexene (2:1 v/v) under 457.5 nm irradiation. The times of irradiation from reactant A to product B are: 0, 10, 20, 30, 40, 60, 105, 150, 240 seconds.

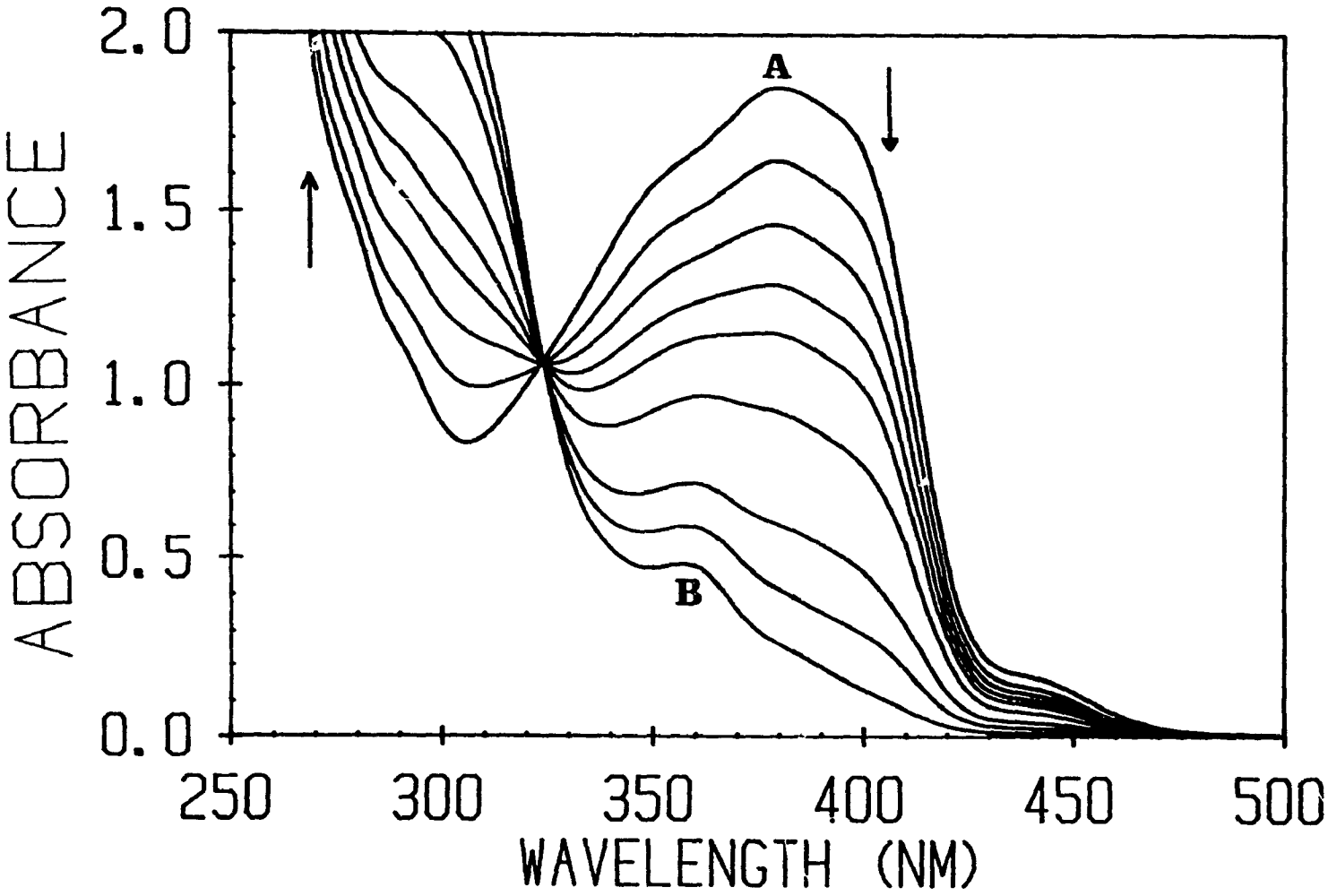

Figure 3.10. Electronic spectral changes for $W(CO)_5$pip in isooctane/ 1-hexene (2:1 v/v) under 436 nm irradiation. The times of irradiation from reactant A to product B are: 0, 30, 60, 90, 120, 180, 300, 600 seconds.

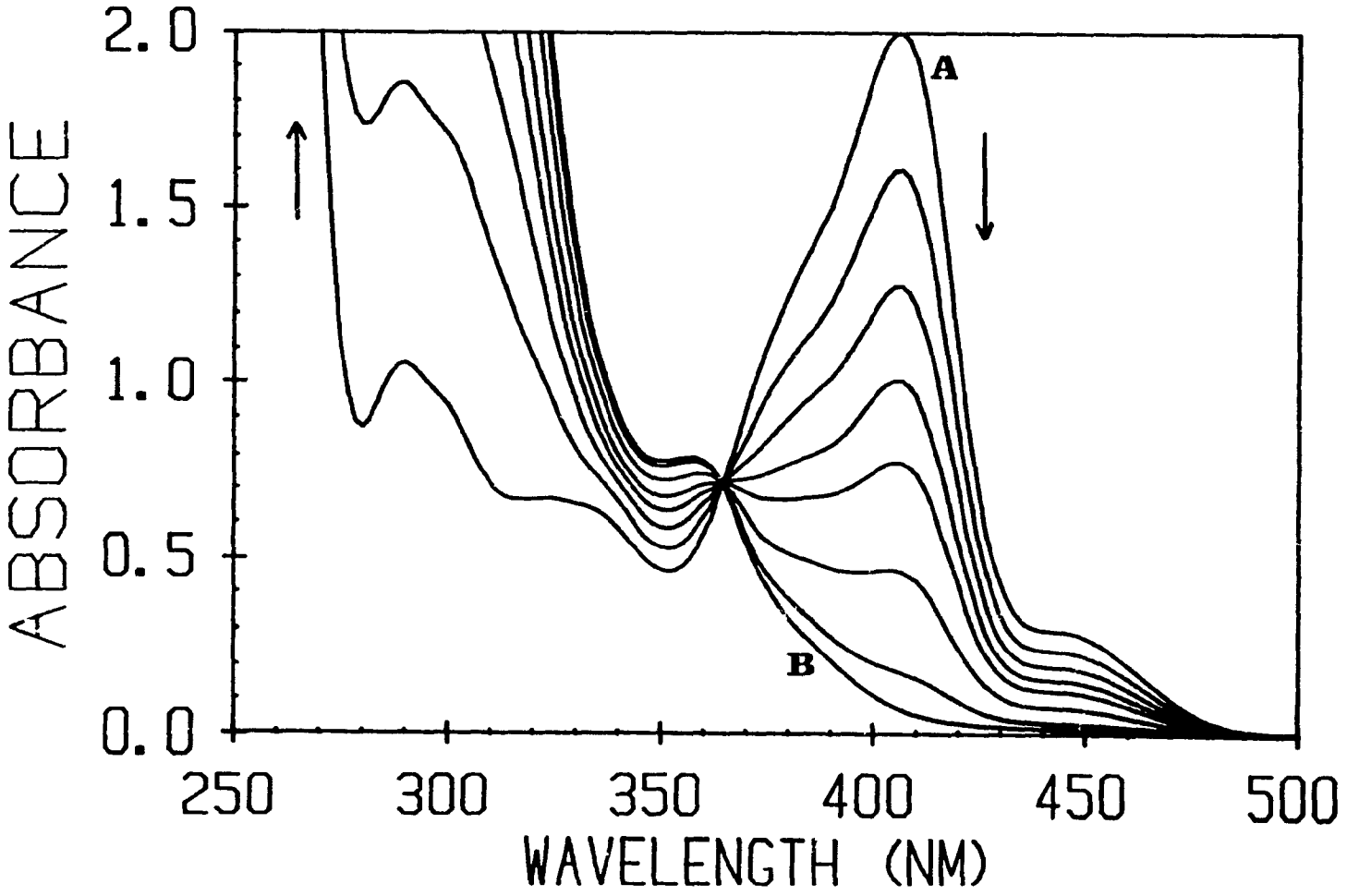

Figure 3.11. Electronic spectral changes for $W(CO)_5$pyr in isooctane/ 1-hexene under 365 nm irradiation. Times of irradiation from reactant A to product B are: 0, 15, 30, 45, 60, 90, 120, 210 seconds.

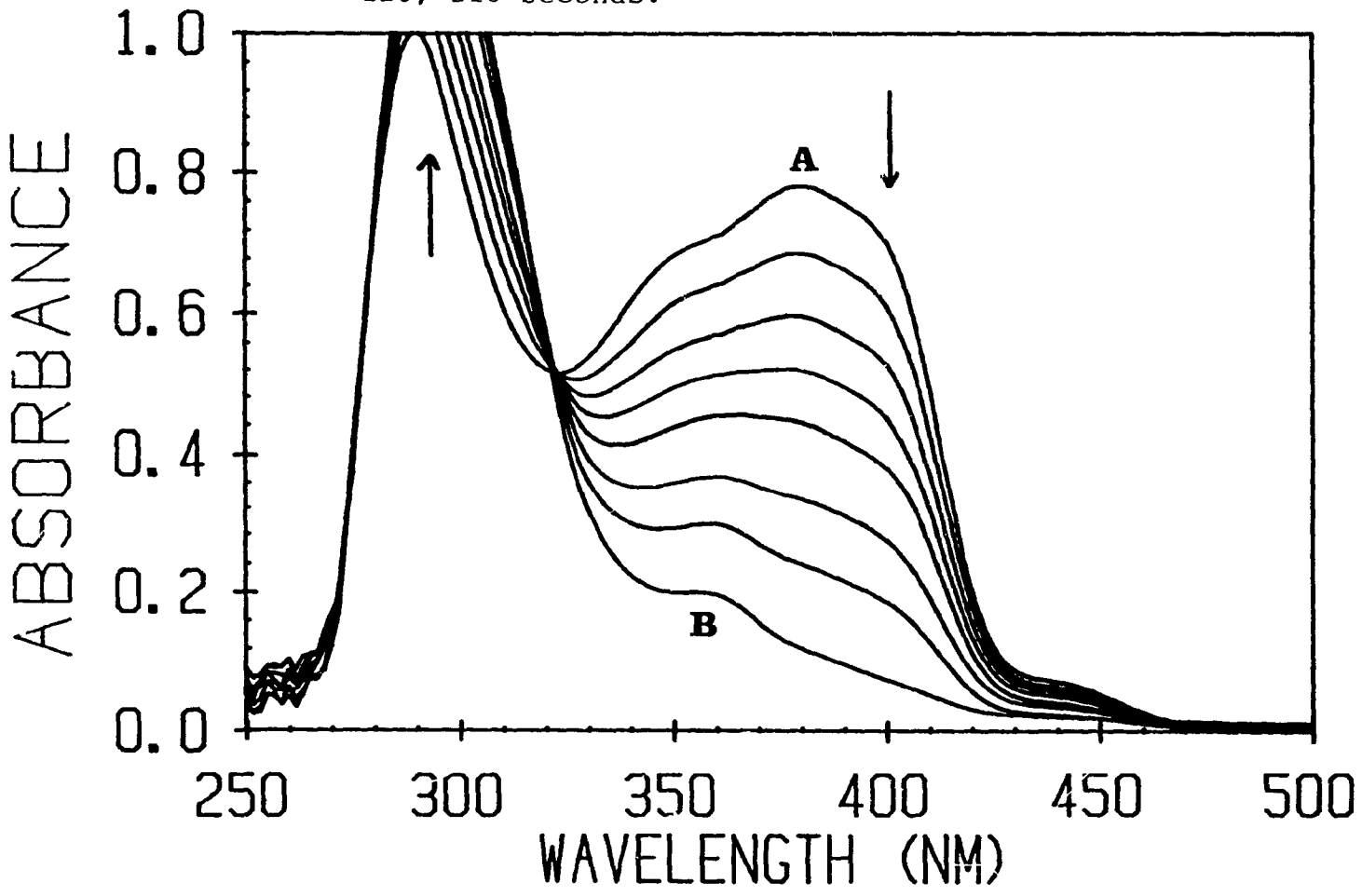

Figure 3.12. Electronic spectral changes for $W(CO)_5$pip in isooctane/ 1-hexene (2:1 v/v) under 365 nm irradiation. The times of irradiation from reactant A to product B are 0,30, 60, 120, 240, 360, 480 seconds.

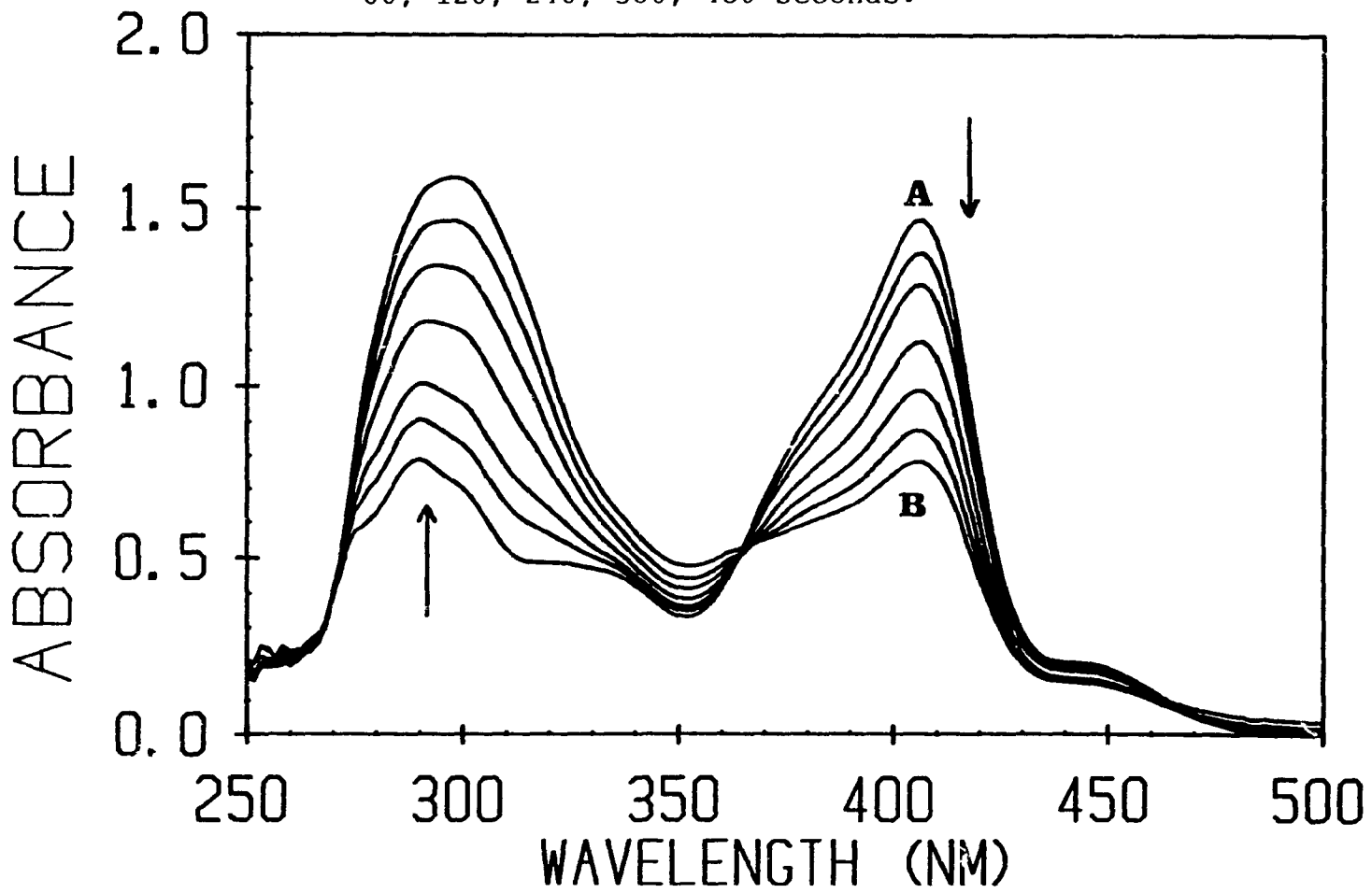

(Figure 3.13). A white precipitate appears at later conversion. Observation of the changes in the spectra for both complexes under $\geq$ 365 nm irradiation reveals that the peaks at 382 nm (pyridine), 404 nm (piperidine) and 442 nm (both) decrease while there is a corresponding increase of the peak at 300 nm. 313 nm irradiation of $W(CO)_5$(piperidine) reveals that while similar changes occur for the peaks at 404 and 400 nm as that observed under > 365 nm irradiation, the peak at 442 nm displays opposite behavior. The clean isosbestic points at 360 nm and 430 nm suggests that only one product is being formed in the early stages of photolysis. It is expected that secondary photolysis of $W(CO)_5$(1-hexene) would take place under 313 nm irradiation since the product absorbs at this wavelength. Low yields of disubstituted products have been reported for similar complexes at this wavelength. Disubstituted products are colored and would not be expected to precipitate from solution. Increased absorbance of the product at longer wavelengths would suggest formation of a disubstituted product at early stages for $W(CO)_5$piperidine.

Overall quantum yields for the photosubstitution of both compounds are given in Table 3.3. Quantum yields for degassed and air-equilibrated samples are compared. As can be observed, there is no significant difference between quantum yields for samples in the presence or absence of oxygen and this indicates that substitution reactions are too fast for oxygen to play a significant role. For both complexes, there is an increase in the quantum yields with a decrease in excitation energy in the LF singlet region (365 - 436 nm) and a significant decrease upon excitation in the LF triplet region (457.5 nm). Quantum yields decrease further for $W(CO)_5$(pyridine) and slightly for $W(CO)_5$(piperidine) at 488.0 nm. The overall yields for $W(CO)_5$(pyridine) in the LF singlet region are slightly higher than those observed for $W(CO)_5$(piperidine). The yields are similar for both compounds at 457.5 nm and reversed at 488.0 nm. At 488 nm, the yields for $W(CO)_5$(piperidine)

Figure 3.13. Electronic spectral changes for $W(CO)_5$pip in isooctane/ 1-hexene (2:1 v/v) under 313 nm irradiation. The times for irradiation from reactant A to product B are: 0, 1200, 2700, 5300, seconds

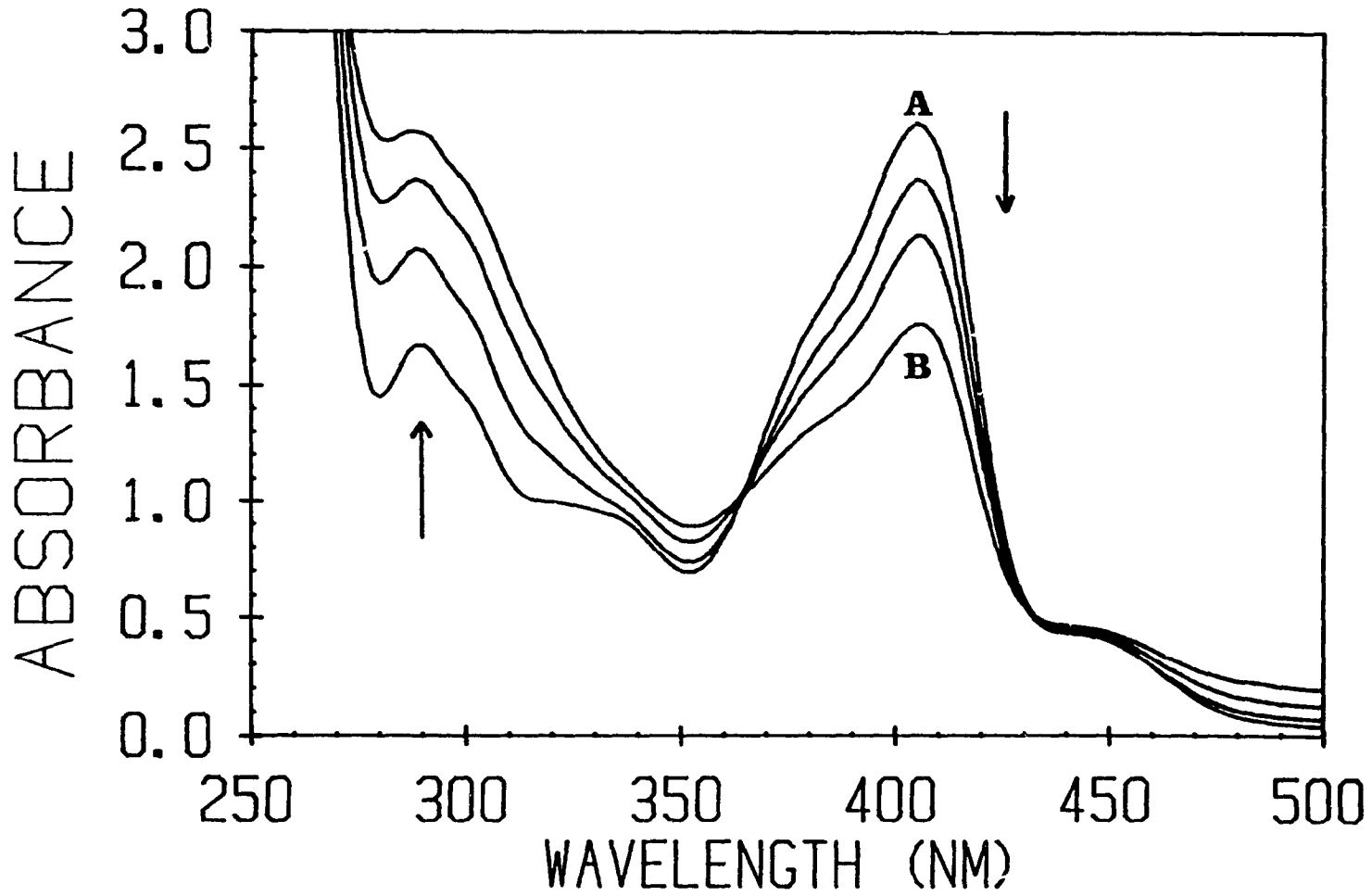

Table 3.3. Photosubstitution Quantum Yields for $W(CO)_5L \rightarrow W(CO)_5$(1-hexene) in Isooctane/1-hexene (2:1)[a,b,c,d]

L		Wavelength				
		313[e]	365[e]	436[e]	457.5	488.0
	N_2	.48(.02)[3]	.53(.02)[4]	.62(.02)[4]	.44(.03)[7]	.23(.03)[16]
pyr						
	O_2	.52(.03)[4]	.54(.02)[11]	.62(.02)[9]	.44(.03)[7]	.23(.01)[7]
		.38(.04)	.50(.05)	.63(.06)	(ref 46)	
	N_2	-	.49(.03)[7]	.54(.02)[2]	.41(.02)[4]	.37(.02)[8]
pip						
	O_2	-	.48(.01)[8]	.53(.02)[5]	.44(.01)[6]	.40(.02)[2]

a) concentrations of reactants are between 1.5-6.5 x 10^{-4} M

b) light intensities are between 3 x 10^{-10} and 2 x 10^{-6} Einsteins/sec

c) numbers in parentheses represent standard deviations

d) superscripts represent the number of trials

e) $\pm$ 10 nm

are significantly higher than those observed for $W(CO)_5$(pyridine). The yield for 313 nm irradiation of $W(CO)_5$(pyridine) slightly lower than those reported for 365 nm irradiation. The yields reported for 365 and 436 nm irradiation of $W(CO)_5$(pyridine) and 436 nm irradiation of $W(CO)_5$(piperidine) are similar to those reported for the substitution of these compounds by 1-pentene, using different irradiation procedures (45,46). Initial concentrations have no significant effect on the quantum yields as is reported in Tables 3.4 and 3.5. There is no significant difference in calculating quantum yields at 365 nm using solutions of $W(CO)_5$pyridine which absorb only 50% of light as compared to solutions which absorb > 95% of the light. Therefore, the quantum yields determined for $W(CO)_5$piperidine at this wavelength using solutions which do not permit total absorption of the light can be treated with confidence.

3.3. MLCT Reactivity

A major difference between the electronic spectra of $W(CO)_5$(pyridine) and $W(CO)_5$(piperidine) is the presence of a W ---> pyridine CT band in the pyridine complex. No corresponding CT transition exists in the piperidine complex. Studies of $W(CO)_5L$ complexes where the MLCT state is the lowest energy state have revealed that the MLCT state is essentially unreactive (14,37). An investigation into the possible contribution of the MLCT state to the overall quantum yields when it lies higher in energy than the first LF singlet state was undertaken. The two solvents, benzene and dichloromethane, were chosen because polarity differences are sufficient to change resolution of the CT and LF bands but neither form stable products which would interfere with rapid coordination of the 1-hexene ligand. As can be seen from the absorption spectra (Figure 3.6), the W ---> pyridine CT band is blue shifted and separated from the LF singlet band when

Table 3.4. Effect of concentration of initial reactant on Photo-substitution Quantum Yields for $W(CO)_5$pyridine ---> $W(CO)_5$(1-hexene) in isooctane/1-hexene (2:1 v/v)

Wavelength		Quantum Yield[a,b]	[$W(CO)_5$pyr] (M)
313[c]	N_2	.48(.02)[3]	5.369×10^{-4}
	O_2	.52(.03)[4]	$5.218 \times 10^{-4} \pm 3\%$
365[c]	N_2	.54(.02)[6]	$2.438 \times 10^{-4} \pm 1.4\%$
		.52(.02)[7]	$4.937 \times 10^{-4} \pm 2.6\%$
	O_2	.52(.02)[5]	8.055×10^{-4}
		.56(.02)[6]	$2.438 \times 10^{-4} \pm 1.4\%$
436[c]	N_2	.65(.04)[3]	1.480×10^{-4}
		.64(.02)[3]	1.852×10^{-5}
		.61(.05)[3]	$4.937 \times 10^{-4} \pm 2.6\%$
	O_2	.68(.03)[1]	1.480×10^{-4}
		.58(.01)[2]	5.067×10^{-4}
457.5	N_2	.43(.03)[4]	$2.794 \times 10^{-4} \pm .3\%$
		.45(.02)[3]	5.369×10^{-4}
	O_2	.42(.01)[4]	2.786×10^{-4}
		.47(.01)[3]	5.369×10^{-4}
488	N_2	.23(.03)[16]	$4.994 \times 10^{-4} \pm 3.8\%$
	O_2	.23(.01)[7]	5.181×10^{-4}

a) numbers in parentheses represent standard deviations

b) superscripts represent number of trials

c) $\pm$ 10 nm

Table 3.5. Effect of concentration of initial reactant on Photosubstitution Quantum Yields for $W(CO)_5$piperidine --->$W(CO)_5$(1-hexene) in isooctane/1-hexene (2:1 v/v)

Wavelength		Quantum Yield[a,b]	[$W(CO)_5$pip] (M)
365[c]	N_2	.49(.03)[7]	3.077×10^{-4}
	O_2	.48(.01)[8]	4.943×10^{-4}
436[c]	N_2	.54(.02)[2]	$5.126 \times 10^{-4} \pm 2.6\%$
	O_2	.53(.02)[3] .54(.01)[2]	3.008×10^{-4} 4.992×10^{-4}
457.5	N_2	.41(.02)[4]	6.224×10^{-4}
	O_2	.44(.01)[6]	6.067×10^{-4}
488	N_2	.37(.02)[8]	6.224×10^{-4}
	O_2	.40(.02)[2]	6.809×10^{-4}

a) numbers in parentheses represent standard deviations

b) superscripts represent number of trials

c) $\pm$ 10 nm

$W(CO)_5$(pyridine) is dissolved in either benzene/1-hexene or dichloromethane/1-hexene (2:1) as compared to isooctane/1-hexene (2:1). The molar extinction coefficients of the CT transition increases while that of the LF singlet correspondingly decreases in the more polar solvents. A slight decrease in the extinction coefficient of the LF singlet transition is observed for $W(CO)_5$(piperidine) in these more polar solvents.

Irradiation of both compounds in either solvent leads to efficient replacement of L by 1-hexene as observed for these complexes in isooctane/1-hexene. Irradiation with wavelengths $\geq$ 436 nm leads to complete conversion with no secondary photolysis (Figures 3.14 and 3.15) whereas the appearance of the white precipitate occurs at approximately 40% conversion under 313 nm and 85% conversion under 365 nm irradiation. Photosubstitution quantum yields for both compounds are reported in Tables 3.6 and 3.7. Comparison between degassed and air-equilibrated samples are included and show that little significant difference occurs in the presence or absence of oxygen. Photolysis at 313 nm of $W(CO)_5$(pyridine) irradiates the MLCT band while 365 nm irradiates overlapping portions of the MLCT and LF singlet bands. The quantum yields in benzene/1-hexene under 313 nm irradiation, within experimental error, are comparable to those observed for 365 nm irradiation. In dichloromethane/1-hexene, quantum yields for 313 nm irradiation of $W(CO)_5$(pyridine) are smaller than those observed for 365 nm irradiation. Separation of the MLCT and LF states is largest for CH_2Cl_2/hexene compared to benzene or isooctane. The wavelength dependence for quantum yields is observed for both compounds in these solvents as is the decrease upon 457.5 nm irradiation. There is an observable decrease in the substitution yields for the pyridine complex when irradiated between 313 and 436 nm in dichloromethane/1-hexene as compared to issoctane/1-hexene. A decrease is also observed for the piperidine complex. 313

Figure 3.14. Electronic spectral changes for $W(CO)_5$pyr in dichloromethane/1-hexene (2:1 v/v) under 436 nm irradiation. The times or irradiation from reactant A to product B are: 0, 10,20,30,60,90,120,240 seconds.

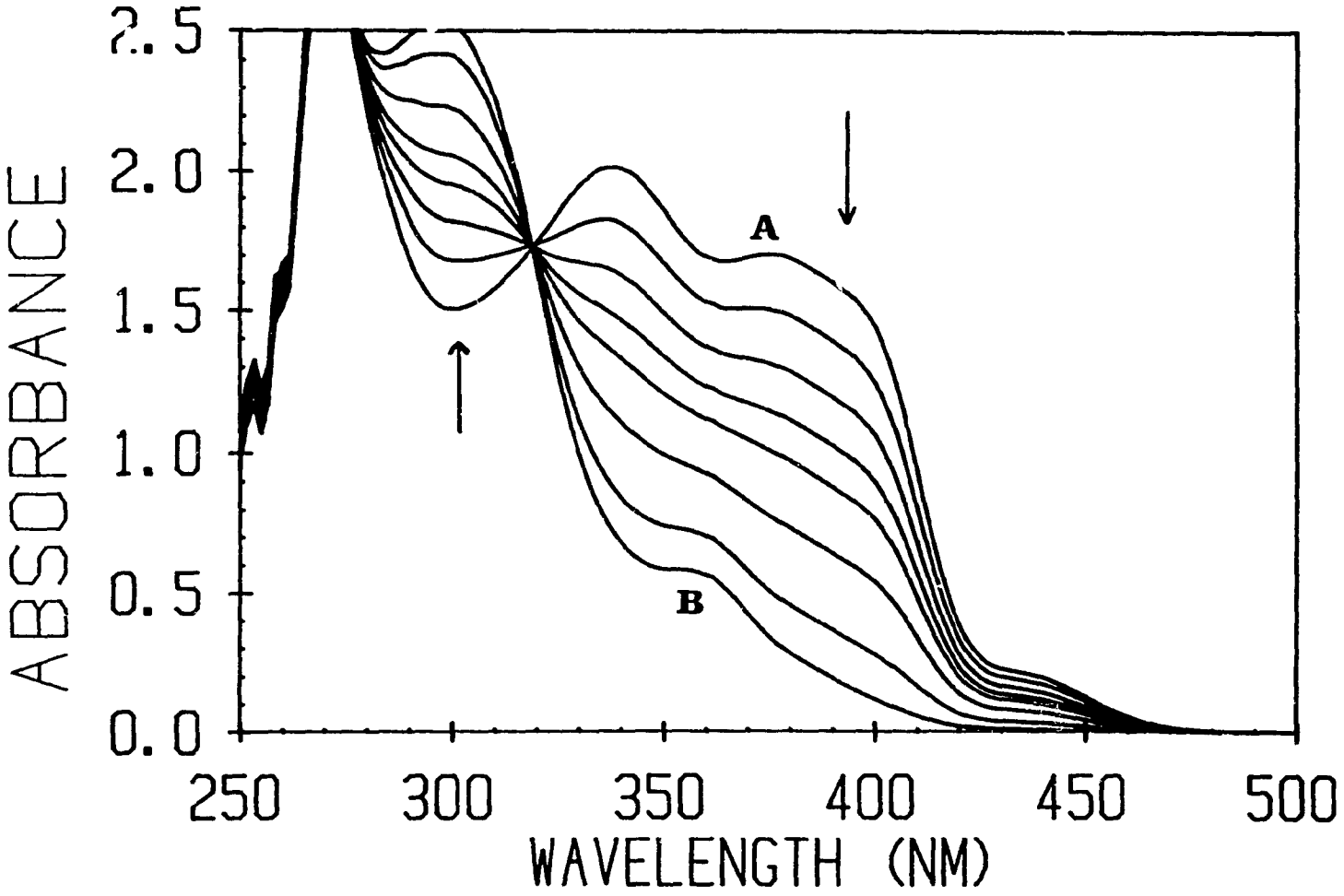

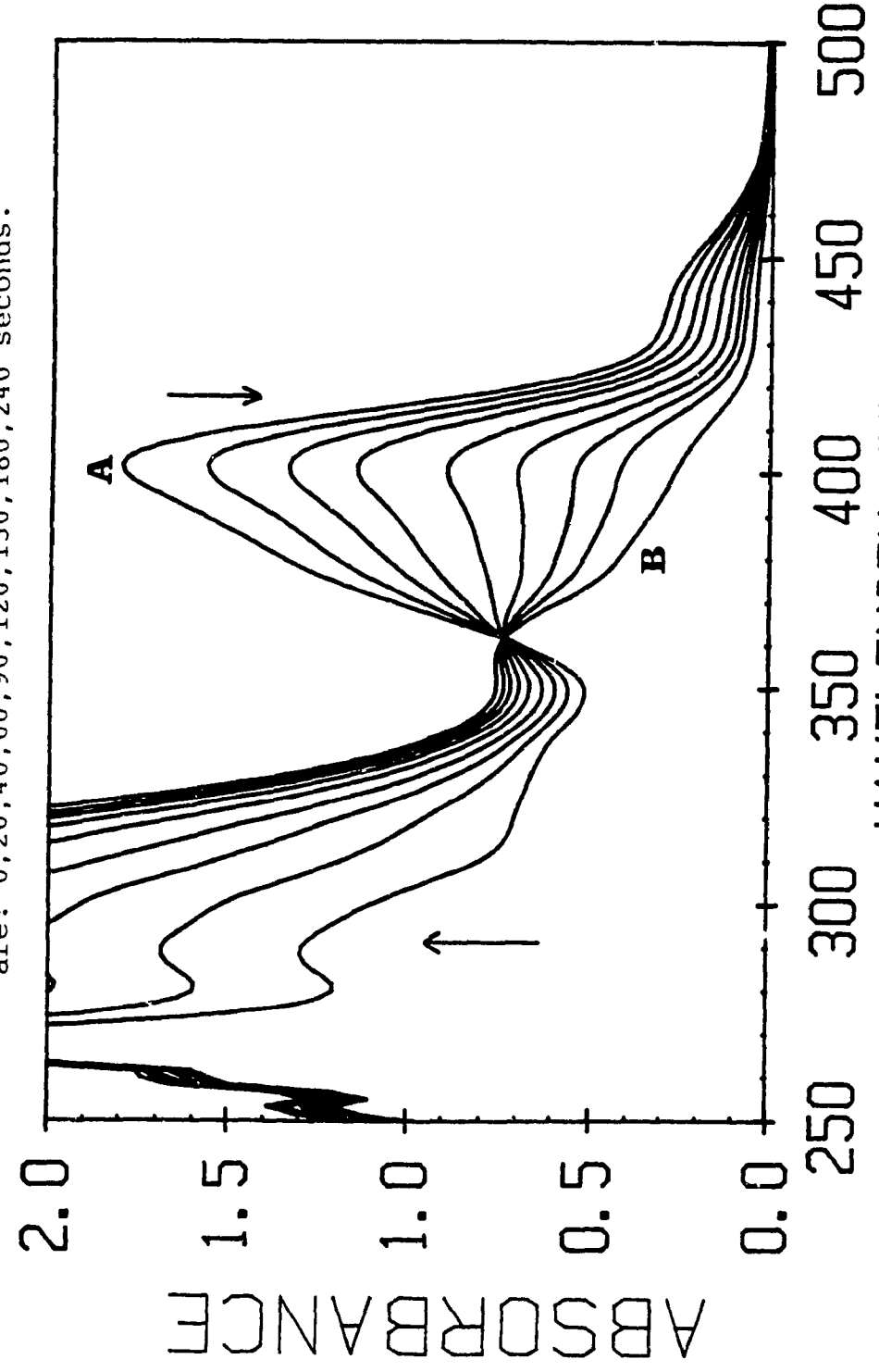

Figure 3.15. Electronic spectral changes for $W(CO)_5$pip in dichloromethane/1-hexene (2:1 v/v) under 436 nm irradiation. The times of irradiation from reactant A to product B are: 0,20,40,60,90,120,150,180,240 seconds.

Table 3.6. Photosubstitution Quantum Yields for $W(CO)_5L$ -> $W(CO)_5$(1-hexene) in benzene/1-hex(2:1)[a,b,c,d]

L		Wavelength			
		313[e]	365[e]	436[e]	457.5
pyr	N_2	.49(.04)[4]	.52(.02)[4]	.57(.03)[7]	.37(.02)[5]
	O_2	-	.53(.02)[4]	.54(.02)[4]	.40(.03)[3]
pip	N_2	-	.42(.02)[4]	.45(.03)[8]	.36(.01)[4]
			.45(.05)	.49(.05)	(ref 47)

a) numbers in parentheses represent standard deviations

b) superscripts represent number of trials

c) concentrations of the reactants are 3 - 6 x 10^{-4}

d) light intensities are between 3.5 x 10^{-10} and 9 x 10^{-7} Einsteins/sec

e) $\pm$ 10 nm

Table 3.7. Photosubstitution Quantum Yields for $W(CO)_5L$ -> $W(CO)_5$(1-hexene) in dichloromethane/1-hex (2:1 v/v)[a,b,c,d]

L		Wavelength			
		313[e]	365[e]	436	457.5
pyr	N_2	.36(.01)[2]	.44(.04)[2]	.51(.02)[2]	.39(.01)[3]
	O_2	.40(.05)[5]	.44(.02)[10]	.54(.01)[9]	.34(.03)[4]
pip	N_2	-	.39(.02)[4]	.41(.03)[8]	.34(.03)[4]
	O_2	-	.42(.01)[4]	.42(.02)[3]	.33(.03)[2]

a) numbers in parentheses represent standard deviations

b) superscripts represent number of trials

c) concentrations of the reactants are 3 - 7 x 10^{-4} M

d) light intensities are between 3.5 x 10^{-10} and 9 x 10^{-7} Einsteins/sec

e) $\pm$ 10 nm

nm irradiation of $W(CO)_5$pyridine in CH_2Cl_2 gives yields which are comparable to the yields produced upon 365 nm irradiation of $W(CO)_5$piperidine in the same solvent. Quantum yields for substitution of piperidine by 1-hexene in benzene/1-hexene are similar to those reported for substitution of piperidine by 1-pentene (45). The decrease in quantum yields for both compounds suggest that a solvent effect is also present. Since MLCT states are reported to be unreactive, the high quantum yields observed for 313 nm irradiation of $W(CO)_5$(pyridine) in all solvents suggest that efficient internal conversion between the MLCT and the LF singlet states are responsible for the MLCT reactivity. The state into which the MLCT state relaxes may account for observed similarities between 313 nm irradiation of $W(CO)_5$pyr and 365 nm irradiation of $W(CO)_5$pip in CH_2Cl_2/hex and supports the phenomenon of wavelength dependence of the singlet states.

3.4. Solvent Dependence

The effect of two groups of solvents, alcohols and chlorinated alkanes, on the photosubstitution quantum yields of $W(CO)_5L$ (L = pyridine, piperidine) was examined. The electronic spectra of $W(CO)_5$pyridine in neat alcohols reveal that resolution of the CT and LF bands occurs due to the polarity of these solvents (Figure 3.5). The electronic spectra of $W(CO)_5$piperidine and $W(CO)_6$ in the alcohols are not significantly changed from those in alkane solvents. Slight decreases in the molar extinction coefficients occur. The CT and LF bands of $W(CO)_5$pyridine are not resolved in the mixed CCl_4/1-hexene or the neat 1-hexene solvents but are resolved in the mixed $CHCl_3$/1-hexene solvents (Figure 3.16). Decreases in the molar extinction coefficients for the LF bands occur in these solvents (Table 3.1). Slight changes occur for $W(CO)_5$piperidine in these solvents (Table 3.1).

Figure 3.16. Electronic spectra of $W(CO)_5$pyr in (A) Chloroform/ 1-hexene (2:1 v/v), and (B) carbon tetrachloride/ 1-hexene (2:1 v/v). Concentrations are 1.7 x 10-4 M.

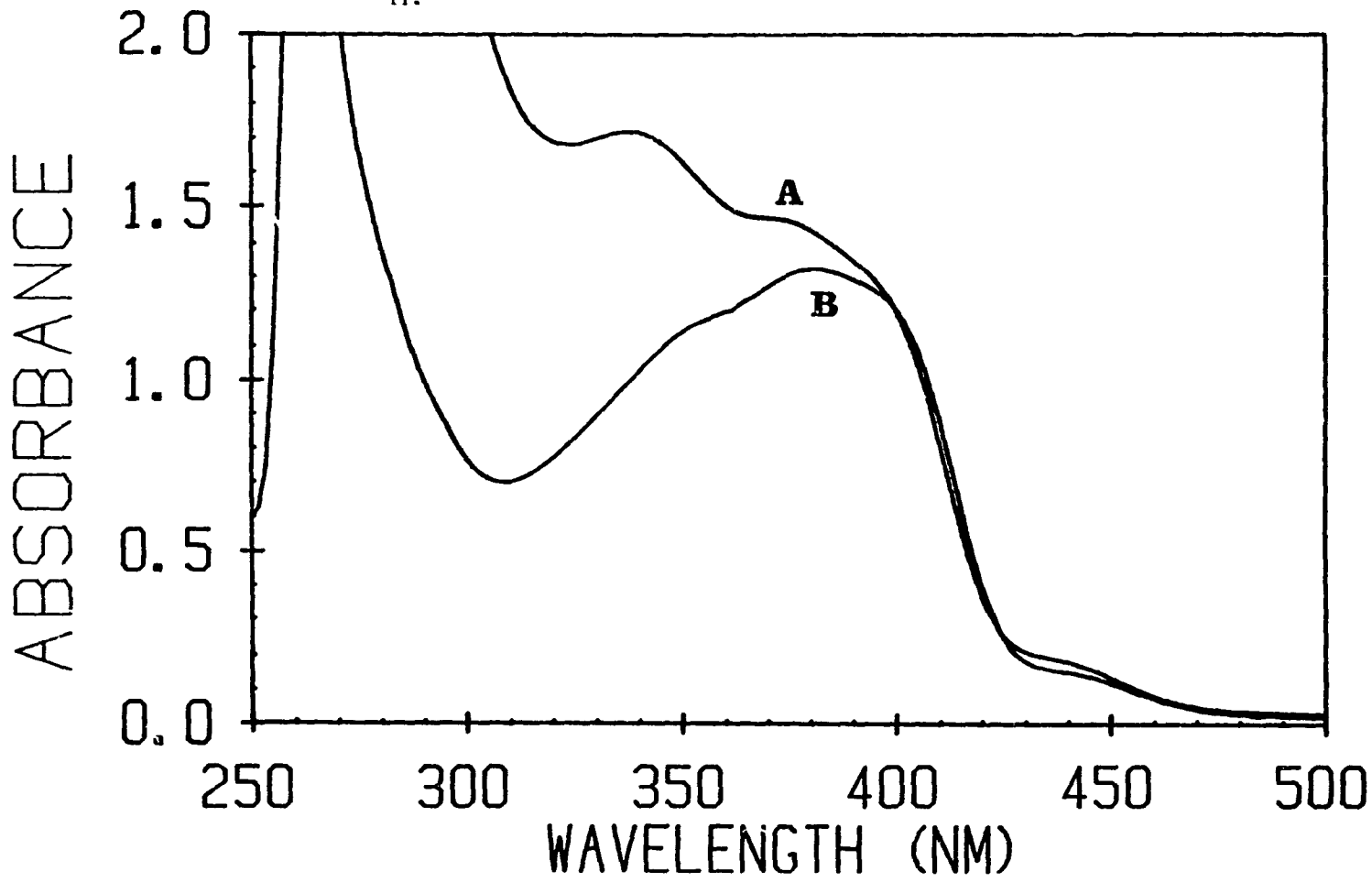

Irradiation into the LF singlet bands of all three complexes in the alcohols or mixed alkane/alcohol solvents leads to efficient replacement of pyridine, piperidine or CO by the OH group of the alcohol (Figures 3.17, 3.18, 3.19). OH is a weaker field ligand than either pyridine or piperidine. It is expected that coordination to $W(CO)_5$ would result in a LF band lower in energy than those observed for either the pyridine or piperidine complex. $W(CO)_5$(alcohol) has two absorption peaks in its electronic spectrum. The low energy peak is at 418 nm and a high energy peak is at 290 nm. These peaks are the same for all the $W(CO)_5$(alcohol) spectra, regardless of the alcohol. There is a clean isosbestic point at 410 nm for $W(CO)_5$pyr and $W(CO)_5$pip in the alcohols from zero to 100% conversion. Photosubstitution quantum yields are given in Table 3.8. As can be observed from the quantum yield data, there is little observable difference for substitution in methanol, butanol or octanol for $W(CO)_5$pyr or $W(CO)_6$ under 365 nm irradiation. The substitution yield in propanol is higher for $W(CO)_5$pyridine. In mixed alkane/propanol solutions, yields do not alter significantly. In contrast, quantum yields for $W(CO)_5$piperidine in propanol, butanol and octanol are essentially the same. Methanol yields are significantly lower. 313 nm irradiation of $W(CO)_5$pyridine reveals that quantum yields are essentially the same for propanol, butanol and octanol as those observed upon 365 nm. The yield for methanol is the same as that observed for 365 nm irradiation of $W(CO)_5$piperidine. The separation between MLCT and LF states in $W(CO)_5$pyr is largest in methanol compared to all other solvents used in this study.

Irradiation into the LF singlet bands of both complexes in the mixed chlorinated solvents leads to efficient replacement of the pyr or pip by 1-hexene (Figures 3.20 and 3.21). The appearance of a blue precipitate and subsequent loss of the isosbestic point are observed at late stages of conversion for both complexes

Figure 3.17. Electronic spectral changes for $W(CO)_6$ in octanol under 365 nm irradiation. The times of irradiation from reactant A to product B are: 0,60,120,180,360,600,1200,2700 seconds.

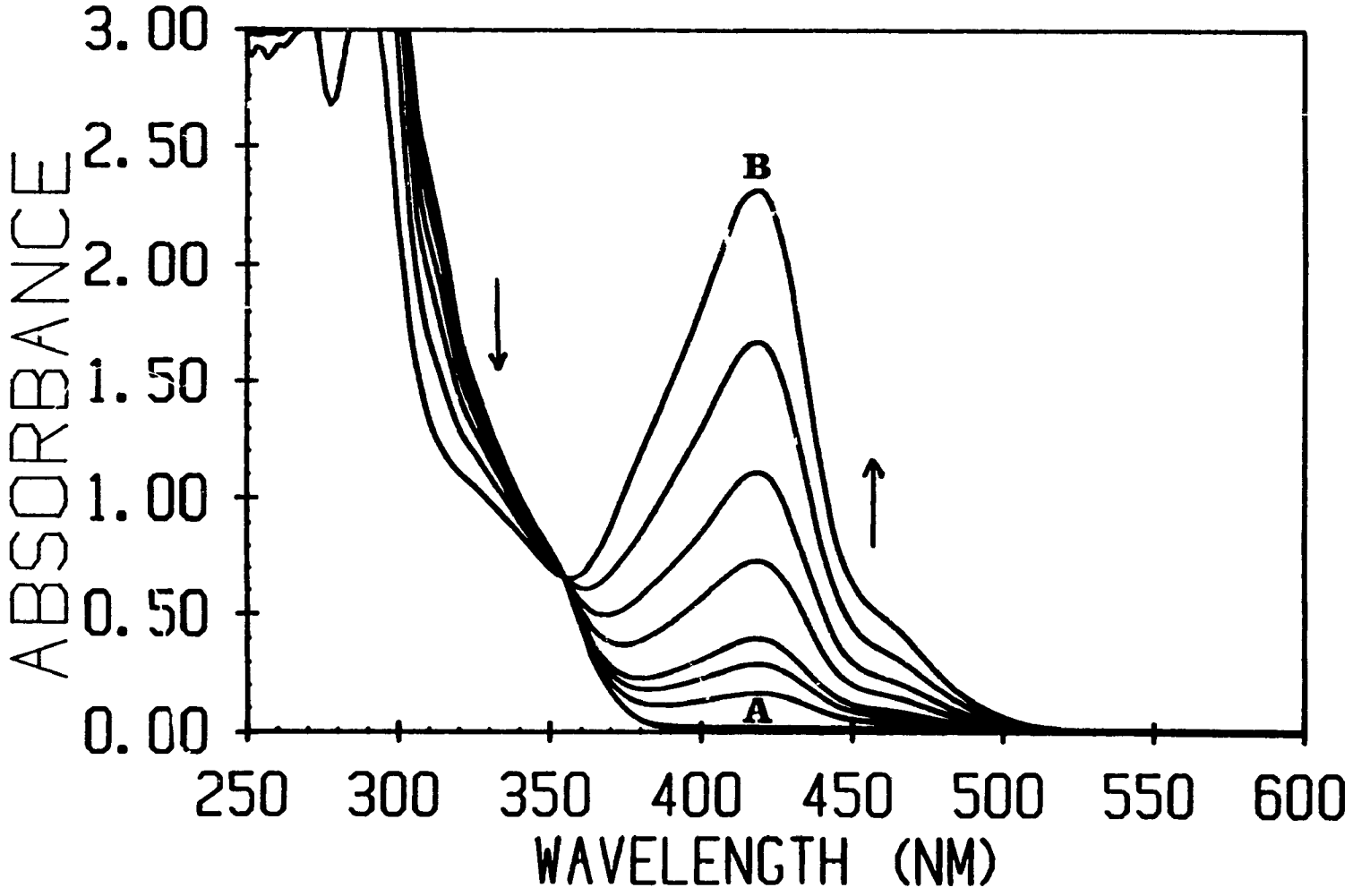

Figure 3.18. Electronic spectral changes for $W(CO)_5$pyr in butanol under 365 nm irradiation. The times of irradiation from reactant A to product B are: 0,60,120,180,300, 420,600 seconds.

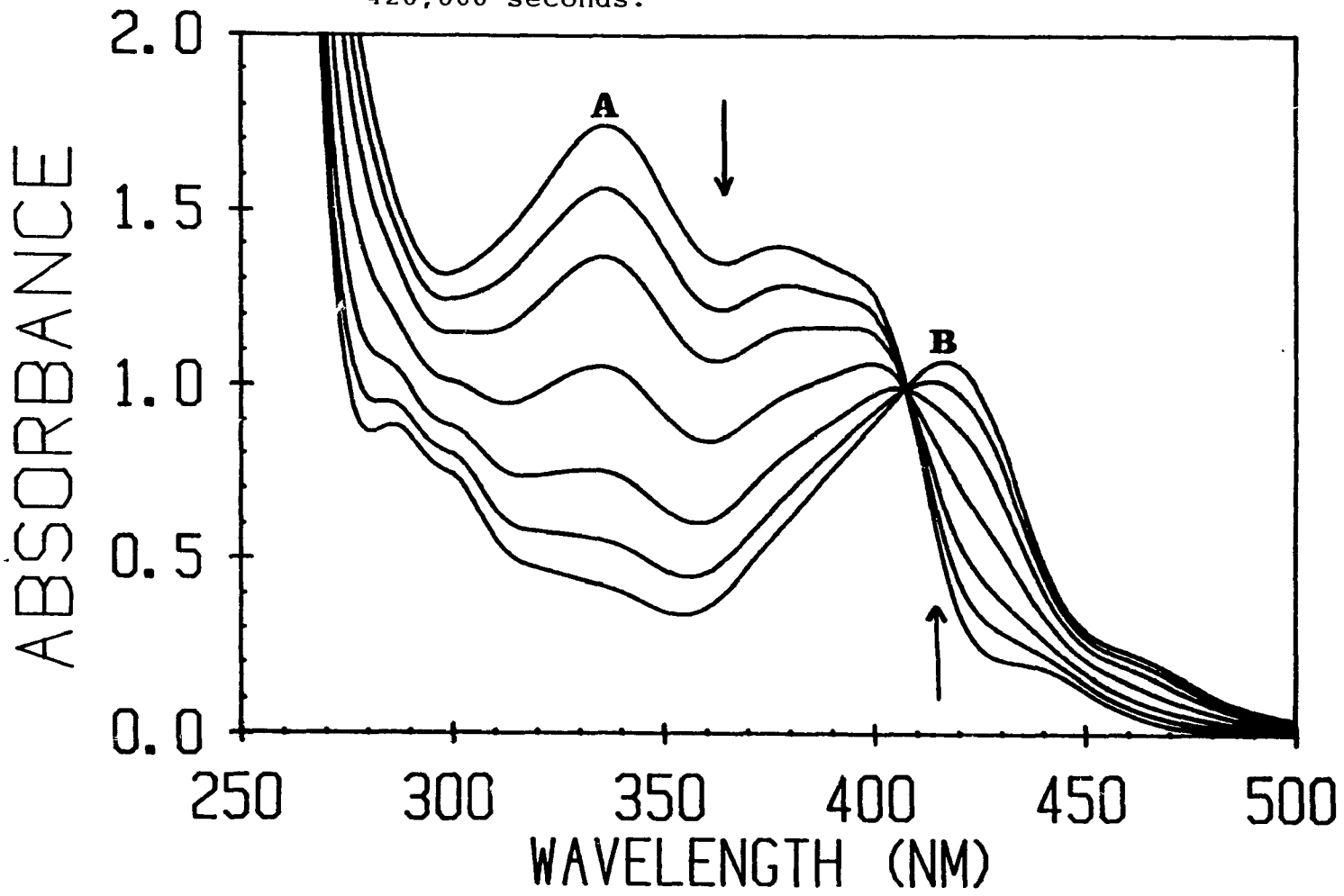

Figure 3.19. Electronic spectral changes for $W(CO)_5$pip in butanol under 365 nm irradiation. The times of irradiation from reactant A to product B are: 0,60,120,240,360, 600,960,1680 seconds.

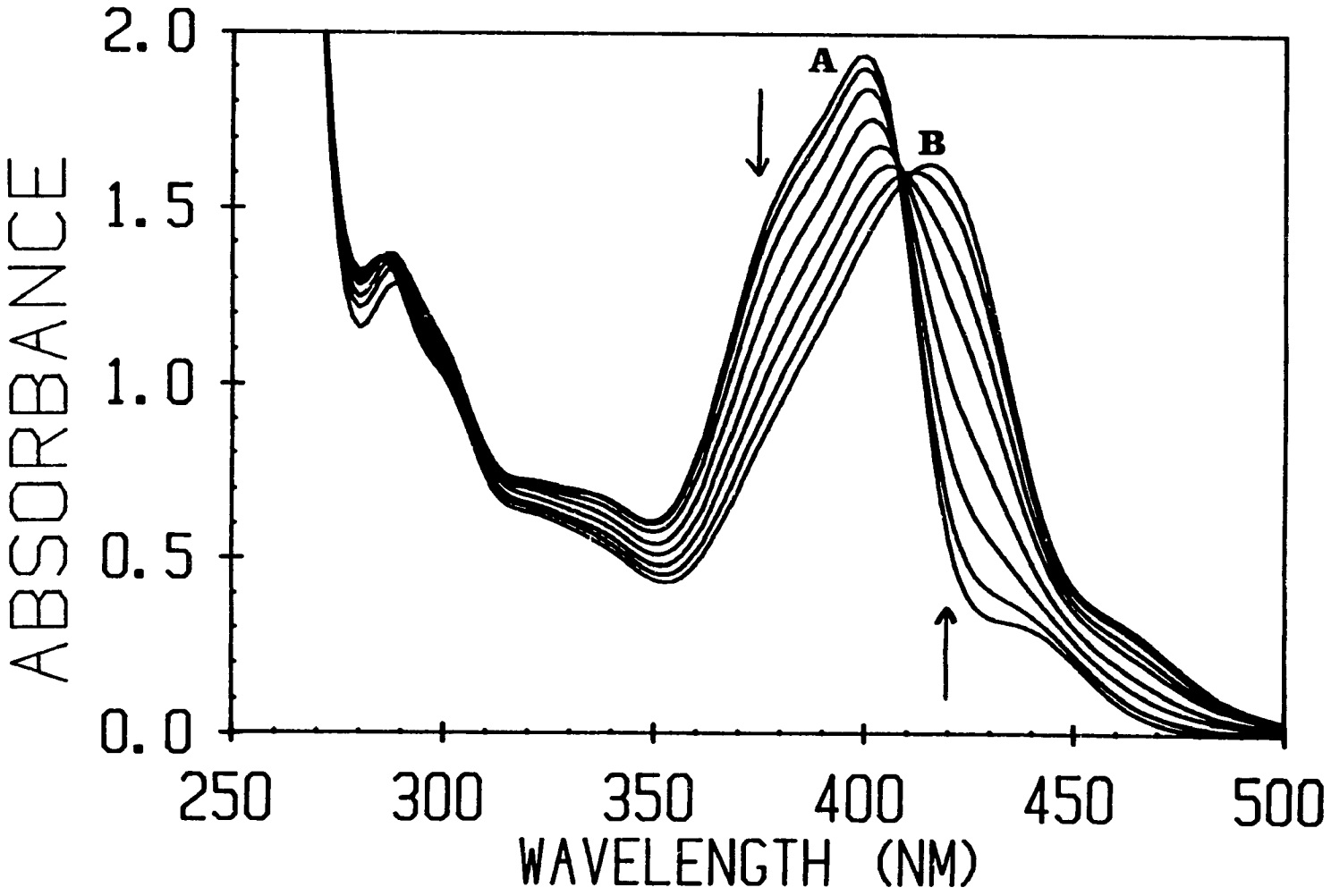

Table 3.8. Photosubstitution quantum yields of $W(CO)_5L$ in 100% n-alcohols[a,b,c,d]

		Wavelength (± 10 nm)	
L	Alcohol	313	365
CO	methanol	-	.89(.09)[12]
	butanol	-	.93(.08)[12]
	octanol	-	.96(.07)[12]
pyridine	methanol	.30(.02)[6]	.44(.04)[8]
	propanol	.55(.06)[8]	.58(.06)[10]
	isooct/prop (9:1)		.56(.05)[8]
	isooct/prop (24:1)		.59(.02)[8]
	butanol	.48(.04)[8]	.48(.04)[16]
	octanol	.52(.06)[8]	.43(.02)[12]
piperidine	methanol	-	.31(.03)[6]
	propanol	-	.41(.02)[6]
	butanol	-	.44(.02)[7]
	octanol	-	.38(.02)[7]

a) concentrations of the reactants are between 3×10^{-4} and 2×10^{-3} M

b) light intensities are between 3.5×10^{-10} and 9×10^{-7} Einsteins/sec

c) numbers in parentheses represent standard deviations

d) superscripts represent the number of trials

Figure 3.20. Electronic spectral changes for $W(CO)_5$pyr in chloroform/ 1-hexene (2:1 v/v) under 436 nm irradiation. The times of irradiation from reactant A to product B are: 0,30,60,90, 120,180,240 seconds.

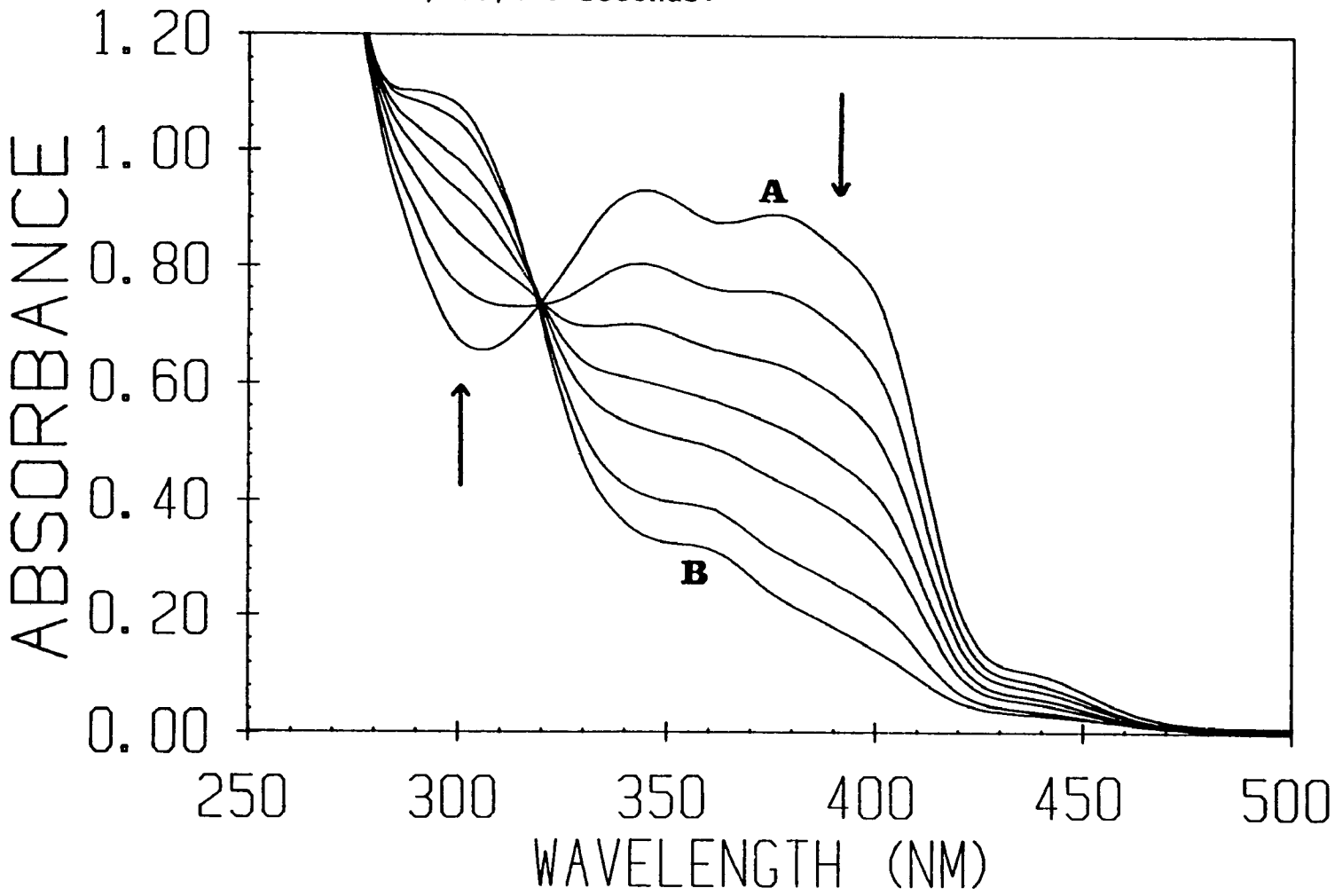

Figure 3.21. Electronic spectral changes for $W(CO)_5$pip in chloroform/ 1-hexene (2:1 v/v) under 436 nm irradiation. The times of irradiation from reactant A to product B are: 0,60, 120,180,240,360 seconds.

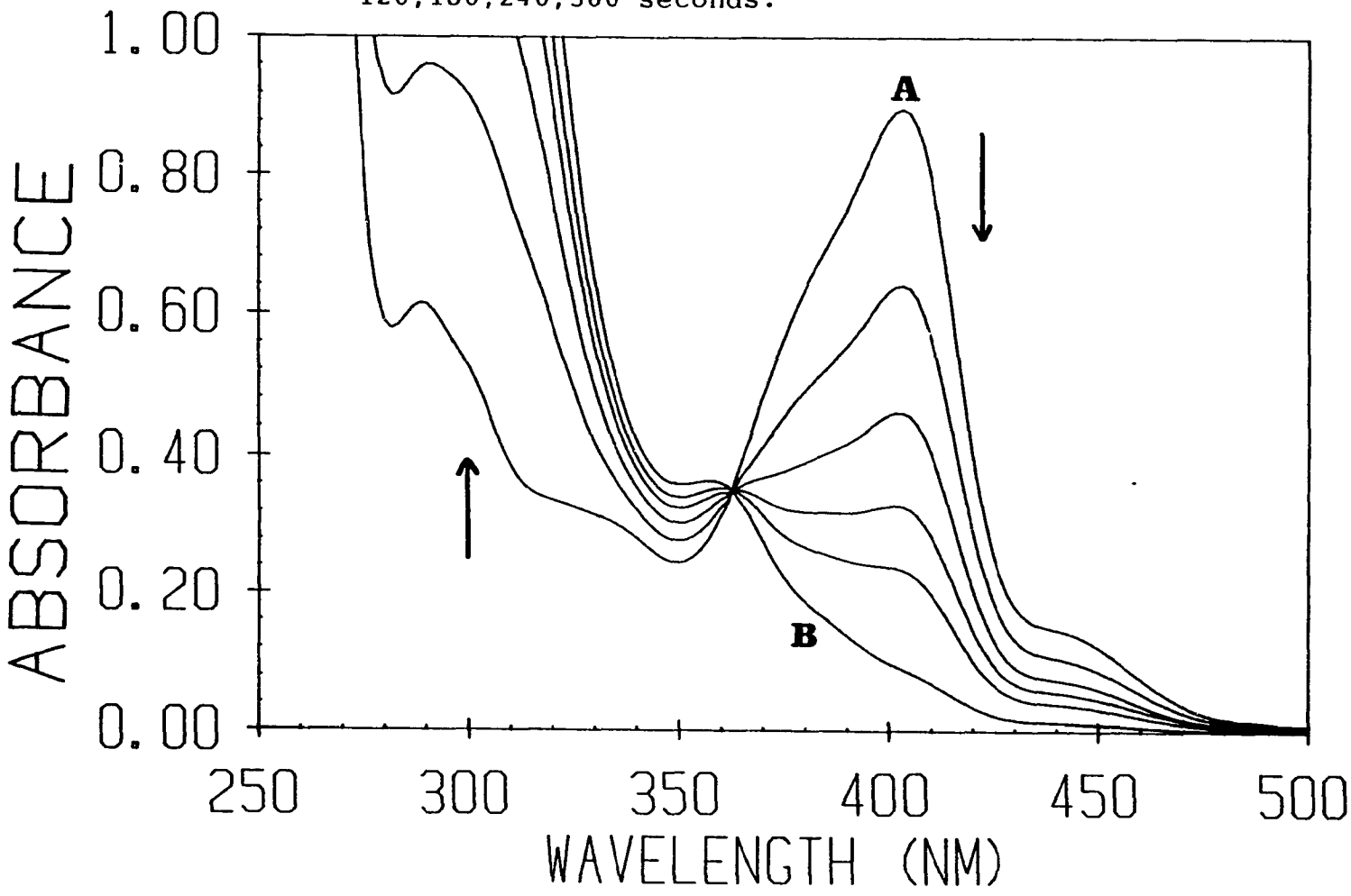

in $CHCl_3$/1-hexene and CCl_4/1-hexene. Removal of the precipitate results in reattainment of the isosbestic point. Quantum yields for 313, 365 and 436 nm irradiation are reported in Table 3.9. As can be observed, the quantum yields in all chlorinated solvents at all wavelengths follow the same pattern. Yields are highest for CCl_4/hex and lowest in CH_2Cl_2/hex and $CHCl_3$/hex. Yields in $CHCl_3$ may be the same or slightly higher than those in CH_2Cl_2 depending on the wavelength of irradiation but both CH_2Cl_2 and $CHCl_3$ are significantly lower than CCl_4. The yields for $W(CO)_5$pyr in CH_2Cl_2 and $CHCl_3$/1-hexene are slightly higher than those of $W(CO)_5$pip in the same solvents. The yields for $W(CO)_5$pyr in CCl_4/1-hex may be considered to be significantly higher than those of $W(CO)_5$pip in the same solvent. The yields of both complexes in CCl_4/1-hex are the highest reported in this study for $W(CO)_5$pyr or $W(CO)_5$pip. The wavelength dependence in the LF singlet region disappears in CCl_4 for both compounds. In CCl_4, 436 nm yields are lower than 365 nm yields.

Irradiation of these complexes in neat 1-hexene leads, as expected, to efficient replacement of pyr or pip by 1-hexene. Spectra are identical to those obtained in isooctane/hexene solvents. The behavior of these complexes is identical to that observed for these complexes in the isooctane, benzene or dichloromethane/1-hexene solvents. A clean isosbestic point is observed at 320 nm from zero to 100% conversion under 436 nm irradiation and precipitation occurs after 85% conversion for 365 nm irradiation. The quantum yields at 365 nm (Table 3.10) are higher than those reported for the mixed alkane/alkene solvents. Changing the concentration of the 1-hexene by mixing it with isooctane has no significant effect on the photosubstitution quantum yields.

Table 3.9. Quantum yields for $W(CO)_5L$ --> $W(CO)_5$(1-hexene)

L	Solvent	Wavelength[a,b,c]		
		313	365	436
pyr	CH_2Cl_2/hex (2:1)	.38(.05)[13]	.44(.05)[8]	.54(.01)[4]
	$CHCl_3$/hex (2:1)	.48(.02)[5]	.47(.06)[8]	.57(.03)[11]
	CCl_4/hex (2:1)	.61(.01)[5]	.80(.02)[6]	.74(.03)[12]
pip	CH_2Cl_2/hex (2:1)	-	.40(.03)[3]	.42(.03)[11]
	$CHCl_3$/hex (2:1)	-	.45(.03)[5]	.50(.04)[17]
	CCl_4/hex (2:1)	-	.68(.02)[6]	.55(.02)[14]

a) $\pm$ 10 nm

b) numbers in parentheses represent standard deviations

c) superscripts represent number of trials

Table 3.10. Quantum yields for $W(CO)_5L$ --> $W(CO)_5$(1-hexene)

L	Solvent	Quantum Yield[a,b] 365 (± 10 nm)
pyr	1-hexene	.60(.03)[9]
	isooctane/1-hexene (2:1)	.55(.03)[9]
	isooctane/1-hexene (10:1)	.53(.03)[3]
	isooctane/1-hexene (20:1)	.53(.02)[5]
pip	1-hexene	.52(.03)[8]
	isooctane/1-hexene (2:1)	.48(.03)[4]

a) numbers in parentheses represent standard deviations

b) superscripts represent number of trials

3.5. Picosecond Spectroscopy

We have studied the transient absorption spectra of $W(CO)_5L$ (L = CO, pyridine, piperidine) in various solvents in order to understand the primary processes which occur in these complexes. The hexacarbonyls of Cr, Mo and W undergo high quantum yield photosubstitution reactions via a primary intermediate of C_{4v} symmetry, $M(CO)_5S$ where S is a solvent molecule. These species have been well characterized in a variety of media (16-21), and display a first ligand field (LF) band which may appear in the visible if the solvent, S, is a sufficiently weak electron donor. If the solvent S allows the first LF band to be detected in the wavelength range 425-675 nm, it becomes possible to monitor the formation of the primary intermediate with the "continuum" pulse produced with the laser system used in this experiment. Three solvents which permit observation of the intermediate $W(CO)_5S$ with our apparatus are the alkanes, perfluoromethylcyclohexane, and the alcohols. In alkanes and alcohols, $W(CO)_5S$, gives LF bands which lie just to the red or blue, respectively, of our probe and the tail of the band may be monitored. In the case of the perfluoro solvent, the entire band is in the visible region as has been reported for the analagous $Cr(CO)_5$complex (24).

Figure 3.22 displays the growth of the absorption maximum for the species $W(CO)_5S$ in perfluoromethylcyclohexane in the period between 0 and 50 picoseconds (ps) after excitation of a solution 18 mM in $W(CO)_6$ with a pulse of 2.5 mJ, 30 ps half-width, at 355 nm. The rate constant at 20° C for the growth of the solvopentacarbonyl species is ~ 3.6×10^{10} s^{-1}. Figures 3.23, 3.24, and 3.25 show the results of picosecond experiments on $W(CO)_6$, $W(CO)_5$pyridine, and $W(CO)_5$piperidine in cyclohexane. For $W(CO)_6$ in cyclohexane, there is an observable growth for the peak at ~ 450 nm from between 0 and 50 picoseconds (Figure 3.23). For $W(CO)_5$pyr (Figure 3.24) and $W(CO)_5$pip in cyclohexane (Figure

Figure 3.22. Transient absorption spectra of $W(CO)_6$ in perfluoromethylcyclohexane between 0 and 50 picoseconds under 355 nm irradiation.

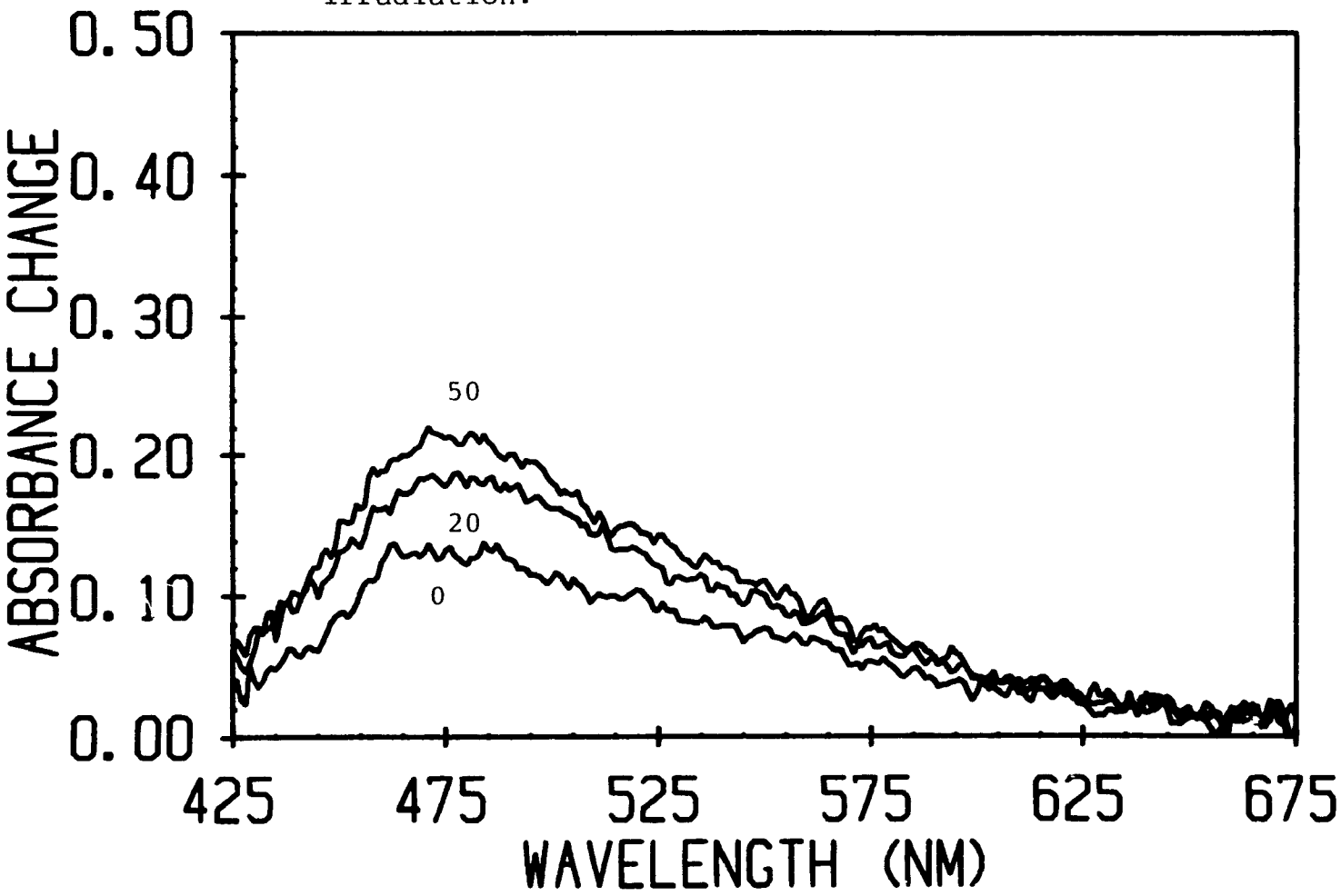

Figure 3.23. Transient absorption spectra of $W(CO)_6$ in cyclohexane between 0 and 50 picoseconds under 355 nm irradiation.

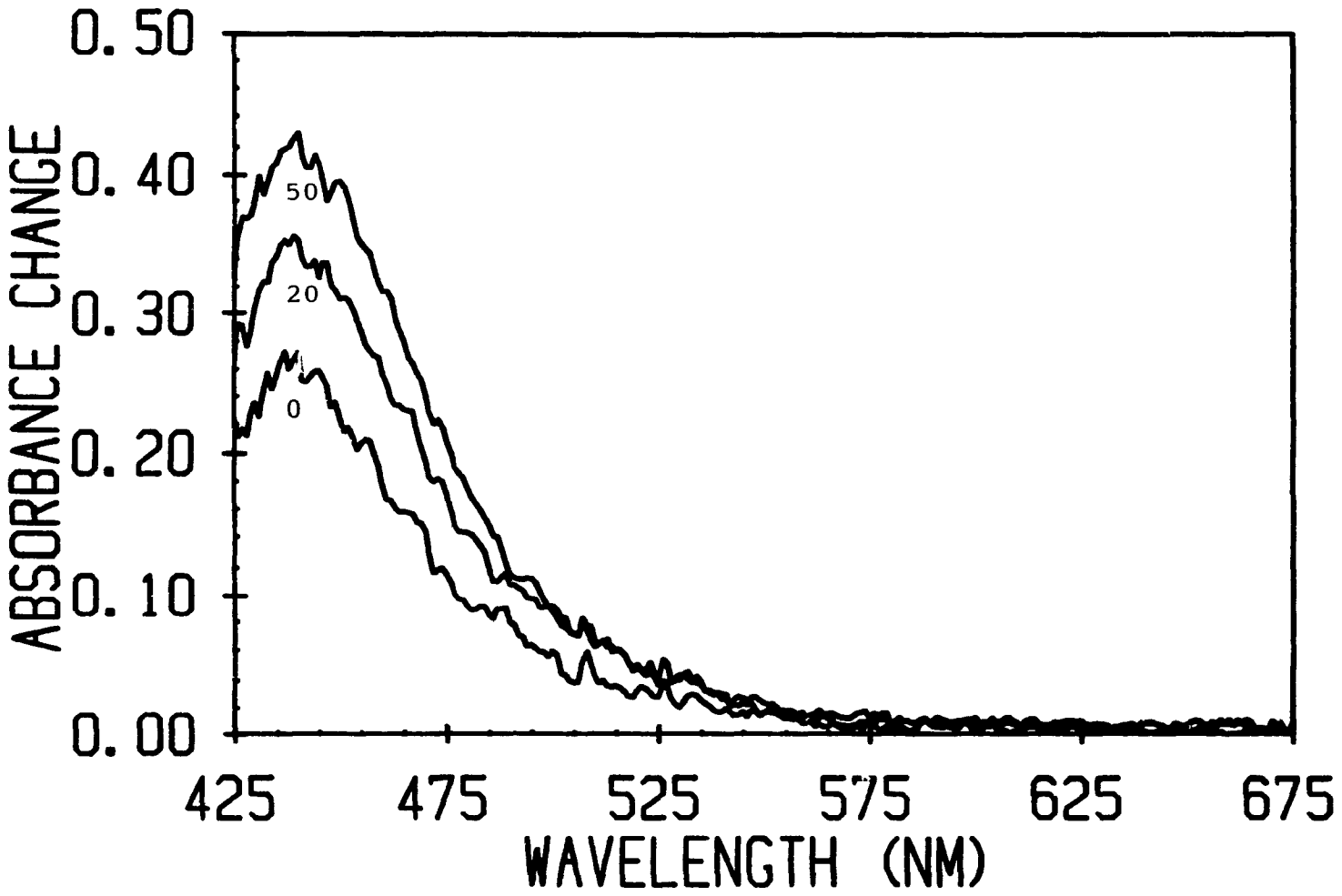

Figure 3.24. Transient absorption spectra of $W(CO)_5$pyr in cyclohexane between 0 and 50 picoseconds under 355 nm irradiation.

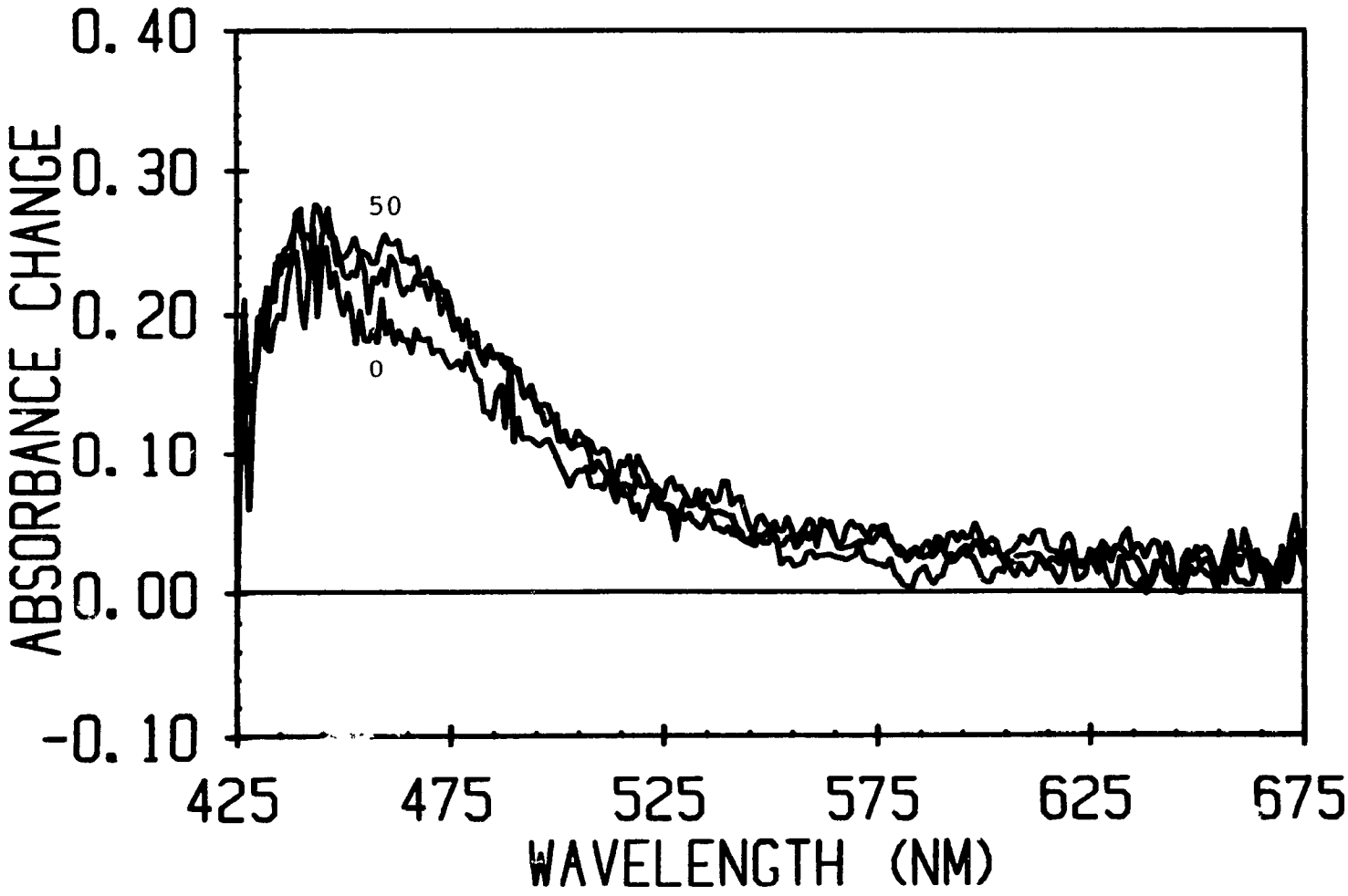

Figure 3.25. Transient absorption spectra of W(CO)5 pip in cyclohexane between 0 and 50 picoseconds under 355 nm irradiation.

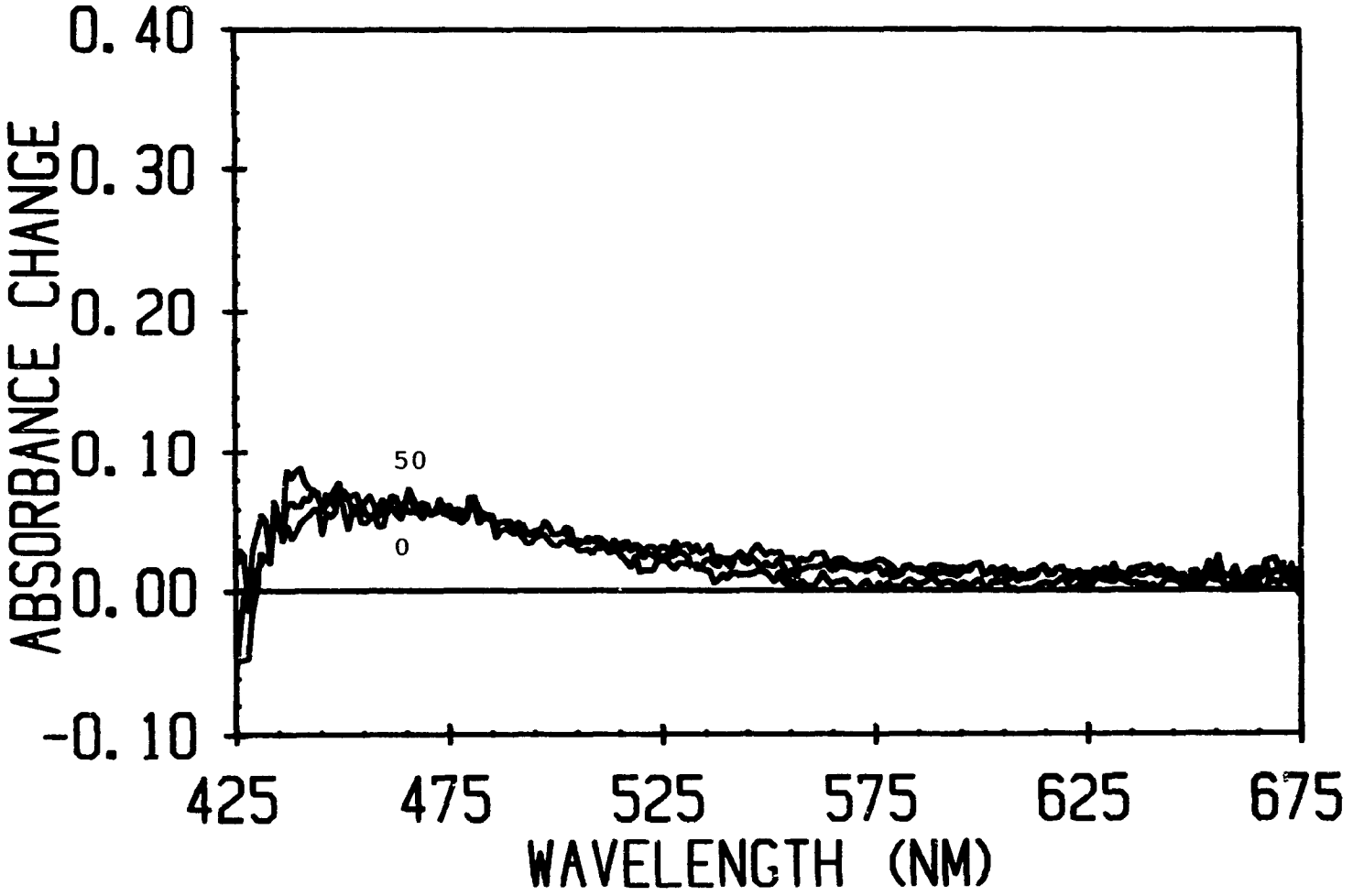

3.25), there is little observable difference in the transient absorbances between 0 and 50 ps. Qualitative examination of the spectra indicates that there is a common $W(CO)_5S$ from all three complexes. A time constant estimated for the formation of $W(CO)_5$(alkyl) from $W(CO)_6$ in cyclohexane is ~ 25 picoseconds. Quantitative examination of all three spectra permits the calculation of the transient extinction coefficient for $W(CO)_5$(cyclohexane). For $W(CO)_5L$ (L = pyr, pip) this value is calculated based on the intensity of the fully developed $W(CO)_5S$ band and the quantum yield for formation of $W(CO)_5$(1-hexene) observed in steady state irradiation experiments in isooctane/1-hexene (2:1 v/v) using 365 nm light. For $W(CO)_6$, the quantum yield for formation of $W(CO)_5$(pyridine) from $W(CO)_6$ in cyclohexane/pyridine (42) was used. The calculated values are given in Table 3.11. The most consistent value was determined from the transient spectra of $W(CO)_5$pyr in cyclohexane. The calculated extinction coefficients are comparable to those observed for LF singlet bands of tungsten analogues. 355 nm irradiation populates a LF triplet state in $W(CO)_6$, a LF singlet state in $W(CO)_5$pip and a combination of a LF singlet and a MLCT state in $W(CO)_5$pyr. The transient spectra of all three complexes indicate that all 355 nm initiated reactions may share the same initial dissociative step.

Picosecond spectra of all three complexes in 1-hexene were also studied (Figures 3.26-3.28). The transient spectra of $W(CO)_6$ in 1-hexene (Figure 3.26) indicates that formation of $W(CO)_5S$, where S is the alkyl portion of the 1-hexene chain, occurs with grow-in from 0 to 50 picoseconds as is seen for this complex in cyclohexane. The product $W(CO)_5$(1-hexene), in which W is bonded to the alkene donor of 1-hexene, does not absorb significantly past 400 nm as is seen from steady state studies. In the transient spectra, the $W(CO)_5$(alkyl) transient decays to form the final $W(CO)_5$(1-hexene) product between 50 ps and 10 nanoseconds. The

Table 3.11. Calculated Molar Extinction Coefficients of transients from $W(CO)_5L$ in cyclohexane at 50 ps

L	λ(nm)	ε($lmole^{-1}cm^{-1}$)	log ε	$log_{450}/log\ \varepsilon_{475}$
CO	450.2	1705 ± 75	3.23	1.09
	475.6	915 ± 50	2.96	
pyr	450.2	2200 ± 150	3.34	1.07
	475.6	1285 ± 95	3.11	
pip	450.2	2410 ± 100	3.38	1.11
	475.6	1095 ± 60	3.04	
Av:	450.2	2045 ± 330	3.31	1.09
	475.6	1115 ± 250	3.05	

Table 3.12. Calculated Molar Extinction Coefficients of transients for $W(CO)_5L$ in 1-hexene at 50 ps

L	λ(nm)	ε($lmole^{-1}cm^{-1}$)	log ε	$log\ \varepsilon_{450}/log\ \varepsilon_{475}$
CO	450.2	851 ± 26	2.97	1.10
	475.6	470 ± 20	2.68	
pyr	450.2	980 ± 100	2.99	1.09
	475.6	565 ± 70	2.75	
pip	450.2	1780 ± 75	3.25	1.09
	475.6	800 ± 76	2.99	
1-hexene	450.2	20.4 ± 4	steady state	
	475.6	15.2 ± 2		

Figure 3.26. Transient absorption spectra of $W(CO)_6$ in 1-hexene between 0 picoseconds and 10 nanoseconds under 355 nm irradiation.

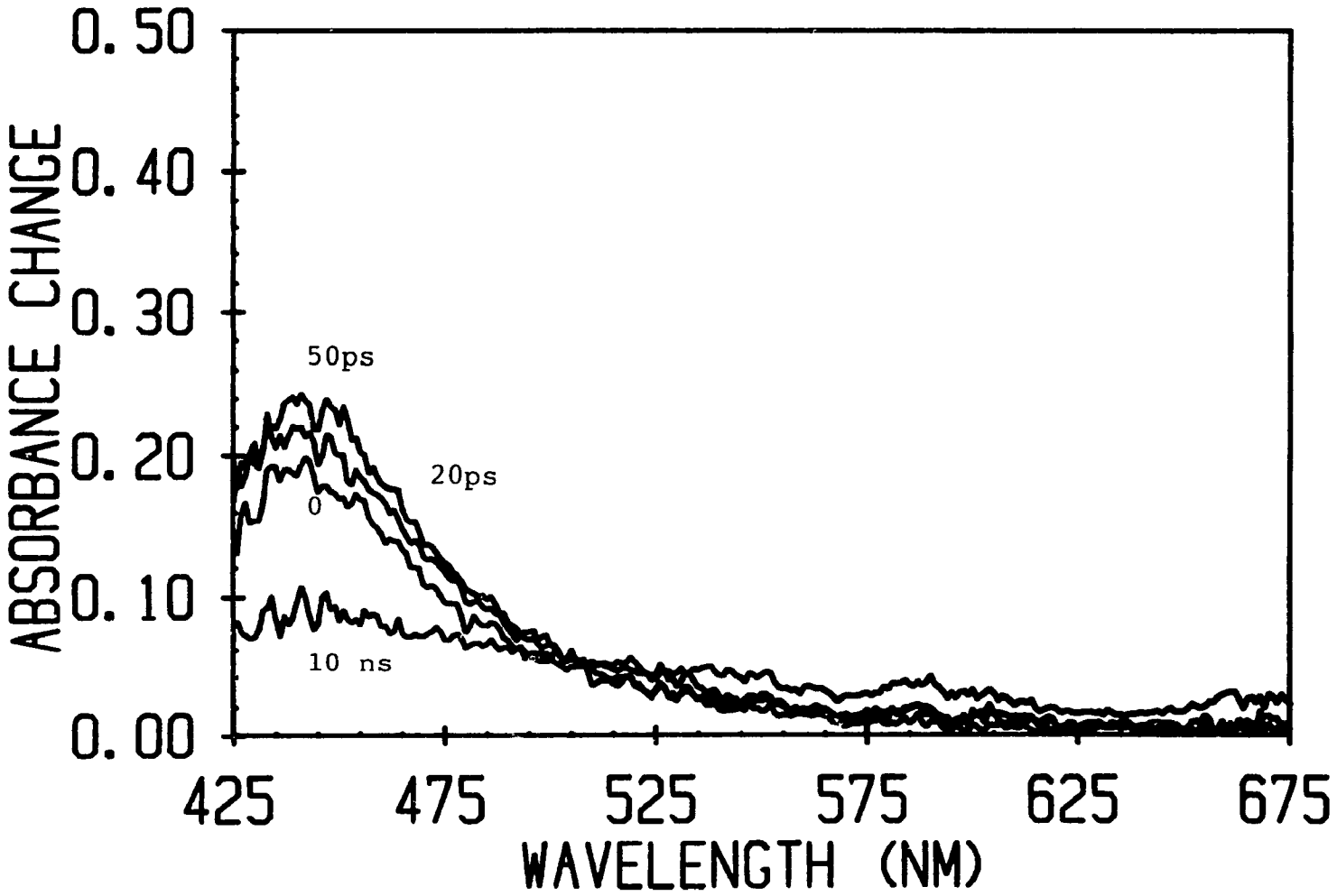

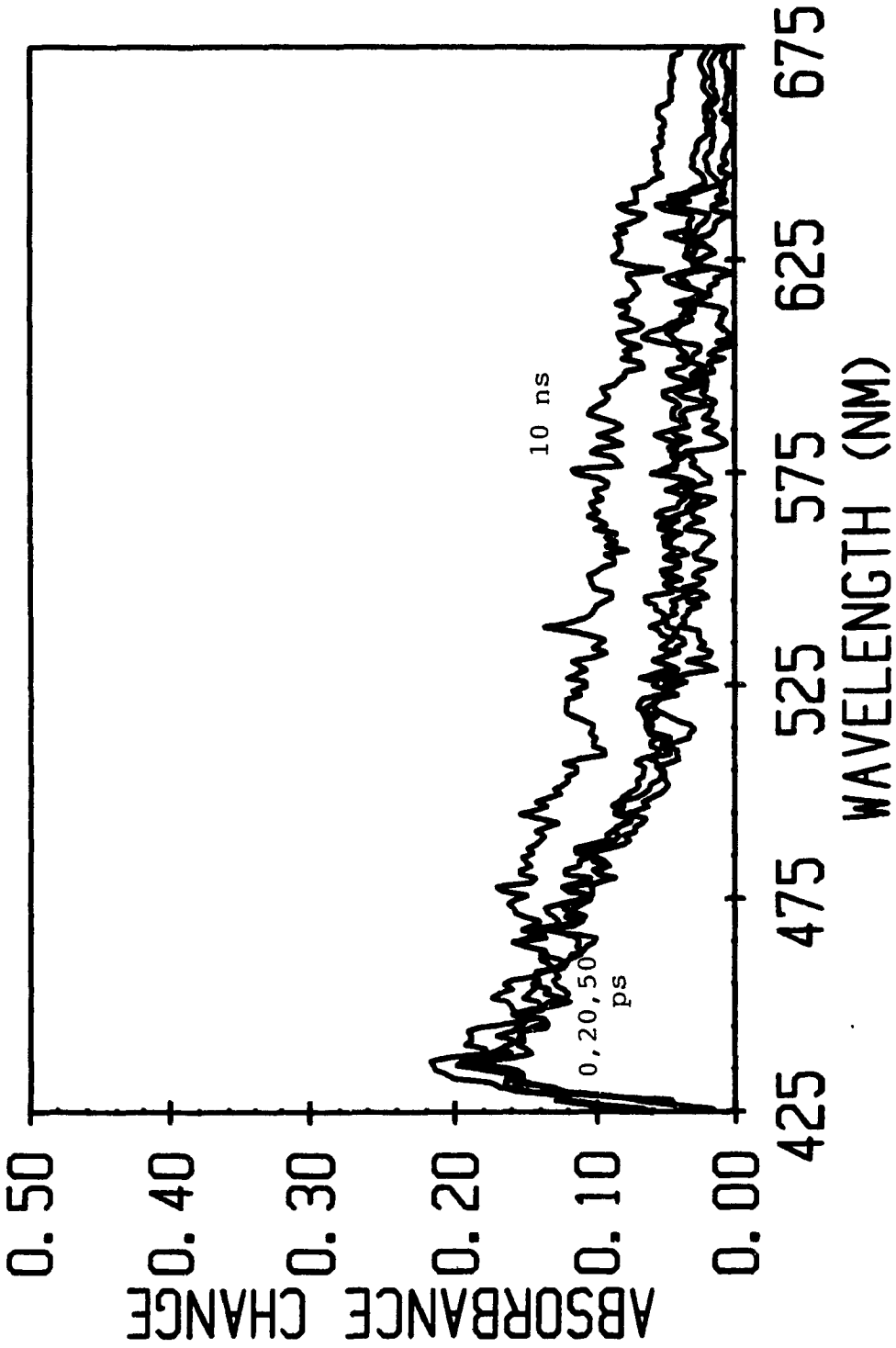

Figure 3.27. Transient absorption spectra of $W(CO)_5$pyr in 1-hexene between 0 picoseconds and 10 nanoseconds under 355 nm irradiation.

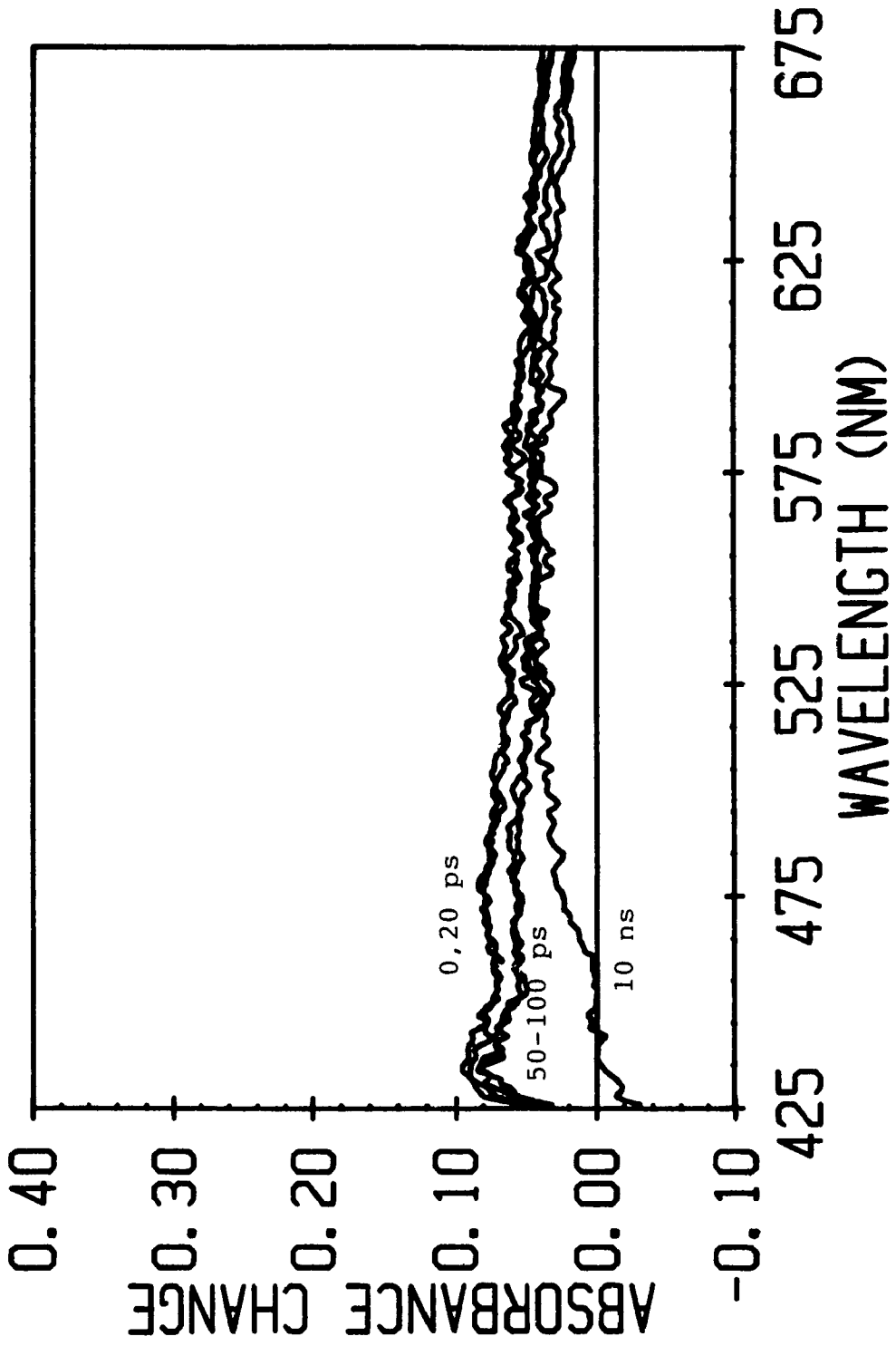

Figure 3.28. Transient absorption spectra of $W(CO)_5$pip in 1-hexene between 0 picoseconds and 10 nanoseconds under 355 nm irradiation.

time constant for formation of $W(CO)_5$(alkyl) from $W(CO)_6$ in 1-hexene is ~ 25 picoseconds, as is observed for this complex in cyclohexane. The transient absorption spectra of $W(CO)_6$ in 1-hexene between 50 ps and 5 ns are shown in Figure 3.29. The transformation time constant is ~ 600 ps. Studies at -10°C are shown in Figure 3.30. The activation energy calculated for the rearrangement is approximately 1 kcal/mole. This indicates that little barrier to rotation from alkyl to alkene products exist. The spectra of $W(CO)_5$pyridine in 1-hexene (Figure 3.27) are very similar between 0 and 50 picoseconds to that observed for this complex in cyclohexane indicating that the initial transient is $W(CO)_5$(alkyl) which is fully developed within 20 picoseconds. At 10 ns, considerable absorbance is observed between 525 and 675 nm. This absorbance is typical of light scattering caused by the presence of a precipitate. The spectra for $W(CO)_5$piperidine shows some similarities to its spectra in cyclohexane (Figure 3.28). At 50 ps, there is some observable absorbance between 425 and 500 nm but there is also considerable absorbance between 525 and 675 nm. At 10 ns, the absorbance has decayed between 425 and 500 nm to negative values. This ground state bleaching suggests that conversion to the 1-hexene product has occurred. The absorbance between 525 and 675 remains reflecting possible light scattering from precipitation. The extinction coefficients have been calculated for the transients in this solvent. Molar extinction coefficients for $W(CO)_5$(1-hexene) at these wavelengths are also given for comparison. The values are given in Table 3.12. The values reported for $W(CO)_5$piperidine may be suspect. This is due to the greater absorbance at longer wavelengths observed for this complex compared to either of the other two complexes. As is observed, the values are approximately 30-50% of the average value reported for the $W(CO)_5$(cyclohexane) transient at 50 ps. Since the highest transient absorbance is observed at 50 ps for both solvents, comparison of the

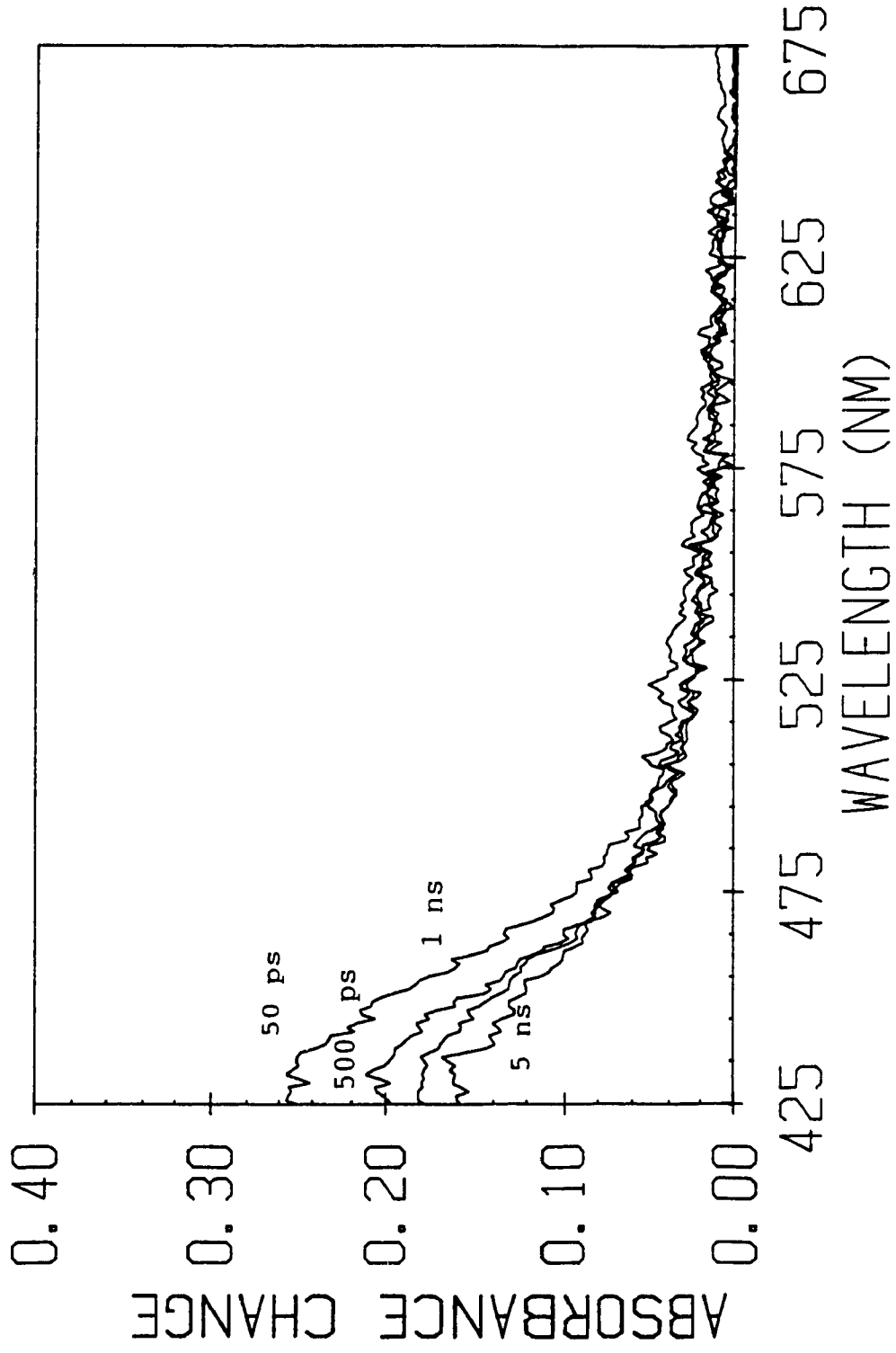

Figure 3.29. Transient absorption spectra of $W(CO)_6$ in 1-hexene between 50 ps and 5 ns at 23°C under 355 nm irradiation.

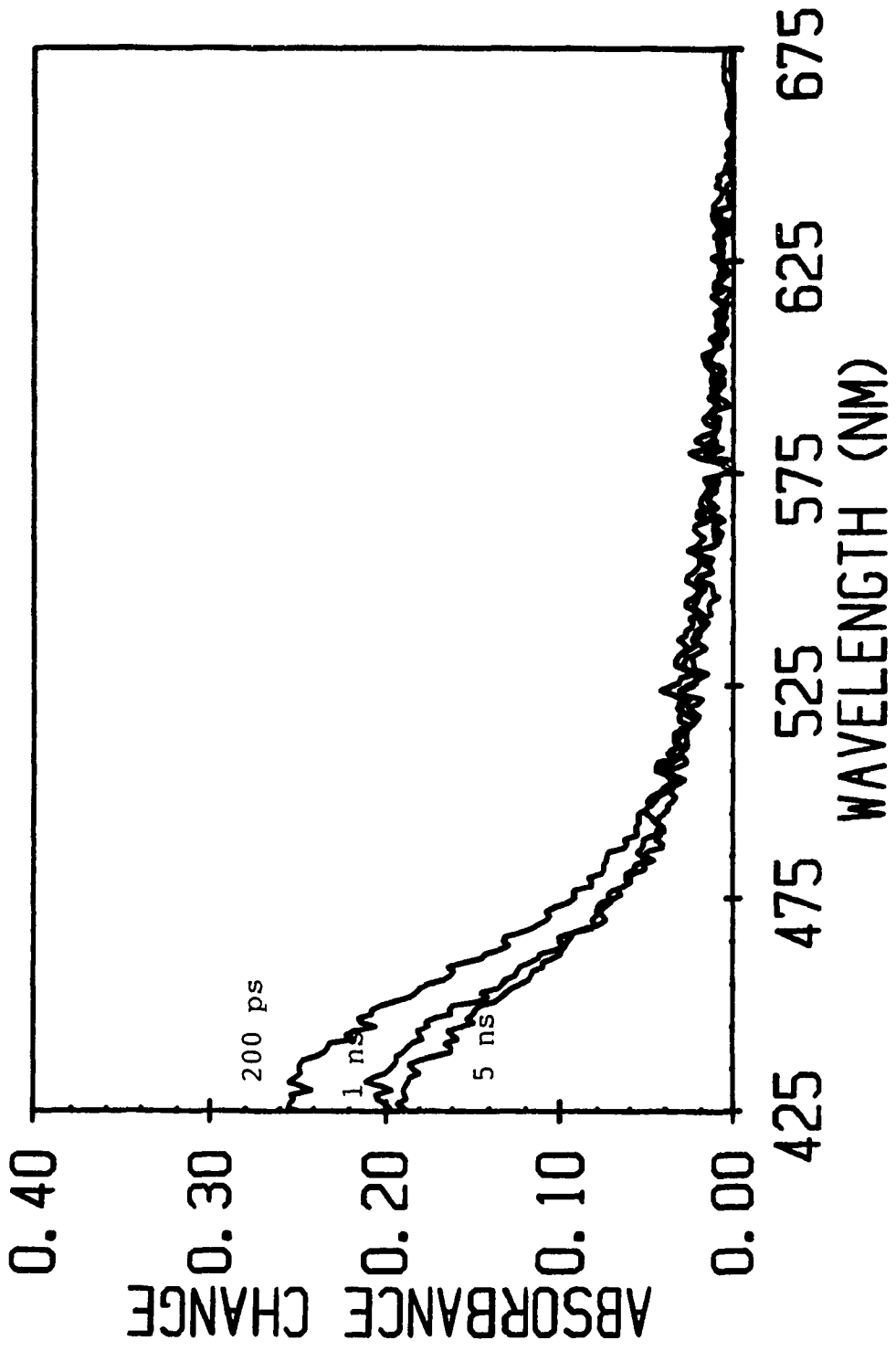

Figure 3.30. Transient absorption spectra of $W(CO)_6$ in 1-hexene between 200 ps and 5 ns at -100 C under 355 nm irradiation.

extinction coefficients suggests that, initially, ≤ half of the molecules undergo coordination with the alkyl portion of the 1-hexene chain. Unlike cyclohexane, 355 nm photolysis of $W(CO)_5$pyr and $W(CO)_5$pip in 1-hexene leads to precipitation. The observed rise at 10 ns for these complexes may indicate that light scattering by the precipitate is occurring.

Steady state photolysis of all three complexes in alcohols show that the electronic spectra of the $W(CO)_5$(alcohol) product has a peak at 418 nm. The picosecond spectra of all three complexes in methanol, butanol, and octanol (Figures 3.31 - 3.39) reveal the presence of a peak at approximately 440 nm. The shape of the peak is narrower than the peak observed for these complexes in cyclohexane and appears to be slightly blue-shifted. For $W(CO)_6$, the behavior in methanol (Figures 3.31) differs from that observed in either butanol or octanol (Figures 3.32 and 3.33). Peak absorbances increase from 0 ps to 10 ns but these increases are not as large as those observed for this complex in cyclohexane. In butanol and octanol, the peak has shifted further to the blue. The peak intensities are the same between 0 and 100 ps but they drop significantly at 10 ns. Absorbances also increase in the 525-675 nm region. For $W(CO)_5$pyridine, the behavior is similar to that of $W(CO)_6$. Differences between successive peaks are hard to discern . The intensity of the 10 ns peak is greater than the 0 ps peak for methanol (Figure 3.34), butanol (Figure 3.35), and octanol (Figure 3.36). Comparison of the spectra indicate that the transient band broadens as the alcohol changes in the order methanol < butanol < octanol. The octanol transient band is closest to matching the broadness of the cyclohexane peak observed for this complex. The behavior for $W(CO)_5$pip is different in all three alcohols. In methanol (Figure 3.37), the peak intensities between 0 and 100 ps are similar and there is a sharp increase at 10 ns. The presence of a peak centred at approximately

Figure 3.31. Transient absorption spectra of $W(CO)_6$ in methanol between 0 ps and 10 ns under 355 nm irradiation.

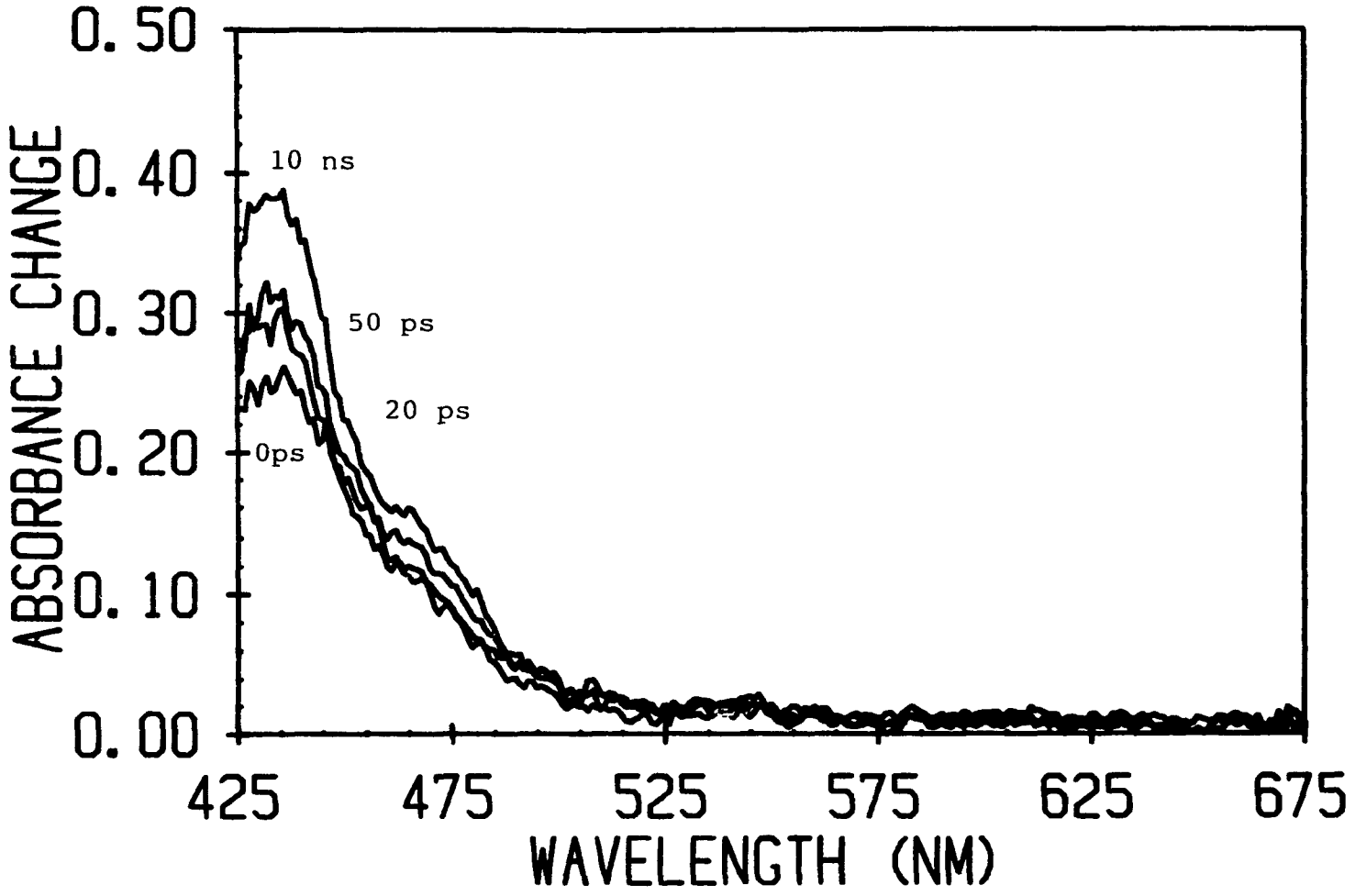

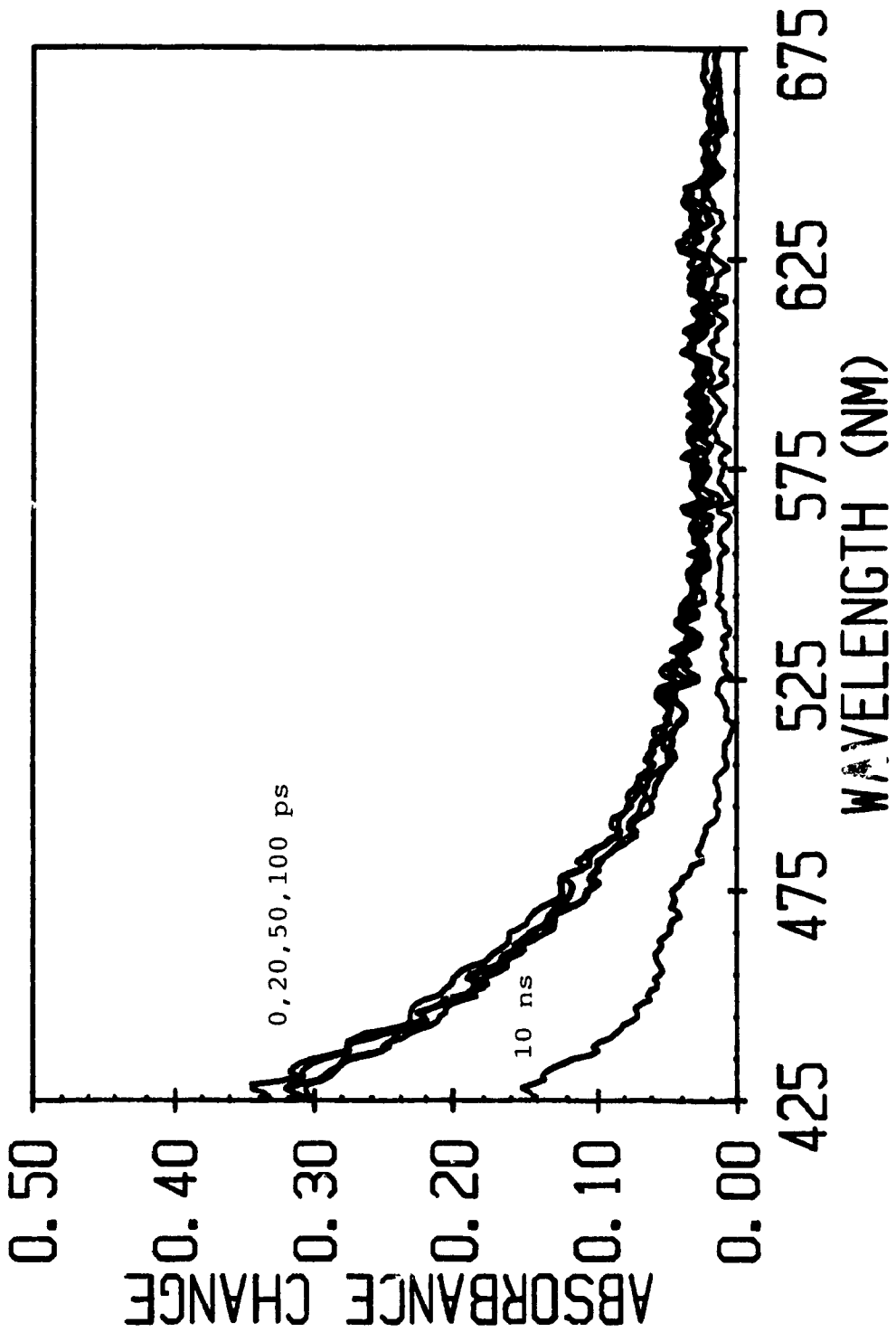

Figure 3.32. Transient absorption spectra of $W(CO)_6$ in n-butanol between 0 ps and 10 ns under 355 nm irradiation.

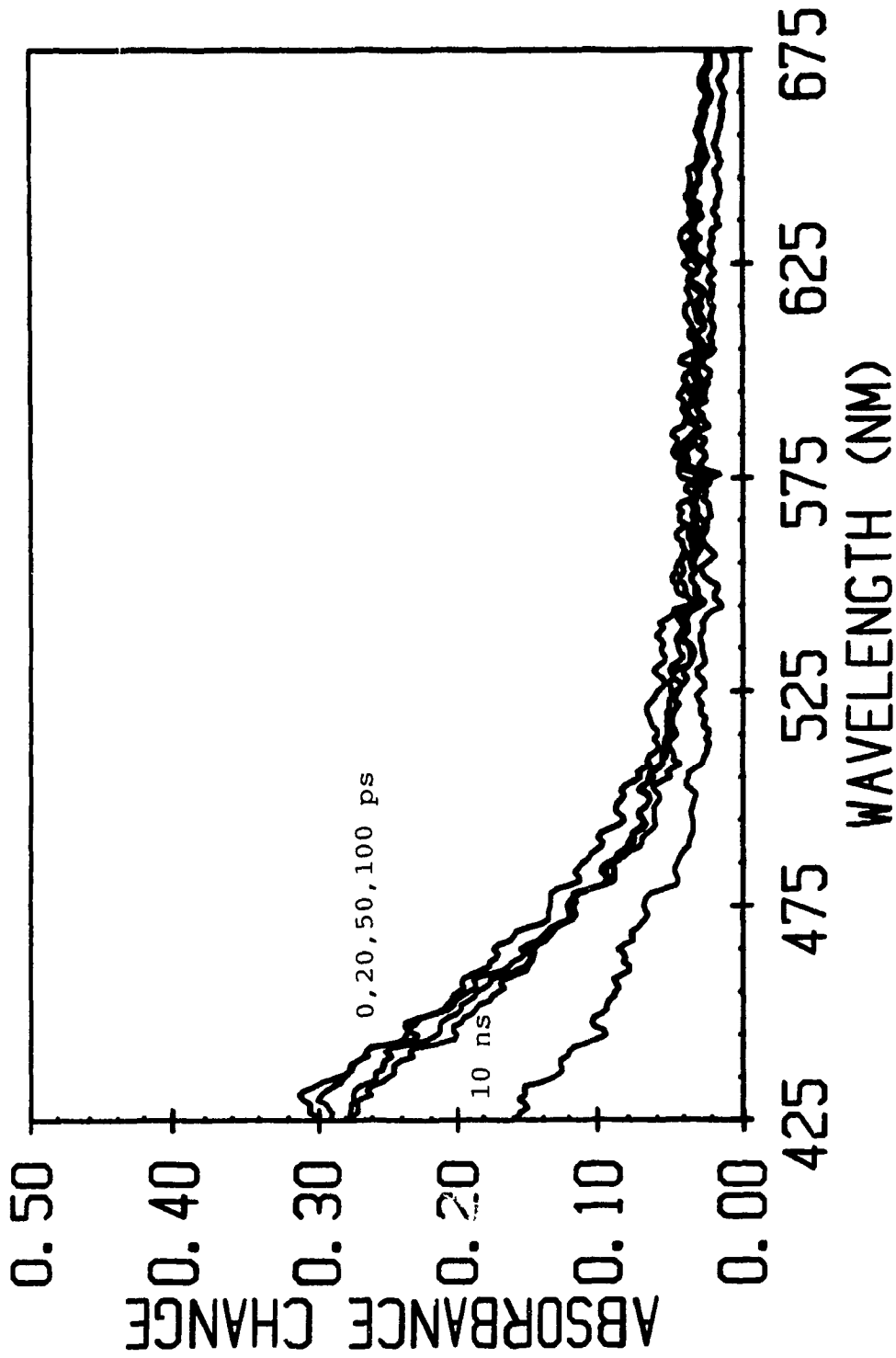

Figure 3.33. Transient absorption spectra of $W(CO)_6$ in n-octanol between 0 ps and 10 ns under 355 nm irradiation.

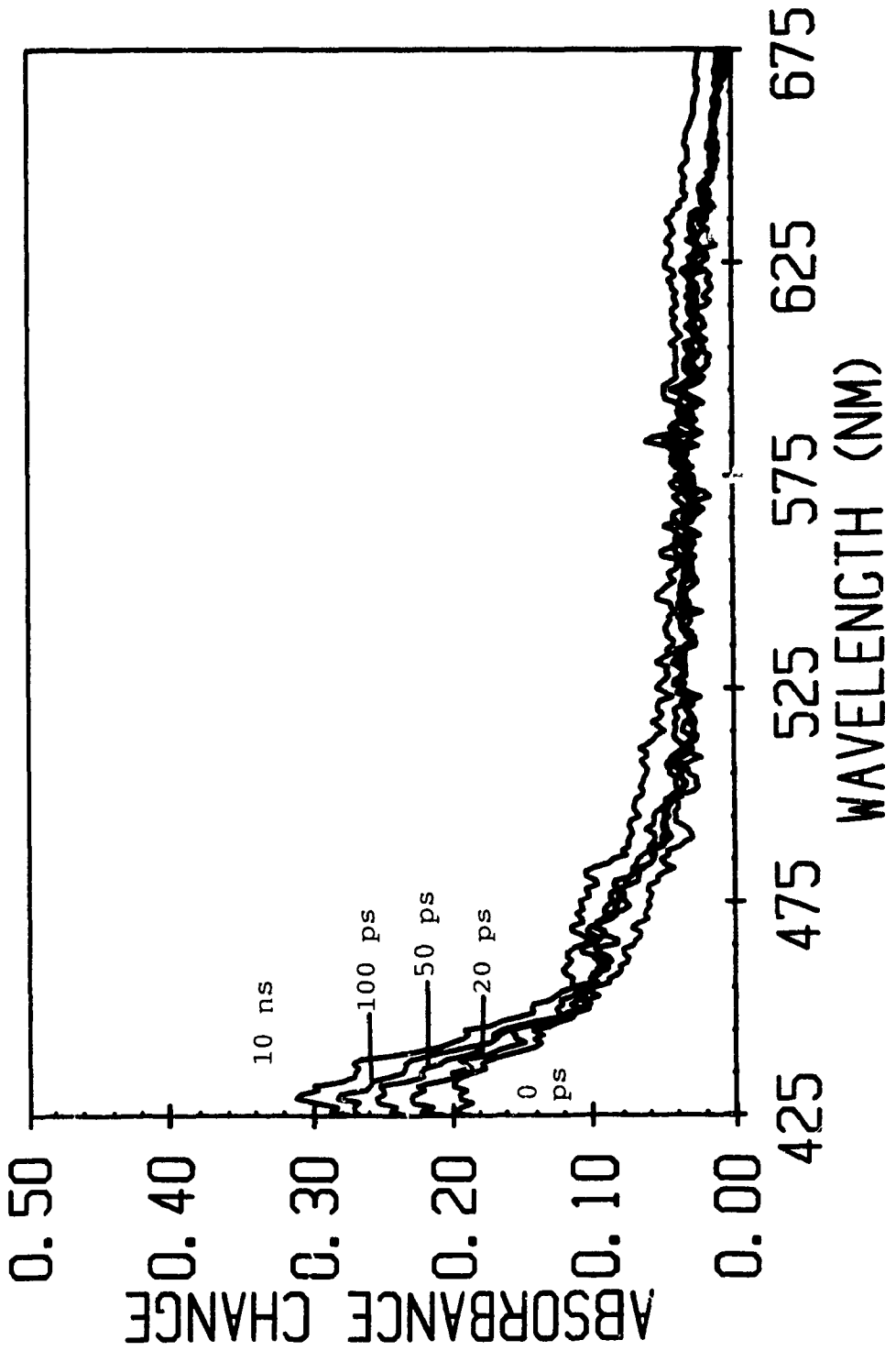

Figure 3.34. Transient absorption spectra of $W(CO)_5pyr$ in methanol between 0 ps and 10 ns under 355 nm irradiation.

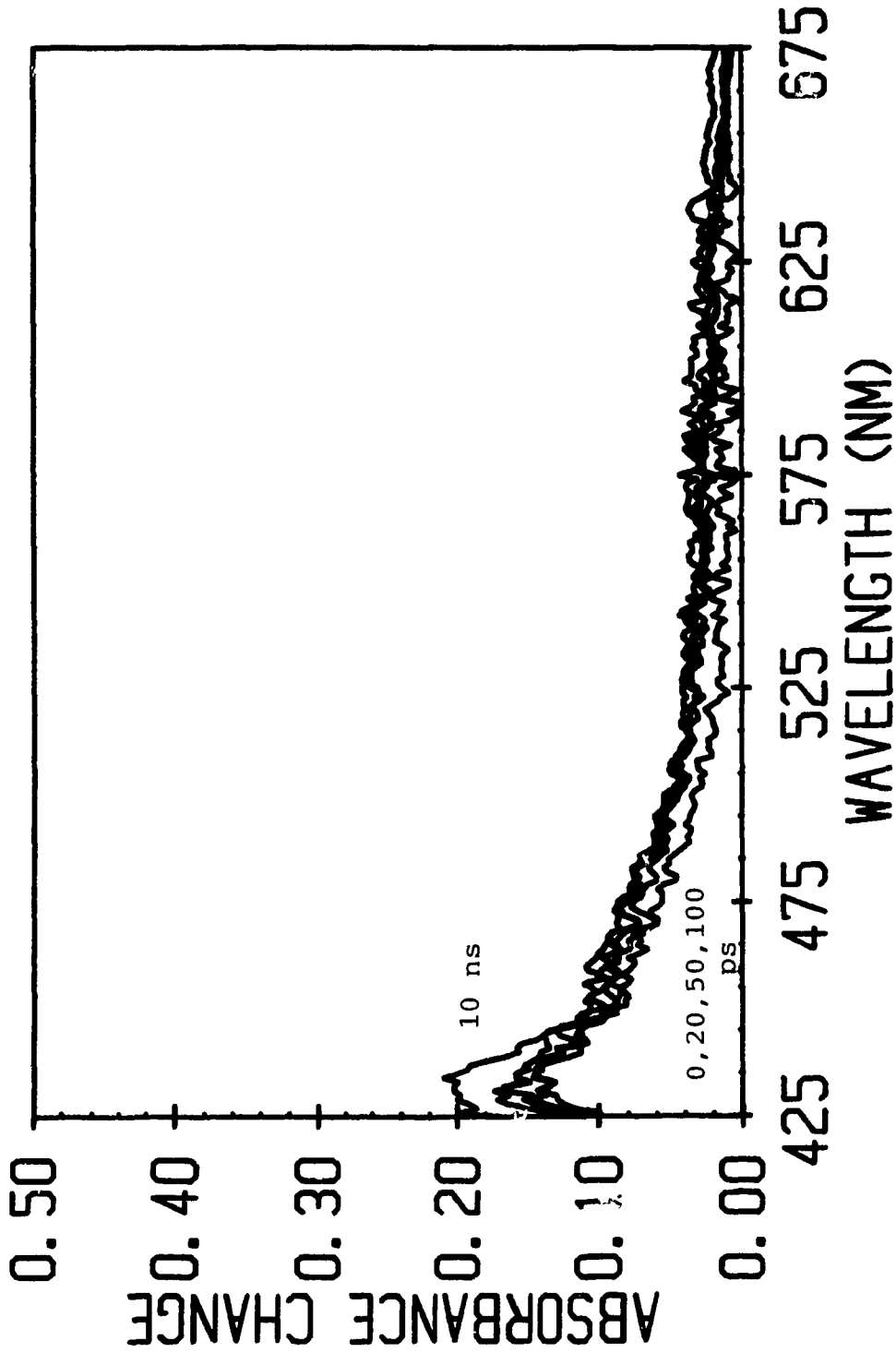

Figure 3.35. Transient absorption spectra of $W(CO)_5$pyr in n-butanol between 0 ps and 10 ns under 355 nm irradiation.

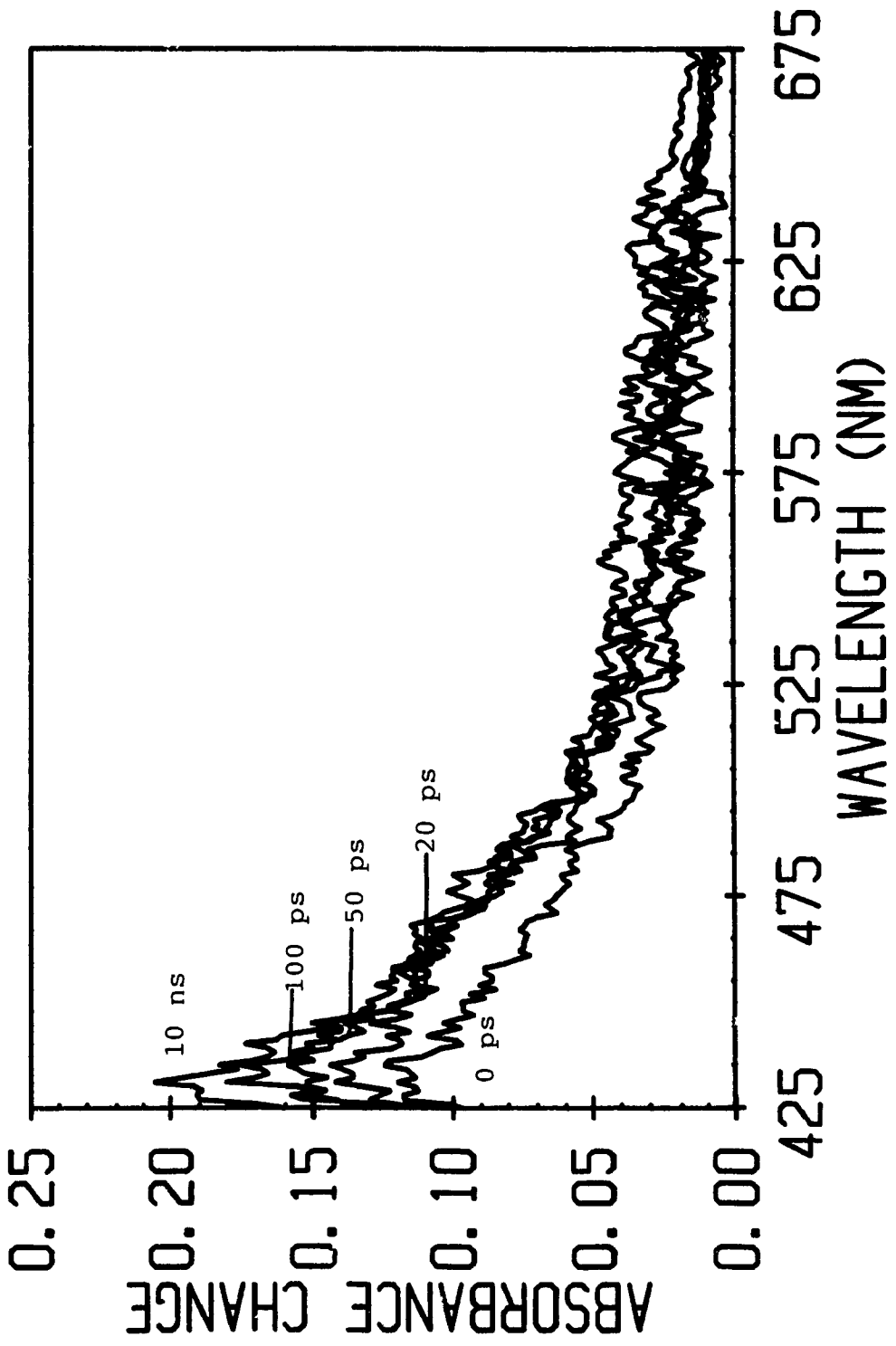

Figure 3.36. Transient absorption spectra of $W(CO)_5$pyr in n-octanol between 0 ps and 10 ns under 355 nm irradiation.

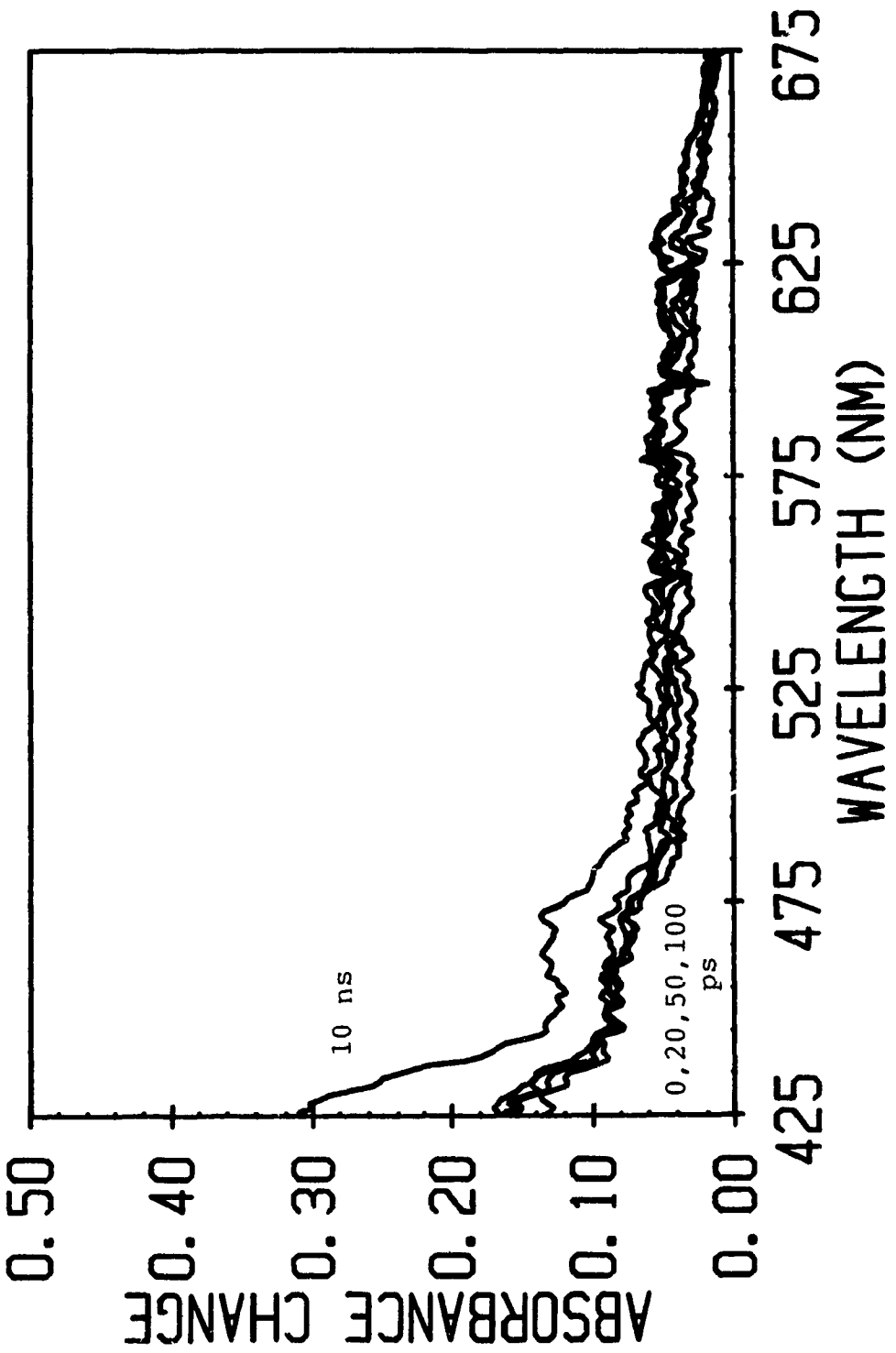

Figure 3.37. Transient absorption spectra of $W(CO)_5$pip in methanol between 0 ps and 10 ns under 355 nm irradiation.

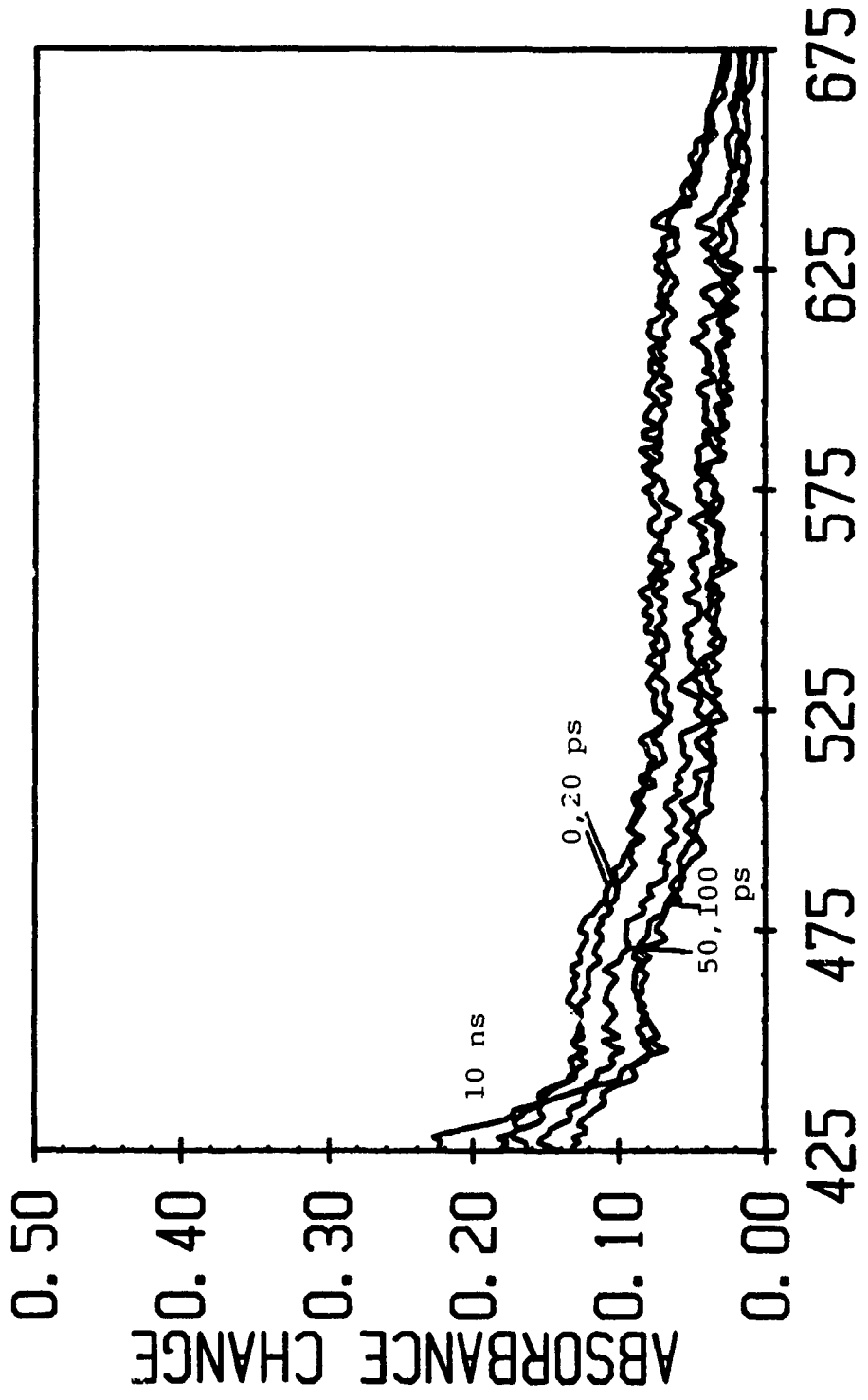

Figure 3.38. Transient absorption spectra of $W(CO)_5$pip in n-butanol between 0 ps and 10 ns under 355 nm irradiation.

Figure 3.39. Transient absorption spectra of $W(CO)_5$pip in n-octanol between 0 ps and 10 ns under 355 nm irradiation.

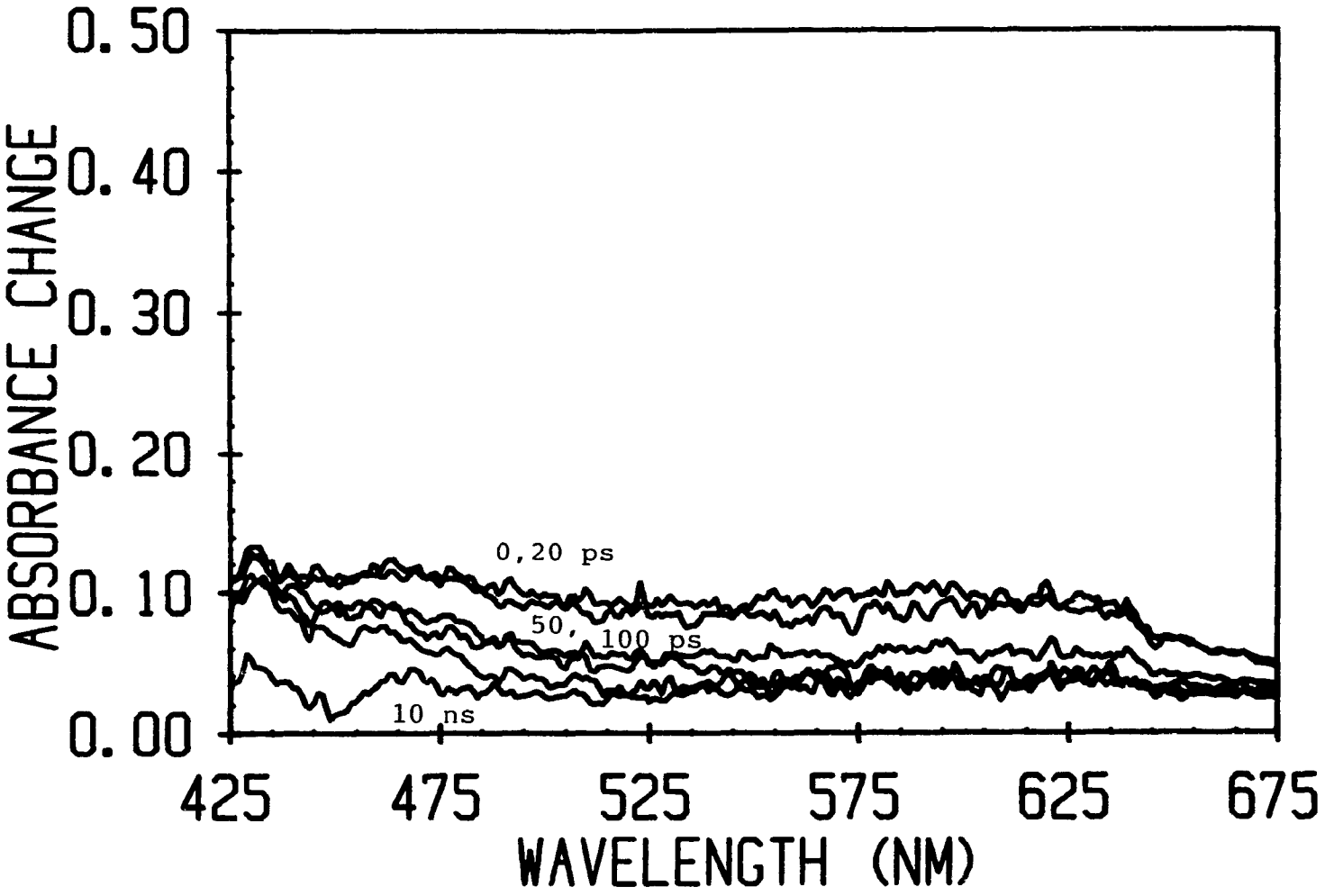

465 nm is apparent at 10 ns. In butanol (Figure 3.38), the peak intensities between 0 and 20 ps are similar and higher than those observed for 50 and 100 ps. The intensity of the peak at 10 ns decreases at around 450-675 nm while it increases at 425 nm relative to the other peaks. Initial absorbances in the 525-675 nm are higher than those observed in cyclohexane for this compound. They decrease between 0 ps and 10 ns for all three alcohols. In octanol (Figure 3.39), the behavior between 0 and 1 ns is similar to that observed for butanol except that the absorbances between 425 and 475 nm decrease while the absorbance between 525 and 675 nm does not change. The peaks are considerably blue shifted as compared to the peak observed for this complex in cyclohexane but the broadness remains. The peak shapes for the alcohol spectra do not correspond as closely to the cyclohexane spectra as do the spectra in 1-hexene. Since the tails of the $W(CO)_5$(alcohol) bands absorb at these wavelengths, the possibility exists that these spectra are composed of both alcohol and alkyl products.

Using the average value calculated for the extinction coefficient of the $W(CO)_5$(cyclohexane) transient and the average value for the extinction coefficients of the $W(CO)_5$(1-hexene) and $W(CO)_5$(OH) products from steady state photolysis, approximate percentages of alkyl transients at 50 ps can be determined for the 1-hexene, butanol and octanol solvents. The alcohol products absorb significantly (Table 3.13) at the wavelength used for the calculation of the alkyl percentages and this absorbance must be taken in account. The 1-hexene products where W is bonded to the double bond of the 1-hexene do not absorb significantly at these wavelengths and the calculations become simpler. The method for calculating these percentages is given in Appendix C. The alkyl percentages are given in Table 3.14. In all three solvents, the percentages of the alkyl transients for $W(CO)_6$ are lower than those for either $W(CO)_5$pip or $W(CO)_5$pyr. In the alcohols, the alkyl

Table 3.13. Calculated Molar Extinction Coefficients of $W(CO)_5L'$ from steady state photolysis of $W(CO)_5L$

L	L'	λ(nm)	ε($l mole^{-1} cm^{-1}$)	log ε	log ε_{450}/log ε_{475}
CO	MeOH	450.2	730 ± 75	2.86	1.13
		475.6	350 ± 35	2.54	
pyr		450.2	845 ± 75	2.93	1.13
		475.6	385 ± 35	2.59	
pip		450.2	705 ± 100	2.85	1.14
		475.6	310 ± 40	2.49	
CO	BuOH	450.2	750 ± 75	2.88	1.13
		475.6	350 ± 35	2.54	
pyr		450.2	935 ± 75	2.97	1.13
		475.6	425 ± 40	2.63	
pip		450.2	690 ± 25	2.84	1.15
		475.6	290 ± 25	2.46	
CO	OcOH	450.2	650 ± 75	2.81	1.10
		475.6	365 ± 35	2.56	
pyr		450.2	970 ± 50	2.98	1.12
		475.6	460 ± 30	2.66	
pip		450.2	750 ± 60	2.88	1.15
		475.6	315 ± 40	2.50	
Av:		450.2	780 ± 110	2.89	1.13
		475.6	360 ± 55	2.56	

Table 3.14. Calculated Alkyl Transient Percentages for $W(CO)_5L$ at 50 ps[a]

L	Solvent	450.2 nm
CO	Butanol	3
	Octanol	15
	1-hexene	41
pyr	Butanol	69
	Octanol	100
	1-hexene	48
pip	Butanol	91
	Octanol	115
	1-hexene	80

a) errors are approximately ± 20%

Table 3.15. Bond Lengths in the ground electronic state of $W(CO)_5L$

Bond	Length (Å)	
	L	
	Pip	Pyr (ref 10)
W-C (axial)	1.96 ± .006	2.00 ± .01
W-C (equatorial)	2.04 ± .007	2.04 ± .02
W-N	2.33 ± .005	2.26 ± .01
C-O (axial)	1.16 ± .008	1.13 ± .01
C-O (equatorial)	1.16 ± .009	1.12 ± .02

percentages are lower for butanol than octanol for all three complexes. These values are not considered to be absolute since they are based on a number of assumptions, however, they can be examined to determine if trends exist. The higher value for the piperidine complex in 1-hexene may be due to problems with light scattering which increase the absorbance values throughout the entire spectrum compared to either $W(CO)_5$pyr or $W(CO)_6$.

Figure 3.40 shows the transient absorption behavior of $W(CO)_5$pyridine in CCl_4/cyclohexane between 0 ps and 10 ns. A blue precipitate is formed during the irradiation. This accounts for the observed scattering in the spectra. Between 0 ps and 10 ns, there is no evidence of coordination to cyclohexane as is observed with this complex in other solvents which have alkyl chains. The quantum yields in this solvent are the highest for this complex.

3.6. X-Ray Crystallography.

The space group for $W(CO)_5$piperidine is $P2_1/C$. The bond lengths are given in Table 3.15. The length of the tungsten-nitrogen bond is 2.33 Å. The length of the carbon-tungsten bond trans to the piperidine ligand is 1.96 Å. The lengths of the cis W-C bonds are 2.04 Å. An ORTEP diagram is shown in Figure 3.41.

Figure 3.40. Transient absorption spectra of $W(CO)_5$pyr in Carbon tetrachloride/cyclohexane (2:1 v/v) between 0 ps and 10 ns under 355 nm irradiation.

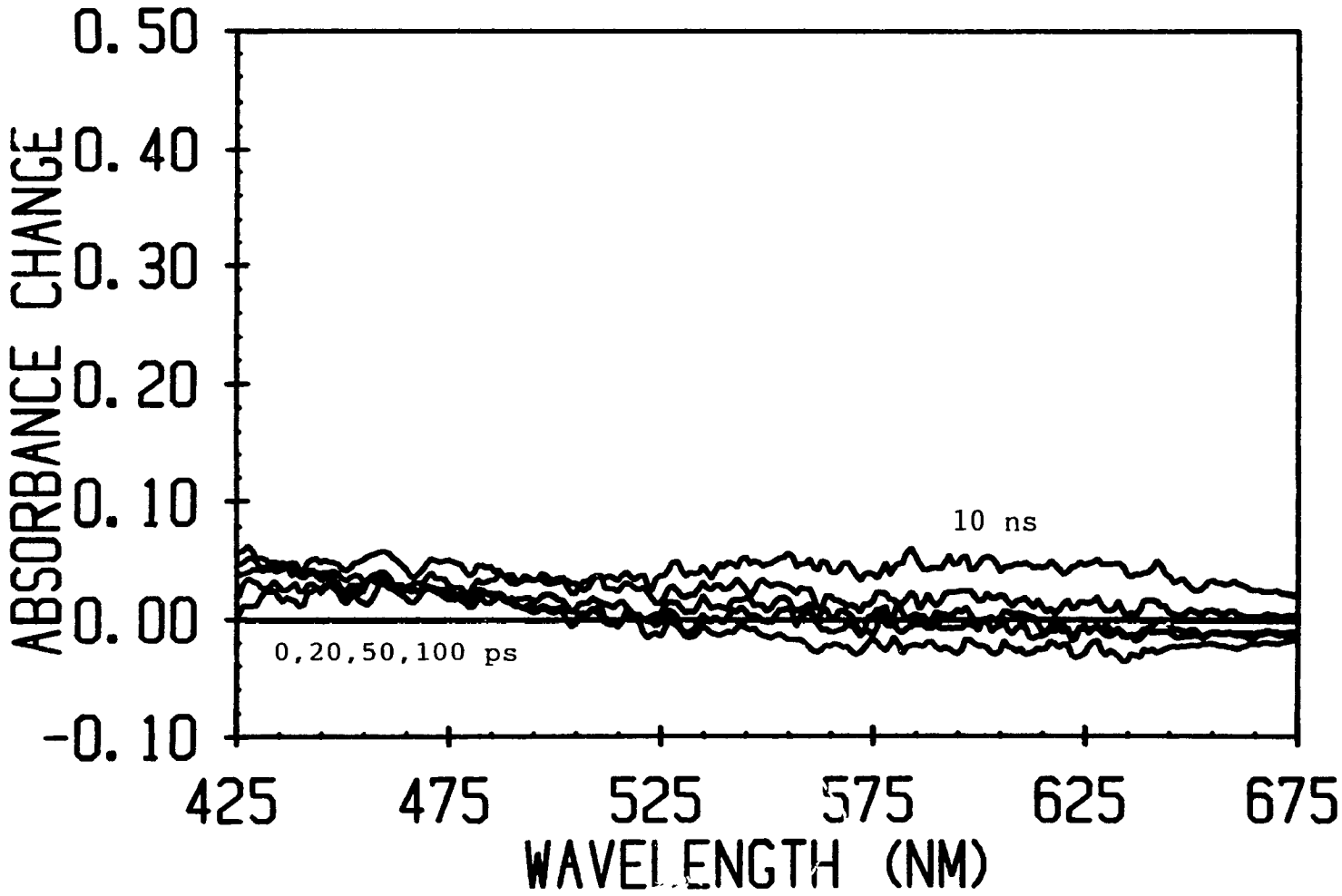

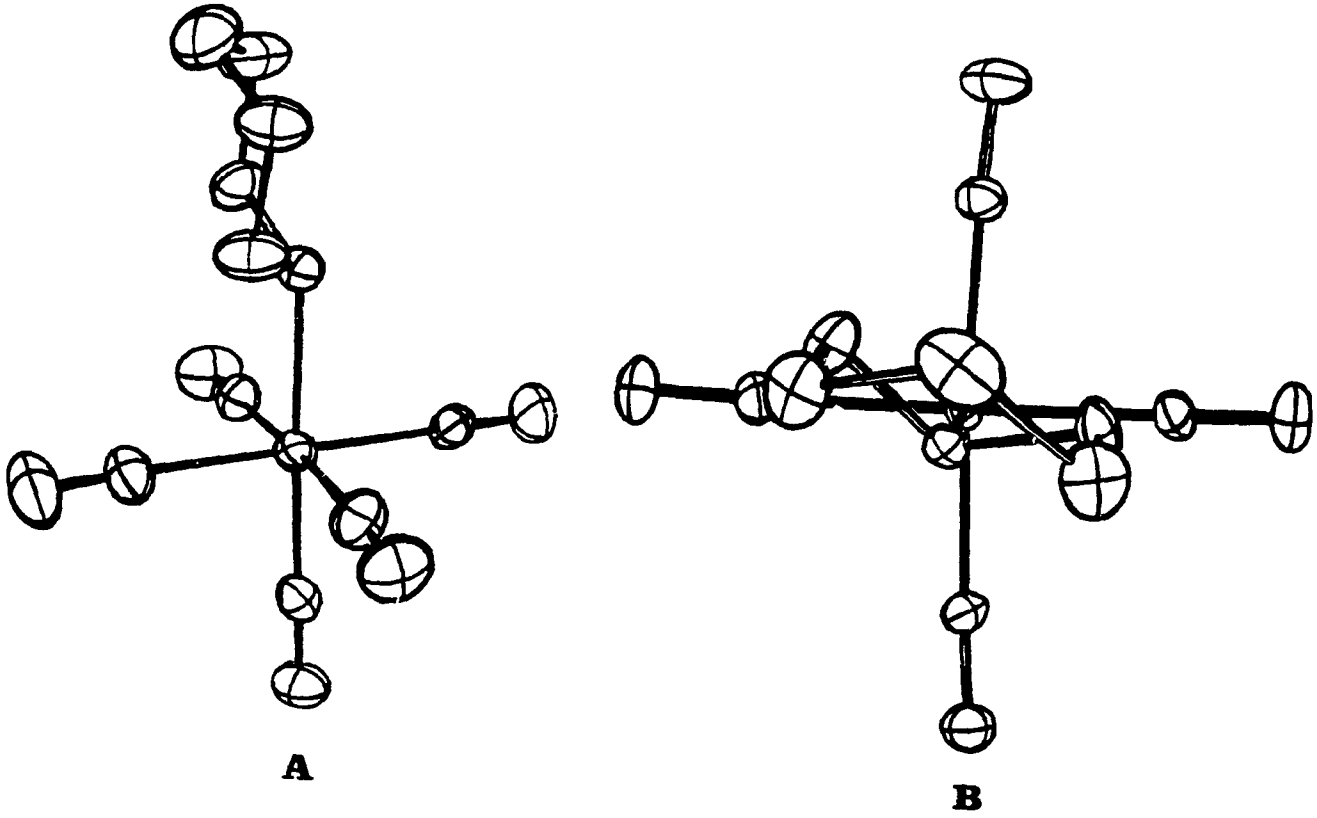

Figure 3.41. ORTEP diagram of W(CO)5piperidine: (A) side view, (B) view down Z axis through piperidine.

4. THEORY AND DISCUSSION

4.1. Bonding in $W(CO)_5L$

4.1.1. $W(CO)_6$

The orbitals which form σ and π-bonds between W and the CO ligands in an octahedral complex such as $W(CO)_6$ have been determined by application of group theory (103,104). Each orbital can be represented by a vector pointing in the appropriate direction for this octahedral complex (Figure 4.1), and the characters of the representation for which these vectors form a basis can be obtained. For the σ-orbitals, the reducible character set can be reduced to $A_{1g} + E_g + T_{1u}$. The corresponding atomic orbitals of W which fall into these categories are:

A_{1g} ---> s

E_g ---> dz^2,$dx^2 - y^2$

T_{1u} ---> px, py, pz

These orbitals will form σ-bonds with the CO ligands.

In a corresponding fashion, a set of π-orbitals can be obtained. π-orbitals differ from σ-orbitals in that they posses a nodal plane. The wave function at a nodal plane has zero amplitude because it changes sign upon passing from one side of the surface to the other. A π-orbital has one nodal surface containing the bond axis. Two orthogonal π bonds are possible between the same two atoms and the nodal planes associated with these orbitals will be mutually perpendicular to each other. Each of the π atomic orbitals for the CO ligands can be represented by a vector which is perpendicular to the nodal plane and points in the direction of the positive values of the wave function (Figure 4.1). The reducible character set for the π-orbitals is reduced to $T_{1g} + T_{2g} + T_{1u} + T_{2u}$. In O_h symmetry there are no metal

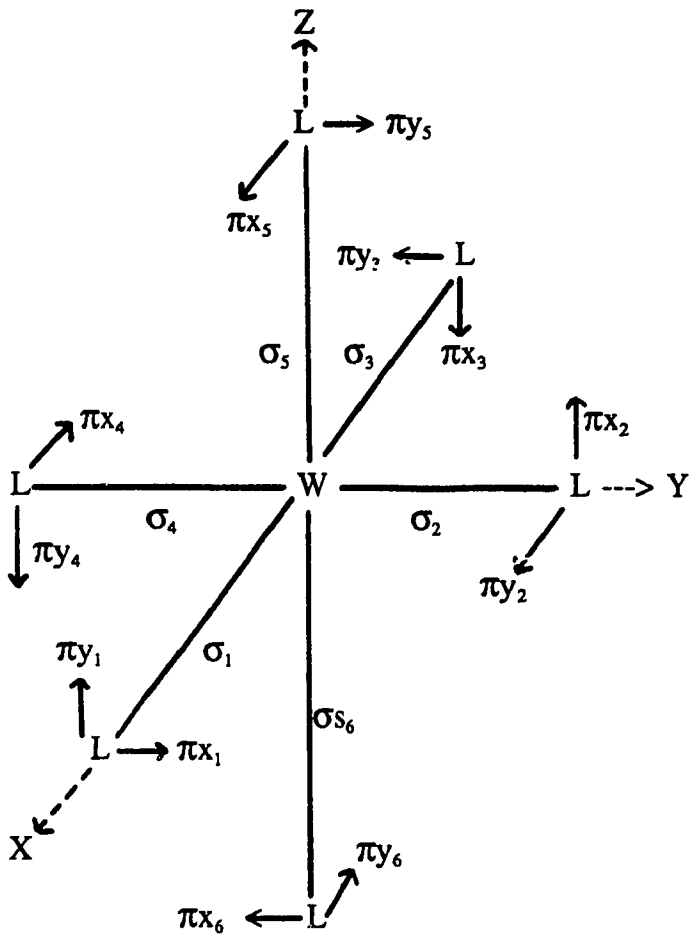

Figure 4.1. Simple diagram indicating vector directions for sigma and pi bonds in an octahedral complex (ref 103)

orbitals with T_{1g} and T_{2u} symmetries so these will be non-bonding in the metal. The corresponding atomic orbitals which fall under the T_{2g} and T_{1u} categores are:

T_{2g} ---> dxy, dyz, dxz

T_{1u} ---> px, py, px

π-bonding can therefore occur with these metal orbitals.

CO, which belongs to the $C_{\infty v}$ linear symmetry group, can form σ-bonds with its sp-hybridized orbital of A_1 symmetry and π-bonds with it Px or Py orbitals of E_1 symmetry. There are corresponding π^* orbitals as well.

A molecular orbital diagram can be constructed from these atomic orbitals in which overlap between orbitals of the same symmetry can occur (Figure 4.2).

B. $W(CO)_5L$ (L = pyridine, piperidine)

The metal orbitals which form σ-bonds with the 5 CO and 1 L ligands are determined in a similar fashion (106). For these orbitals, the reducible character set for these C_{4v} complexes reduces to $3A_1 + B_1 + E$. The corresponding metal orbitals are:

A_1 ---> pz, s, dz^2

B_1 ---> $dx^2 - y^2$

E ---> px, py, dxz, dyz

The σ-orbitals will consist of 3 orbitals of A_1 symmetry, one orbital of B_1 symmetry and 2 orbitals of E symmetry. Since the orientation of the orbitals in a C_{4v} complex is similar to that of an O_h complex, no σ-overlap is expected with the dxz

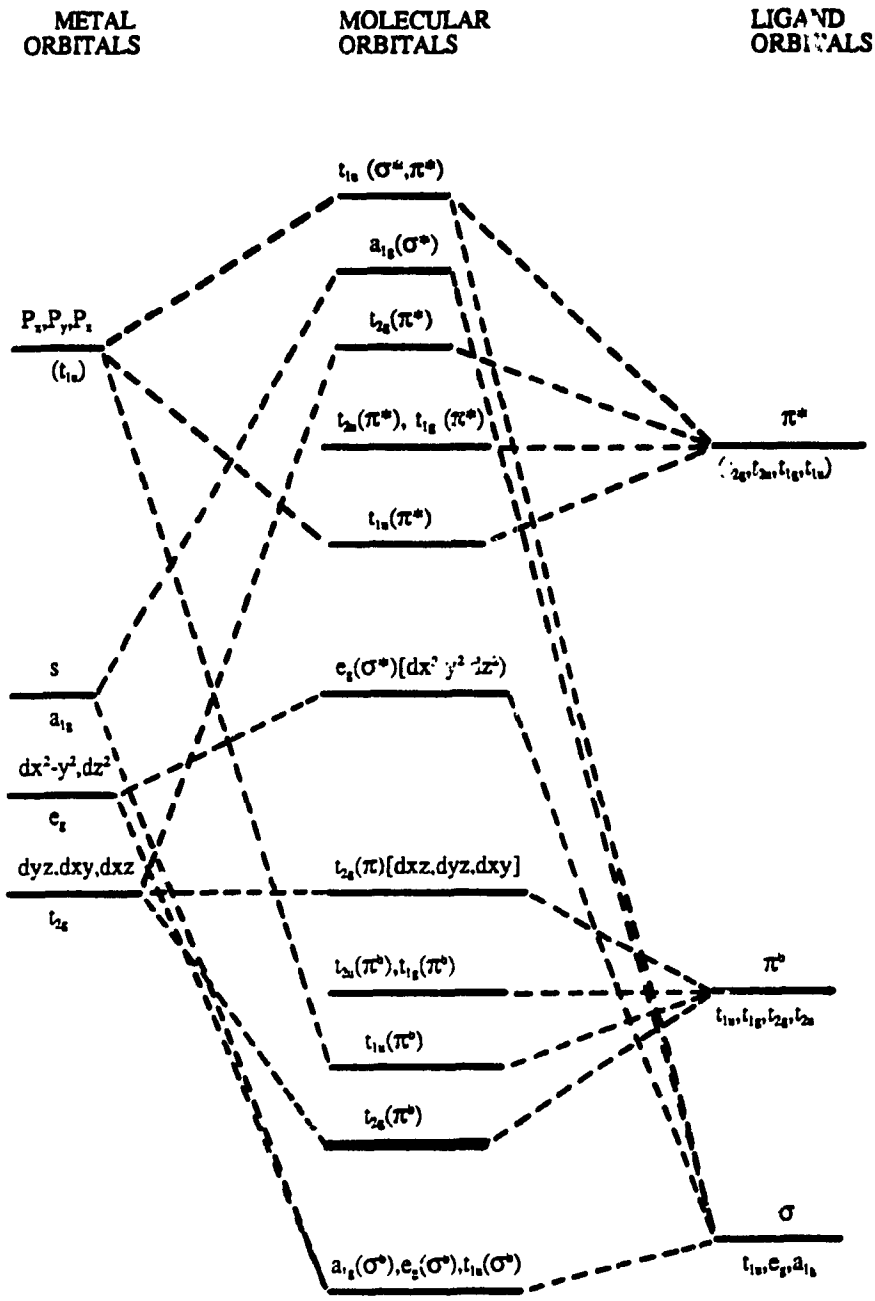

Figure 4.2. Molecular orbital diagram for a d^6 complex in an octahedral field. Interactions between the pi* orbitals of CO and the metal t_{2g} orbitals are not shown. The overlap between these two sets of orbitals would lower the energy of the molecular t_{2g} relative to the metal t_{2g} orbitals due to stabilization from metal to CO back-bonding (ref 104).

and dyz orbitals. The complete orbital set for σ-bonding will consist of the s,px,py,pz, dz^2 and dx^2-y^2 orbitals. The pyridine complex has low-lying π-orbitals which can accept electron density. The piperidine complex does not. A molecular orbital diagram of a C_{4v} complex is given in Figure 4.3.

In either octahedral or C_{4v} complexes, the number of electrons placed into the σ-bonding molecular orbitals is 18, 12 from the 6 ligand orbitals and 6 from the metal d orbitals. Electrons from the π orbitals of the ligands fill the π-bonding molecular orbitals. Excitation of an electron occurs generally from the highest occupied molecular orbital (HOMO) which is one of the metal t_{2g} orbitals to the lowest unoccupied molecular orbitals (LUMO) which is one of the e_g orbitals. The e_g orbitals are σ-antibonding orbitals. Excitation to higher orbitals is possible depending on the energy available.

4.2. Photoreactivity.

In this section, the following aspects observed for the photochemistry of both $W(CO)_5$pyr and $W(CO)_5$pip will be addressed. First, there is the observation that loss of L is preferred over loss of CO. Second, there is a wavelength dependence for LF singlet irradiation. Third, LF singlet yields are higher than LF triplet yields. Fourth, $W(CO)_5$pyridine undergoes photosubstitution of L under direct MLCT irradiation. Fifth, the solvent affects the yields for both complexes in a consistent manner.

4.2.1. Relationship between Reactivity and Spectroscopy.

The photosubstitution behavior observed in $W(CO)_5L$ complexes, where L is an N-donor, reveals that two distinct substitution processes, loss of L or loss of CO, can occur. In these C_{4v} complexes, by convention, loss of L can occur only from

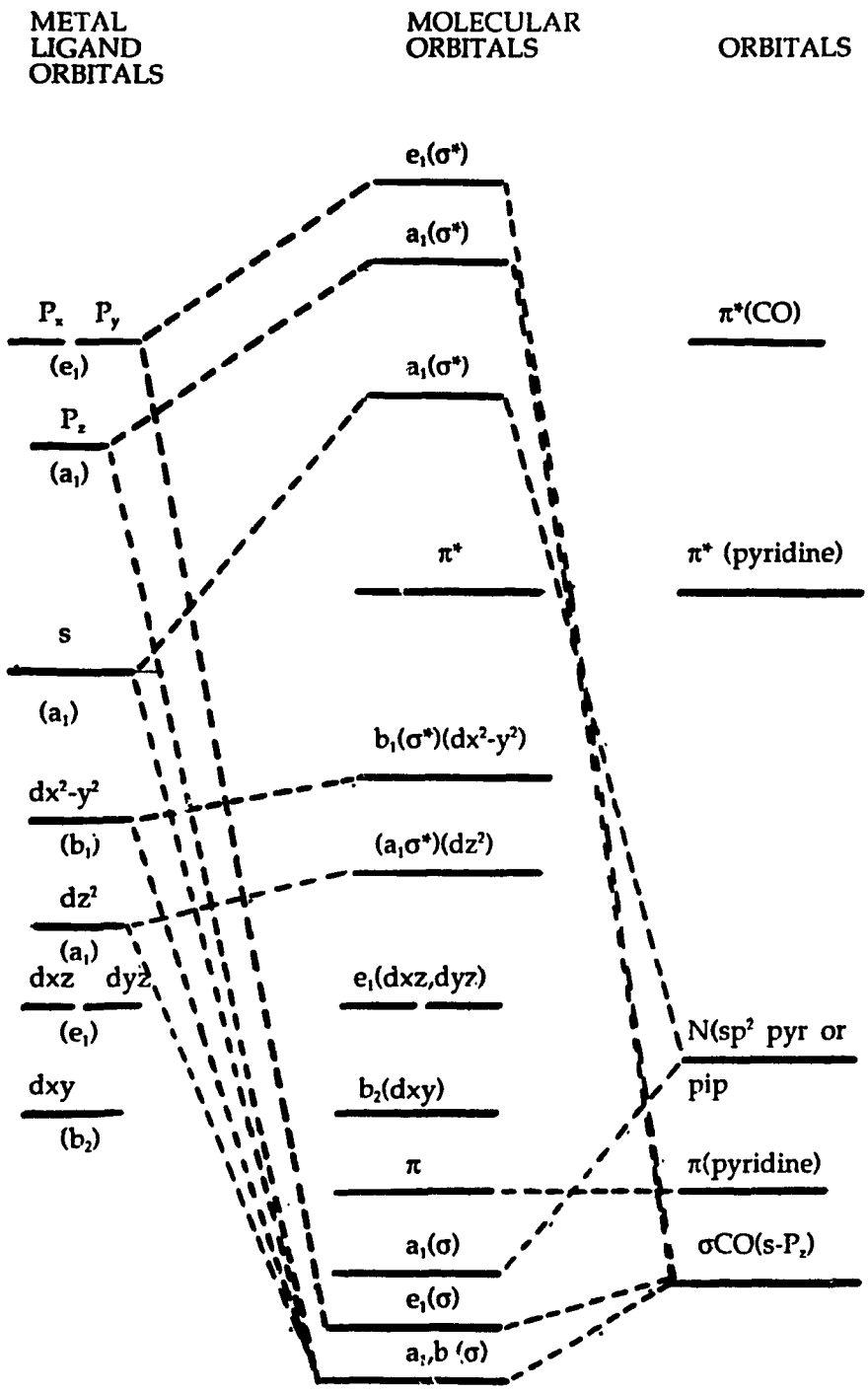

Figure 4.3. Simplified molecular orbital diagram for a C_{4v} complex $W(CO)_5$pyr or $W(CO)_5$pip.

an axial position in the molecule whereas loss of CO can occur from either an axial or an equatorial position. It is often observed that loss of CO is very inefficient as compared to loss of L and both processes are dependent on the wavelength of excitation. This observation suggests that not only is axial labilization more prominent than equatorial labilization but it is unidirectional as well since parallel loss of the CO trans to the L ligand upon low energy excitation is not competitive with loss of L.

Several theoretical models (107-111) have been proposed which attempt to account for observed photochemical behavior in transition metal complexes. One of the simplest models uses molecular orbital theory to predict which axis of a six-coordinate complex will be photolabilized by identifying which of the metal orbitals are predominant components of the photoactive state (110). In a d^6 octahedral complex, the lowest energy transition is t_{2g}^6 ---> $t_{2g}^5 e_g^1$ (Figure 4.4a). The e_g orbitals are σ-antibonding between the metal and the ligands and these orbitals consist of the degenerate dx^2-y^2 and dz^2 orbitals. The result is ejection of an equatorial or an axial ligand. For complexes such as $W(CO)_6$ in which the CO molecules are good π acceptor ligands, depopulation of the $d\pi$ t_{2g} orbitals which are π-bonding between metal and ligand, and population of the e_g σ^*-antibonding orbitals presumably leads to an increased excited state reactivity over complexes which are only good σ-donors. When the symmetry of the molecule is reduced to C_{4v}, the degeneracy of the e_g orbitals is lifted and the dz^2 orbital lowers in energy compared to the dx^2-y^2 orbital (Figure 4.4b). Population of either of these orbitals depends on the excitation energy. The lowest energy excitation is from the dxz, dyz orbitals to the dz^2 orbital. The ligands bonded in the dz^2 direction (axial to the metal) are expected to be labilized. In this circumstance, it is expected that selective labilization of one of the ligands on the z axis should occur.

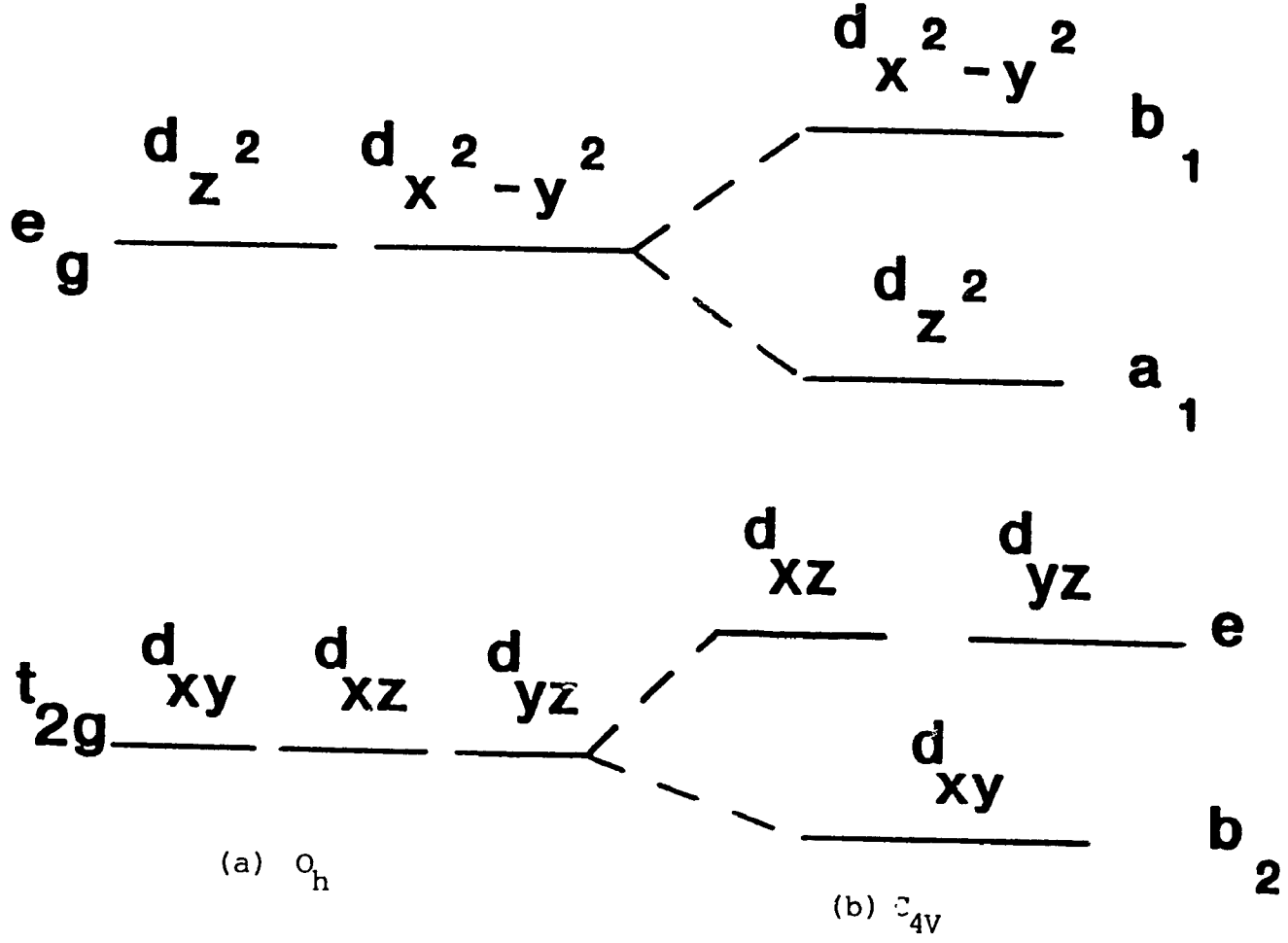

Figure 4.4. Splitting of orbitals from octahedral symmetry to C_{4V}.

For $W(CO)_5$pyr or $W(CO)_5$pip, population of the $dx^2 - y^2$ state can potentially labilize an equatorial CO. Population of the dz^2 can selectively labilize the axial CO or the unique ligand. Labilization of the equatorial COs in these complexes has been reported to be inefficient compared to loss of pip or pyr. Axial CO labilization has not been confirmed experimentally. Zink and Dahlgren (46) have argued that loss of equatorial CO over axial CO is due to the high bond order of the W--C bond which is trans to the pyridine or piperidine ligand. C--O force constants (k) calculated from carbonyl infrared stretching frequencies of these complexes in cyclohexane infer that the force constant for the trans W--C bond is less than for the cis W--C bonds. The larger the value of k, the weaker the metal-carbon bond is in the ground state since both σ donating and π acceptor orbitals are antibonding with respect to the C--O bond. This behavior is expected to be similar in the excited state. Excitation from the dxz, dyz orbitals into the dz^2 orbitals is expected to labilize the ligands bonded in the dz^2 direction. In order to labilize the metal-CO bond, a large σ^* population must be received in the excited state and it must have a low initial metal-carbon bond order. Since the bond order for the trans metal-carbon bond is high, a low substitution yield is expected and observed. Higher energy excitation results in population of the equatorially-directed dx^2-y^2 orbital which is associated with the σx^2-y^{2*} antibonding orbitals. The equatorial COs lie in the xy plane and since the bond orders of the cis W-C bonds are lower than those of the trans W-C bonds greater substitution lability is expected. Experimentally, the substitution quantum efficiency for this process is low. The theoretical model does not explain this observation satisfactorily. Loss of L which is also observed at higher energies is explained by efficient internal conversion between states which are σxy and σz^2 antibonding.

An alternative model has been proposed by Hollebone et al (111) to explain the

excited state reactions of coordination compounds. In Hollebone's model, rapid reaction from an excited state requires decay along selected nuclear coordinates. Hollebone (111) has developed vectorial selection rules for identification of such coordinates based on the treatment of vibrational coordinates by subduction from the group describing fluctuations of a spherical mass distribution. This provides vibrational quantum numbers entirely analogous to electronic quantum numbers for subduction analysis of angular momentum selection rules. Since $W(CO)_5L$ systems produce a fully equilibrated $W(CO)_5S$ spectrum in a few picoseconds, they are obvious candidates for analysis in the fast limit.

The simplest of Hollebone's selections rules is the octapole rule for angular momentum changes in a transition. The objective of the octapole rule is to identify the vibrational mode coupling the excited state to the ground state. The octapole rule, $\Delta T = 3$, governs both the vibronic intensity and the probability that reaction will occur along a specific coordinate. It is factored into the following components:

$$\Delta J + \Delta V = \Delta L + \Delta S + \Delta V = \Delta T = 3 \qquad (4.1)$$

The vibrational component can simply be determined by:

$$\Delta V = 3 - (\Delta L + \Delta S) \qquad (4.2)$$

where ΔJ is the change of electronic angular momentum quantum number, ΔV is the change of the vibrational angular momentum number, ΔL is the change in orbital momenta and ΔS is the change in spin momenta. The observed ΔV can be converted to V_{EX} (EX = excited state) by assuming that $V_{GR} = 0$ (GR = ground

state) in the following relation:

$$\Delta V = (V_{EX} - V_{GR}) = V_{EX} \qquad (4.3)$$

This is applicable at room temperature for vibrations higher than 400 cm^{-1}.

In a d^6 octahedral system, the first two excited states are:

$^1T(D)$

$^3T(P)$

If the primary product is, like the intermediate $W(CO)_5S$ which is formed in less than a few ps, a $^1A(D)$ state (O_h symmetry), then the reaction process is ^1T ---> ^1A and requires $\Delta V = 3$. ^3T ---> ^1A requires $\Delta V = 1$ as described as follows:

Transition	ΔL	ΔS	ΔV	(O_h)
$^1T_1(D)$ <--- ^1A (D)	0	0	3	t_{1u} buckle
$^3T_1(P)$ <--- $^1A_1(D)$	1	1	1	t_{1u} stretch

In octahedral symmetry, the requirements of the point group imply a t_{1u} vibration of which there are two types. The vibration corresponding to $\Delta V = 1$ is the asymmetric stretch t_{1u} shown in Figure 4.5a. In this mode, appropriate to the triplet, there is substantial extension along one axis and the ligand on that axis should be susceptible to substitution. On descent in symmetry to C_{4v}, the Hollebone prompt reaction model gives the same prediction as the thermally equilibrated state model for reactivity from the triplet which will be discussed later.

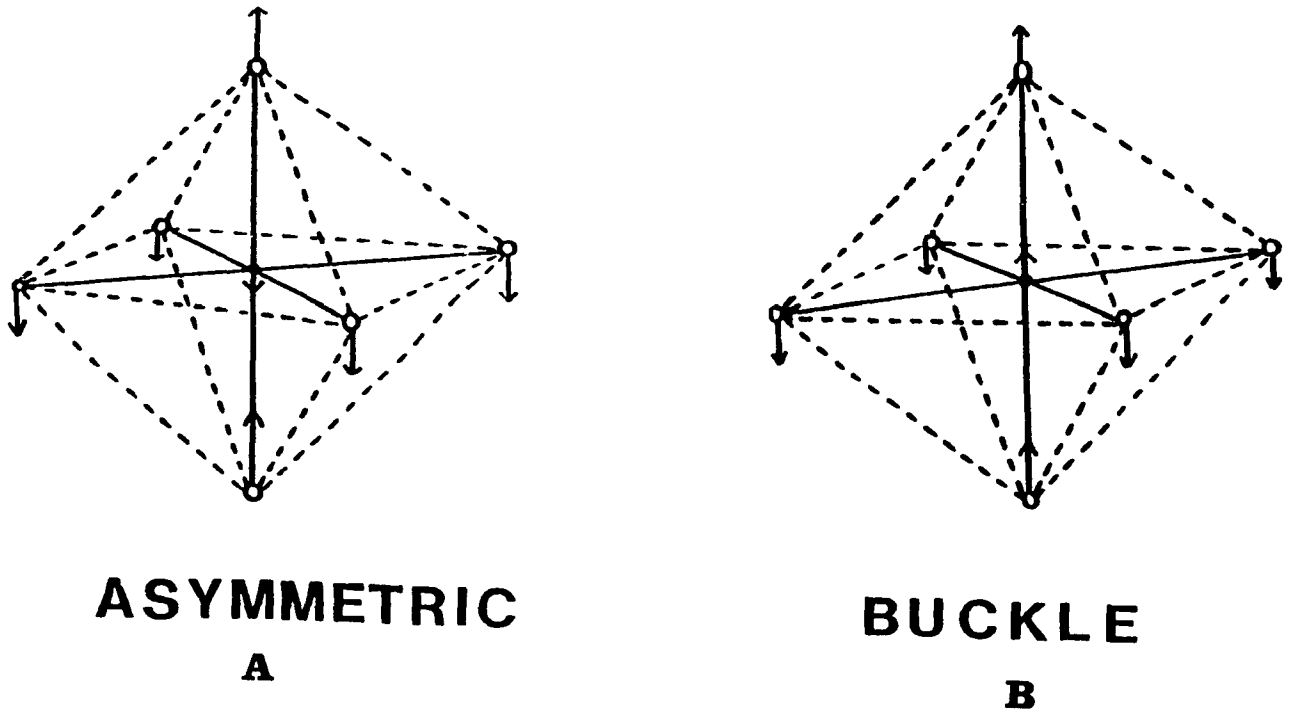

Figure 4.5. Simple diagram indicating t_{1u} asymmetric and buckle stretch modes.

From the singlet, $\Delta V = 3$. The t_{1u} is called a "buckle" and is shown in Figure 4.5b. This mode, which is also responsible according to the Hollebone model for the efficient photosubstitution from ^4T Cr(III) d^3 species, is expected to be very reactive toward substitutions via a non-selective path because the metal is highly exposed to second sphere (solvating) molecules on four octahedral faces above the x,y plane in Figure 4.5b. This explanation accounts for the decrease in reactivity from the singlet to triplet regions.

Wavelength dependence can also be accounted for using this model. This requires consideration of the C_{4v} components. Octahedral ^1T correlates with ^1E and ^1A in C_{4v}. ^1E is the lower electronic state and ^1A is the upper. The wavelength dependence suggests more efficient substitution on irradiations of ^1E than ^1A. Hollebone and Stillman (112) have shown that vibronic coupling is a vector product which must conserve overall degeneracy. The splitting of the octahedral t_{1u} "buckle" vibration into e_u and a_u requires the combination of the E electronic state with the a_u vibration and the A electronic state with the e_u vibration. Thus, excitation of the lower electronic state leads to selection of a relaxation pathway buckling to release the L ligand of $W(CO)_5L$. In contrast, excitation of the higher ^1A electronic state, which is doubly degenerate, leads to selection of a relaxation pathway along either the x or y direction where the more exposed ligand is a CO not an L.

4.3. Triplet Reactivity

Tutt and Zink (9) have calculated the excited state distortions of $W(CO)_5$pyridine and $W(CO)_5$piperidine from emission and preresonance Raman spectra using time-dependent theory (113). Time-dependent theory provides a detailed understanding of excited-state distortions by determining the motions of a

wavepacket on a final multidimensional electronic state potential hypersurface using emission, absorption and Raman spectra. During emission, the initial wavepacket, ϕ, begins on the upper potential surface and propagates on the lower potential surface which is displaced relative to the upper surface. The opposite occurs for absorption. The displaced wavepacket, $\phi(t)$, evolves according to the time-dependent Schrodinger equation. The overlap of both the initial and time-dependent wavepackets, $\phi/\phi(t)$, gives rise to the absorption or emission spectra. The overlap is maximum at $t = 0$ and decreases as the wavepacket moves away from its initial position. It is given by:

$$<\phi/\phi(t)> = \exp\{-\Sigma_k[(\Delta^2_k/2)(1-e^{-i\omega_k t})-i\omega_k t/2]-iE_o t/h - \Gamma^2 t^2\} \quad (4.4)$$

where E_o is the energy difference between the minima of the two potential surfaces, Γ is the damping factor, ω_k and Δ_k are the frequency and displacement, respectively, of the kth normal mode. The emission spectrum is the Fourier transform of the overlap and is given by:

$$I(\omega) = C\omega^3 \int_{-\infty}^{\infty} e^{i\omega t} <\phi_k/\phi_k(t)> dt \quad (4.5)$$

The absorption spectrum is given by:

$$I(\omega) = C\omega \int_{-\infty}^{\infty} e^{i\omega t} <\phi_k/\phi_k(t)> dt \quad (4.6)$$

where C is a constant and ω is the frequency of emitted or absorbed radiation. The frequencies and displacements can be experimentally determined from preresonance Raman spectroscopy, and the energy difference E_o and the damping factor Γ can be

obtained from the electronic and/or emission spectra.

For Raman spectroscopy, the initial wavepacket propagates on the upper excited electronic potential surface and the overlap of $\phi(t)$ with the final state ϕ_f is of interest. The Raman scattering amplitude is given by:

$$\alpha_{fi}(\omega_i) = \int_0^\infty e^{i\omega_i \cdot \Gamma_t} \langle \phi_f / \phi_i(t) \rangle \, dt \tag{4.7}$$

Because it is difficult to experimentally obtain values of the scattering cross-section, the relative intensities of two normal modes are usually determined. The ratio of intensities is given by:

$$I_k / I_k' = \Delta_k^2 \omega_k^2 / \Delta_k'^2 \omega_k'^2 \tag{4.8}$$

The intensities in the Raman spectra are related to the displacements and the absorption spectrum becomes:

$$I(\omega) = C\omega \exp[-\omega\text{-}E)^2/2\sigma^2] \tag{4.9}$$

where $2\sigma^2$ is the width of the electronic absorption spectrum at 1/e of the height. $2\sigma^2$ is also related to the displacement by:

$$2\sigma^2 = \Sigma \Delta_k^2 \omega_k^2 \tag{4.10}$$

$2\sigma^2$ is found experimentally from the absorption spectra, the ratio of the Δs is found from Raman spectra and the individual Δ_ks are calculated by pairwise comparison of the Raman intensities. The displacements, Δ_ks, can be converted

from dimensionless normal coordinates to lengths and angles by transforming to the desired units. Emission and absorption spectra can be calculated from the calculated displacements and can be compared to experimental spectra as a check of the validity of the distortion measurements.

This technique requires information derived from both emission and Raman spectra and in the case of $W(CO)_5$pyridine or $W(CO)_5$piperidine is limited to the triplet region. Tutt and Zink used the 476.5 and 488.0 nm lines of an argon ion laser for the preresonance Raman spectra of $W(CO)_5$pyridine and $W(CO)_5$piperidine, respectively. The distortions that they calculated can be used to explain the differences we observed at 488.0 nm for these two complexes.

Tutt and Zink (9) observed that for $W(CO)_5$pyridine, the most elongated bond in the excited state is the W--N bond which is extended by 18 pm. The trans W--C bond is extended 12 pm. The bond length changes for $W(CO)_5$piperidine are larger. The W--N bond is extended by at least 30 pm (a limit in the analysis) and the trans W--C bond is extended 25 pm. These results were shown to conform to ligand field predictions in which the ^3E state (dz^2 <--- dxz,dyz in 1st order) has larger dz^2 character than dx^2-y^2 character to the extent that the unique ligand is weaker in ligand field strength than CO. Tutt and Zink pointed out that triplet photoreactivity is correctly predicted on the assumption that increased distortion in the vibrationally equilibrated excited state correlates with a smaller barrier to substitutional reactivity. This approach provides a good account of our data at 488.0 nm. A Hollebone analysis would reach the same conclusion.

4.4. MLCT Reactivity and Solvent Dependence.

The electronic spectra of $W(CO)_5$pyridine reveals the existence of a solvent-sensitive W ---> pyridine CT band when polarity changes of the solvent are

sufficient to resolve it from the corresponding LF band. This provides the opportunity to study the MLCT behavior of this complex when the MLCT state is higher in energy than the LF state. To date, the study of the photoreactivity of MLCT states has dealt with those complexes whose MLCT states are lower in energy than the corresponding LF states (32-38). Excitation into the MLCT bands of complexes such as $W(CO)_5L$ (L = 4-cyanopyridine, 4-acetylpyr, 4-formylpyr, 4-benzoylpyr) (14) or $Ru(NH_3)_5X^{2+}$ (X = a substituted pyridine) (114) reveals that the photoreactivity with respect to loss of L or X is relatively less efficient than the corresponding LF excitation. Loss of CO from $W(CO)_5L$ is also inefficient.

The curve-fitting program (101) described previously was used to deconvolute the bands in the 300-500 and 350-500 nm regions of the electronic spectra of $W(CO)_5$pyr and $W(CO)_5$pip, respectively. Examples of the deconvoluted Gaussian spectra are shown in Figures 4.6 - 4.9. The band maxima determined from the curve-fitting program for all the solvents used in this study are given in Appendix D. The four bands in $W(CO)_5$pyr represent, from highest to lowest energy, transitions to the MLCT, ^1A, ^1E and ^3E states, respectively. In $W(CO)_5$pip, the three bands represent, from highest to lowest energy, transitions to the ^1A, ^1E and ^3E states, respectively. The bands are not well resolved and tend to overlap each other significantly depending on the solvent. According to the deconvoluted spectra 313, nm for $W(CO)_5$pyr, 365 and 436 $\pm$ 10 nm irradiation for both populates primarily, but not exclusively, the MLCT, ^1A and ^1E states, respectively. As we have observed with our experimental results, irradiation into all of these states leads to efficient substitution of pyridine or piperidine. Since MLCT reactivity is very inefficient in complexes where the MLCT state is lowest in energy, MLCT reactivity in $W(CO)_5$pyr must be due to efficient internal conversion from the higher energy MLCT state to the lower energy LF singlet states. The rate of conversion into

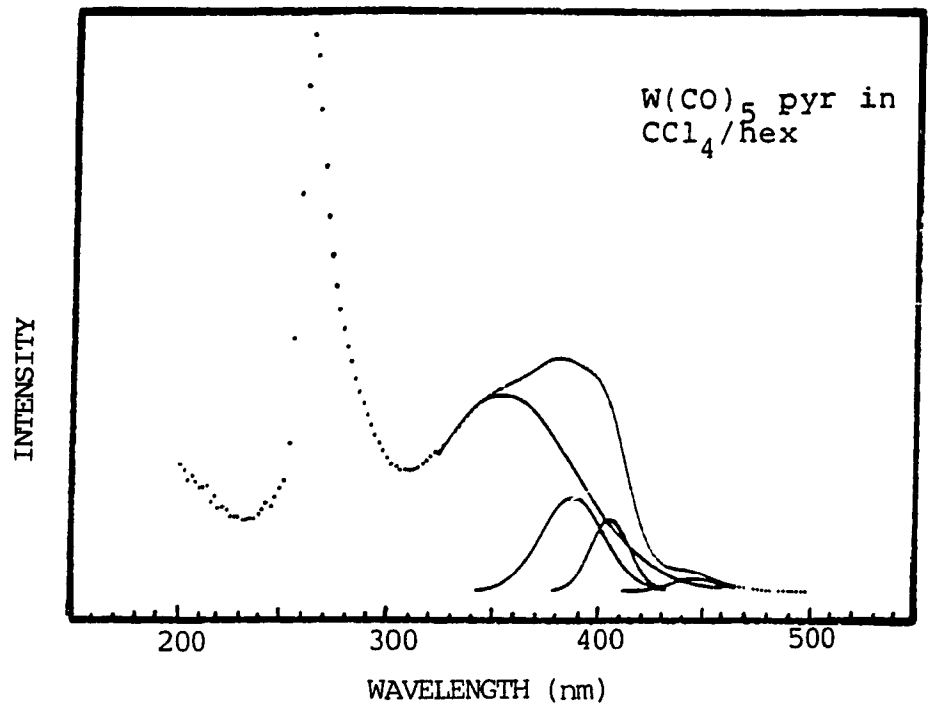

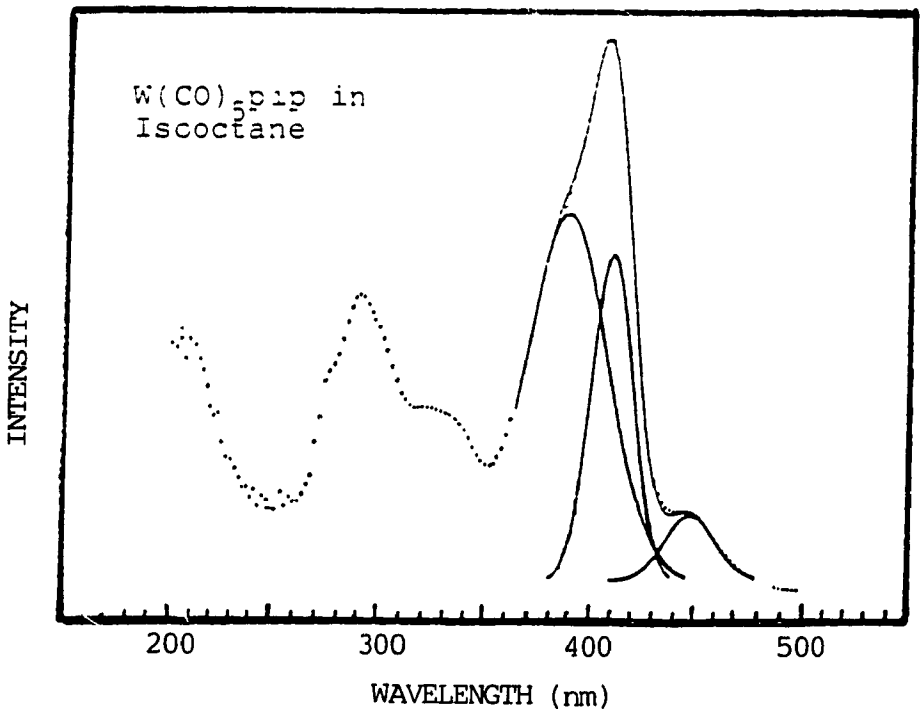

Figure 4.6. Deconvoluted spectral bands for $W(CO)_5$pyr in CCl_4/1-hexene and $W(CO)_5$pip in isooctane.

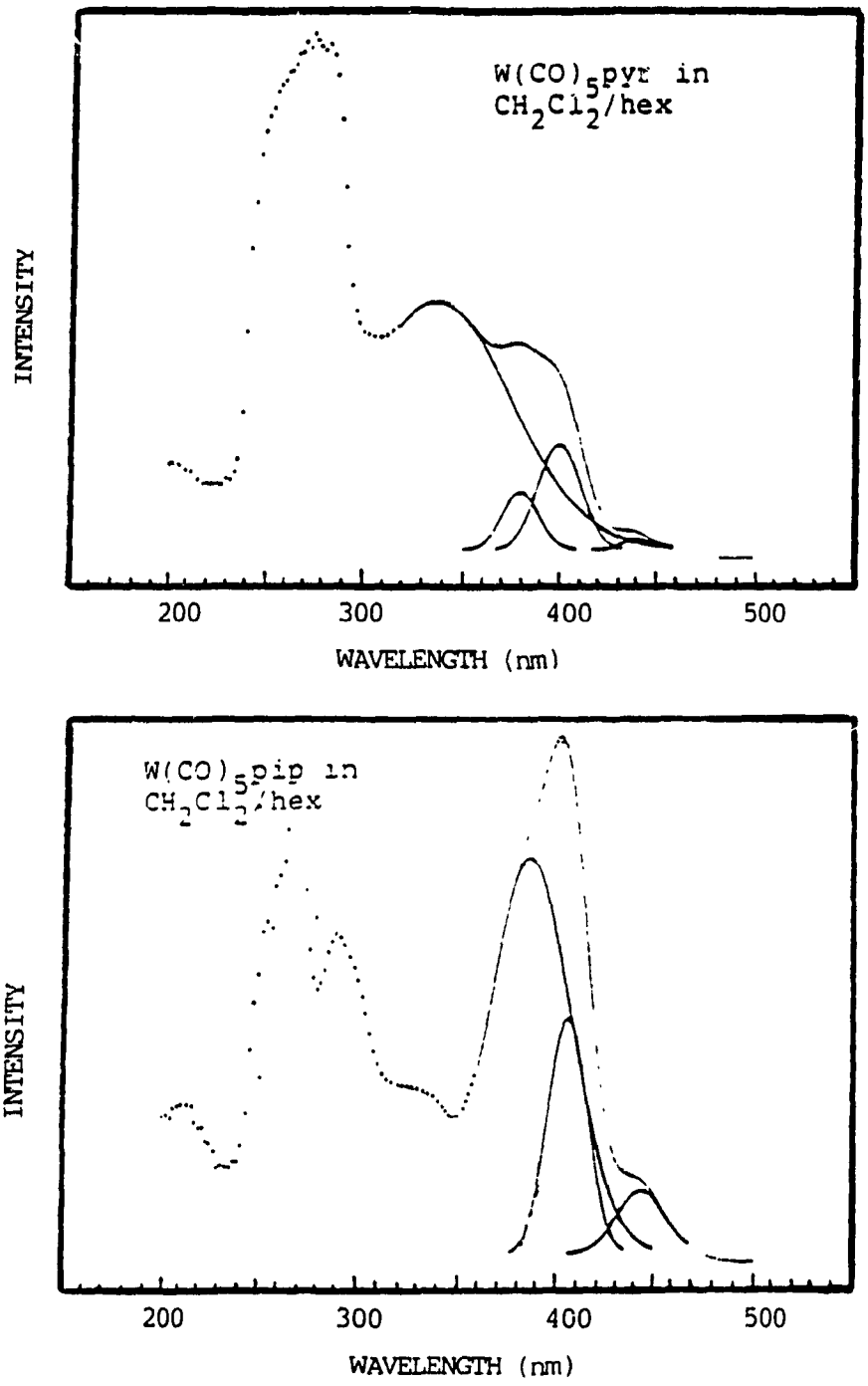

Figure 4.7. Deconvoluted spectral bands for $W(CO)_5$pyr in CH_2Cl_2/1-hexene and $W(CO)_5$pip in CH_2Cl_2/1-hexene.

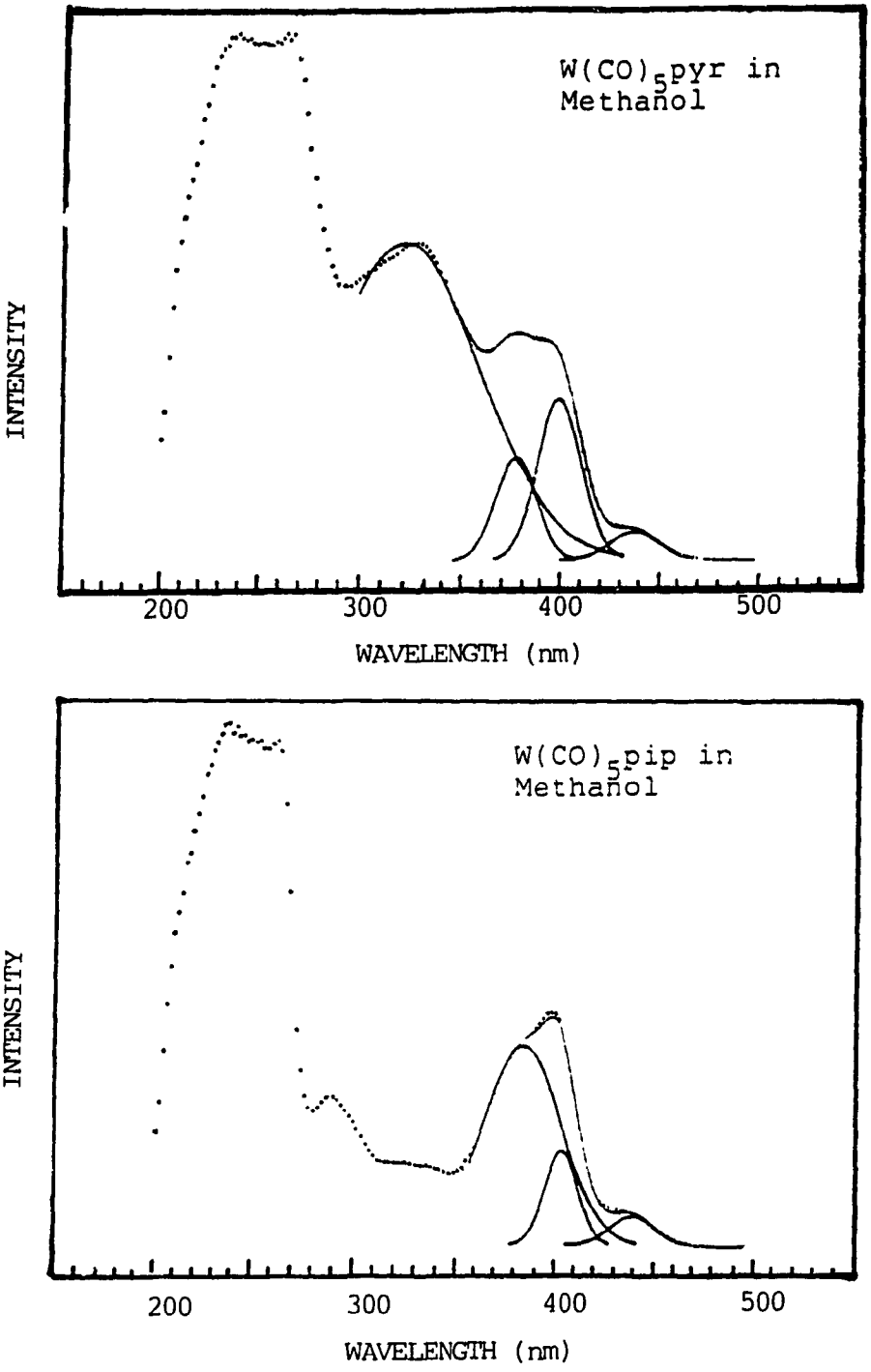

Figure 4.8. Deconvoluted spectral bands for $W(CO)_5$pyr and $W(CO)_5$pip in methanol.

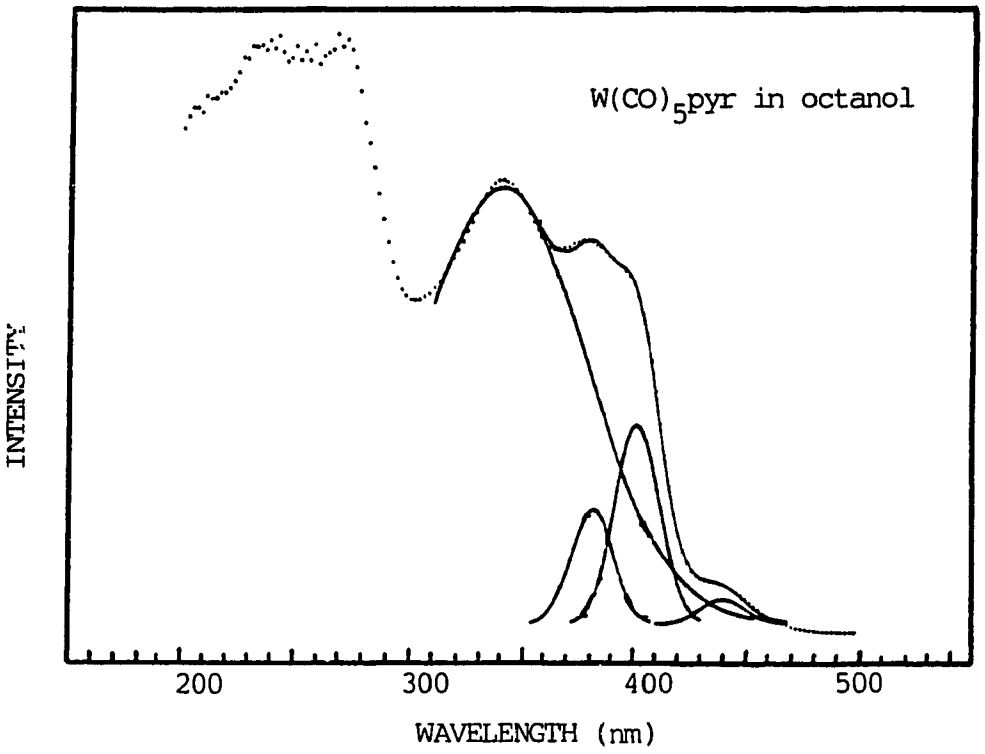

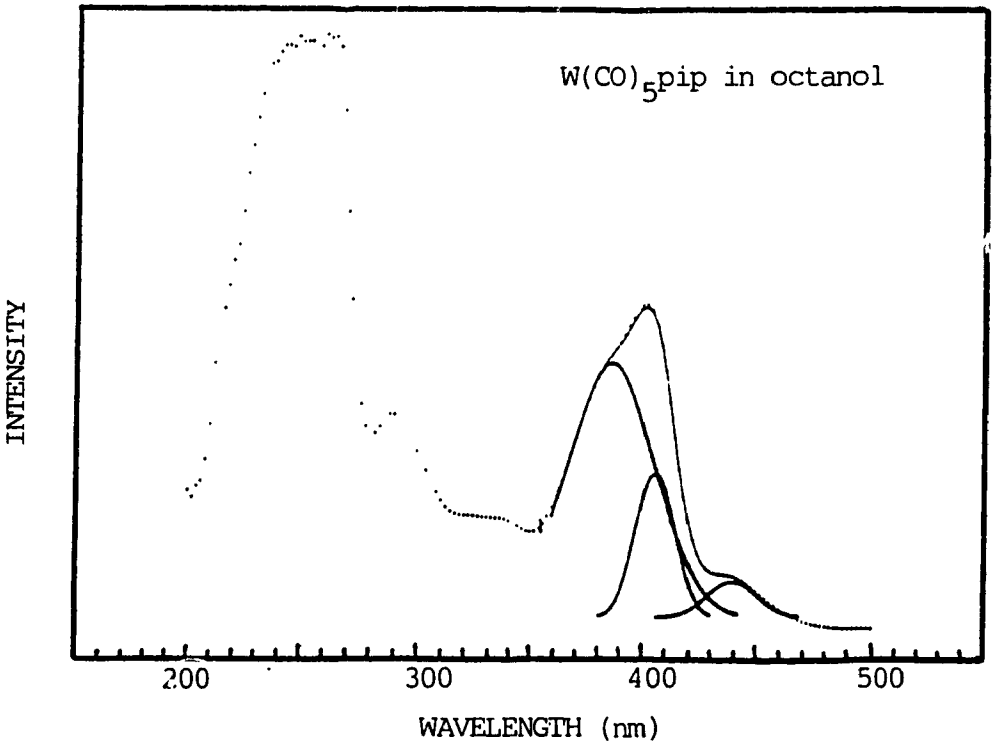

Figure 4.9. Deconvoluted spectral bands for $W(CO)_5$pyr and $W(CO)_5$ pip in octanol.

either the ^1A or ^1E state apparently depends on the proximity of the CT state to the LF states. According to Hollebone's rules (111), the ^1A state leads to buckling along the x or y axis and release of an equatorial CO. The ^1E state leads to buckling along the z axis and release of pyr or pip. Competition exists between release of CO, release of pyr or pip and vibrational relaxation to the ground state. CO molecules are more tightly bound to the metal than pyr or pip and since only monosubstituted products are observed under the conditions used in these experiments, competition between vibrational relaxation from the ^1A state and conversion from the ^1A to the ^1E state becomes more important.

When the MLCT and LF states are mixed in $W(CO)_5$pyr, competitive internal conversion to the ^1A and ^1E states exist. When the MLCT and LF states are separated, the state into which the MLCT relaxes depends on the energy difference between the respective MLCT and LF states. The greater the MLCT-^1E energy difference, the greater is the probability that internal conversion will occur to the ^1A state before conversion to the ^1E state. This is supported by the following experimental evidence. In CH_2Cl_2/hex, $CHCl_3$/hex and methanol, the three solvents which produce the largest energy differences between the CT and LF states in $W(CO)_5$pyr, MLCT (313 nm) irradiation gives yields which are comparable to 365 nm yields of $W(CO)_5$pip in the same solvents. This indicates that relaxation from the MLCT state is primarily into the higher energy ^1A state followed by competition between relaxation to the ground state and internal conversion into the reactive ^1E state. In other solvents, such as the remaining alcohols, the energy separation is not enough to exclusively relax into the ^1A state. Relaxation into the ^1E state is competitive. This explains why 313 and 365 nm irradiation of $W(CO)_5$pyr give essentially the same yields.

In $W(CO)_5$pip, the significant overlap between the ^1A and ^1E states and

comparable rates of vibrational relaxation from the ^1A state to the ground state or internal conversion to the ^1E state could account for the same yields observed in propanol, butanol, and octanol under 365 nm irradiation. There are three solvents whose yields for both complexes can be considered to be significantly different: methanol, CH_2Cl_2 and CCl_4. Experiments with I_2 in the chlorinated solvents (74,75) have revealed that the rates of vibrational relaxation of I_2 decrease in the order $CH_2Cl_2 < CHCl_3 < CCl_4$. We can observe that 313 nm irradiation of $W(CO)_5$pyr and 365 and 436 nm irradiation of both compounds display yields which increase in the same order. We can speculate that the vibrational relaxation rate from the ^1A state decreases in the same order enhancing the probability of internal conversion to the ^1E state. In CH_2Cl_2 and $CHCl_3$/hex, the CT and LF states are separated in $W(CO)_5$pyr by the same degree. Relaxation from the MLCT state, upon 313 nm irradiation, to the ^1A state in competition with relaxation to the ^1E state should occur to the same extent in both solvents. A slower relaxation time in $CHCl_3$ would enhance internal conversion to the ^1E state and account for the higher yield. In CCl_4, the CT and LF states are mixed. Again, a slower relaxation time and the closer proximity between MLCT and ^1E states would account for the even higher yield observed in this solvent. For 365 nm, the interpretation for both complexes is the same. Slower vibrational relaxation accounts for higher yields by virtue of enhanced probability of internal conversion to the reactive ^1E state. The presence of the CT component in $W(CO)_5$pyr can account for the increased yields compared to $W(CO)_5$pip. This solvent trend is also observed for 436 nm irradiation of both complexes but in CCl_4, the wavelength dependence between 365 and 436 nm disappears. Yields for 436 nm irradiation of both complexes in CCl_4 are lower than those obtained upon 365 nm irradiation. This can be explained using the same argument. The slower vibrational relaxation in CCl_4 and the close proximity of the ^1E and ^3E

states allow for intersystem crossing under 436 ± 10 nm irradiation into the less reactive ^3E state. This lowers the overall quantum yields. This solvent behavior can be used to speculate on the behavior of these complexes in methanol. If vibrational relaxation is faster than in any of the other solvents studied, 313 nm irradiation of $W(CO)_5$pyr would result in internal conversion to the ^1A state followed by rapid relaxation to the ground state. 365 nm irradiation of $W(CO)_5$pip would give the same result.

4.5. Polymerization of 1-hexene.

The appearance of a white precipitate occurs upon 313 and 365 nm irradiation of either $W(CO)_5$pyr or $W(CO)_5$pip in all solvents containing 1-hexene as an entering ligand. The peak of the lowest energy absorption band of $W(CO)_5$(1-hexene) is at 350 nm with peaks of higher energy bands at ≤ 290 nm. Precipitation is observed only after 85% conversion of $W(CO)_5$L (L = pyr, pip) under 365 nm irradiation and after 40% conversion under 313 nm irradiation of $W(CO)_5$pyr. No precipitation, except at late stages of conversion in CCl_4, is observed for irradiations ≥ 436 nm. In all solvents, the $W(CO)_5$(1-hexene) product may be undergoing a polymerization of 1-hexene upon absorption of light by the product at 313 or 365 nm. Two proposed mechanisms leading to formation of cyclic and straight chain hexene polymers are given in Scheme I and II. The polymer may contain alkyl chains only or may precipitate from solution containing the metal. Since the precipitate was formed in small amounts, collection and analysis was difficult.

4.6. Transient Absorption Spectroscopy.

For the monosubstituted complexes studied here, the overall quantum yields for mono- or disubstituted reactions, whether combined or alone, are less than

SCHEME I.

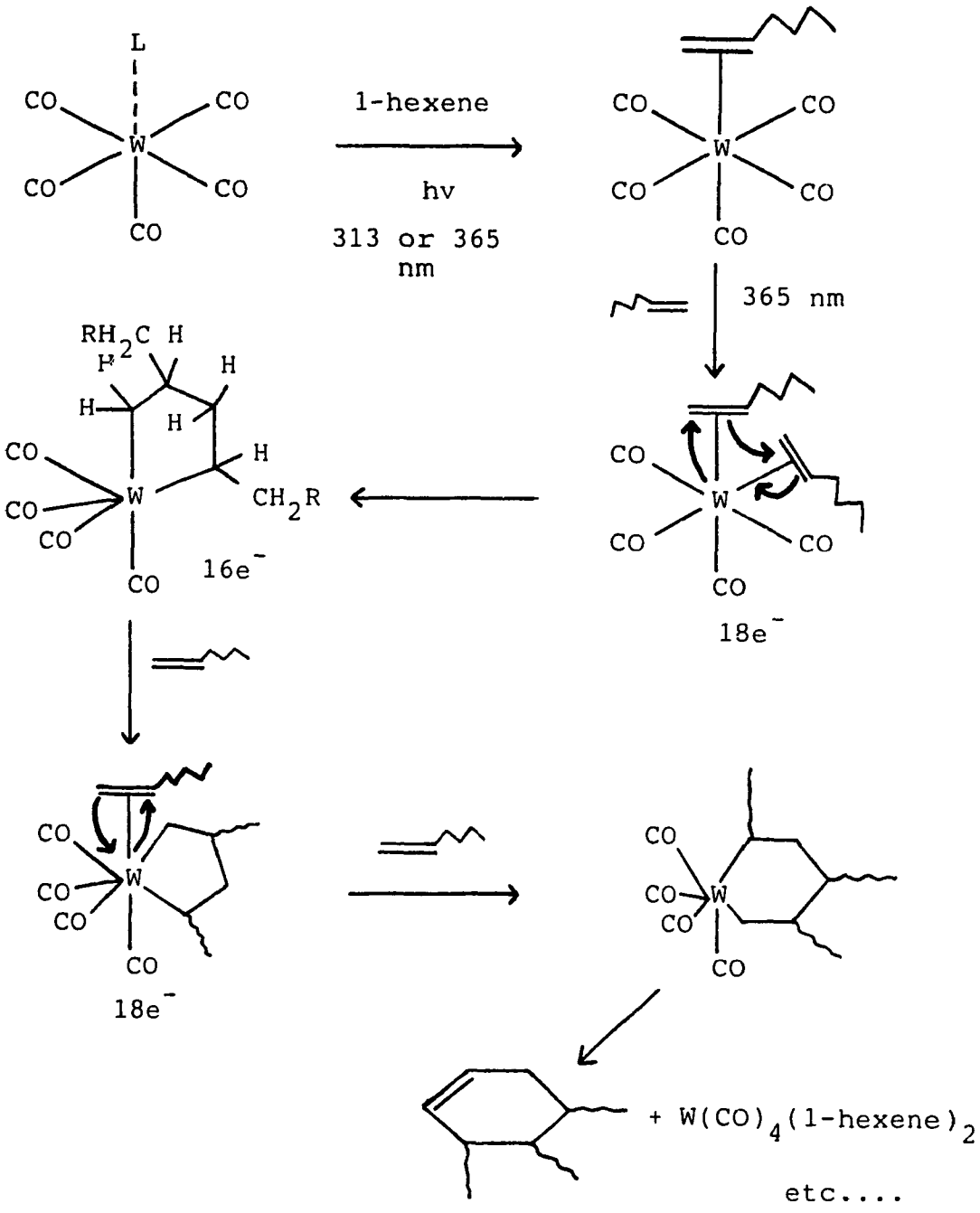
L
CO
W
1-hexene
hv
313 or 365 nm
365 nm
RH_2C H
H
CH_2R
16e⁻
18e⁻
18e⁻
+ $W(CO)_4(1\text{-hexene})_2$
etc....

SCHEME II.

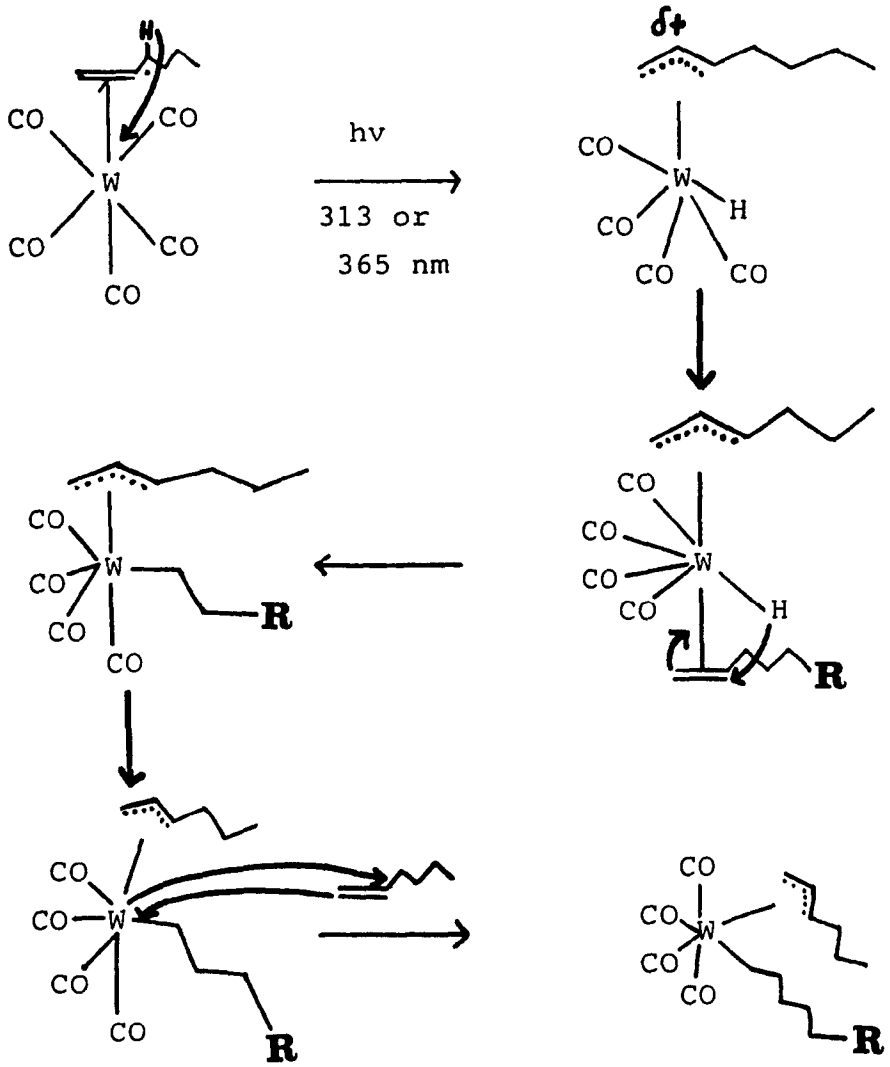

unity. This inefficiency may be attributed to recombination of dissociated fragments due to cage effects or direct nonradiative decay to the ground state from the electronically excited $W(CO)_5L$ species. Viscosity differences may reveal the cage effect. This has been observed with photoredox quantum yields of $Co(NH_3)_5NCS$ in glycerol/water solutions (115). The greater density of solvent molecules inhibits fragment separation and increases the probability of recombination. In a series of related solvents, such as the alcohols, which exhibit large differences in viscosities, a parallel increase of quantum yields with decreasing viscosity would suggest that recombination accounts for values less than unity. Increasing the wavelength of irradiation, theoretically, should lead to increased quantum yields because of the increased separation of fragments caused by energy in excess of that required to dissociate the molecule. As the distance between fragments increases, the probability of recombination decreases. In our studies, these effects are not observed. It is possible, given the results with the chlorinated solvents, that efficient vibrational relaxation to the ground state accounts for the yields less than unity.

Whatever occurs in the primary event can have a considerable effect on the final outcome. In an effort to understand the solvent dependence observed for photosubstitution reactions of the substituted tungsten carbonyls, we have studied the transient behavior between 0 ps and 10 ns in various solvents to determine if a relationship can be found. Simon and his co-workers investigated the behavior of $Cr(CO)_6$ in methanol and pentanol in order to examine the dynamics of solvation (31,84). They compared their results with those obtained upon flash photolysis of $Cr(CO)_6$ in cyclohexane whose band maximum is centered around 520 nm and is very broad compared to the band formed upon irradiation of $Cr(CO)_6$ in either alcohol. The band for the $Cr(CO)_5$(alcohol) transient is centred at around 460 nm

reflecting the greater interaction with the Cr metal. The transient rise time to form $Cr(CO)_5(MeOH)$ was observed to be slower than the rise time for formation of $Cr(CO)_5$(cyclohexane)(31). The slower rise time was attributed to solvent reorganization and coordination to the ground state $Cr(CO)_5$ fragment. The coordination time is faster than the Debye relaxation time of 50 ps. In pentanol solutions (84), instantaneous signals for coordination of the alkyl portion of the alcohol chain and the hydroxyl portion of the alcohol were observed at 520 nm and 460 nm, respectively. The 520 nm signal decayed with time while the 460 nm signal increased reflecting the time of rearrangement from alkyl intermediate to final alcohol product. Simon (84) calculated the percentage of alkyl coordinated intermediate by determining the ratios of alkyl/hydroxyl transients from the observed absorbances at 520 nm and 460 nm. He assumed that the extinction coefficients at the peak maxima of the alkyl and hydroxyl transients were the same and under conditions of similar power and concentration he established that greater than 50% of the photofragments were initially coordinated by hydroxyl groups. Simon and his co-workers were able to follow the very early transient behavior using a laser with time resolution of .8 ps.

Spears and his co-workers (110) investigated the transient absorption spectra of $Cr(CO)_6$ in THF using the 266 nm line of a Nd/YAG laser with a 20 ps pulse and an IR detection system. They disagreed with the assignment of Simon et al that solvent bonding was correlated with the fast risetime (.8 - 2.5 ps) observed for this complex in the alcohols because this assumption was based on UV-Vis spectral bands which lack detail. Observation by Spears et al of changes in the CO vibrational frequencies of $Cr(CO)_6$ demonstrates a slower reaction rate for solvent bonding to $Cr(CO)_5$. In THF, two binding sites are available, an H atom and an O atom site. Bonding of $Cr(CO)_5$ to an H atom gives a CO frequency at 1961 cm^{-1}

similar to the 1965 cm^{-1} frequency observed for $Cr(CO)_5$(cyclohexane). Bonding of $Cr(CO)_5$ to an O atom gives a CO frequency at 1937 cm^{-1} similar to the 1935 cm^{-1} frequency reported for $Cr(CO)_5$MTHF(O) (MTHF = methyltetrahydrofuran). According to theoretical predictions by Hay (117), two species can be formed upon decomposition of $Cr(CO)_6$ to an excited $Cr(CO)_5$ state. These are a square pyramidal (SP) species and a trigonal bipyramidal (TBP) species with singlet and triplet ground states, respectively (Figure 4.10). The triplet TBP species is metastable and converts to the thermodynamically more stable SP species. According to observations by Spears et al (116), the SP species prefers to bind THF via its O atom whereas the TBP species can coordinate equally to a C-H group or an O atom. Formation of the TBP species where $Cr(CO)_5$ is bound to a C-H group leads to rearrangement to the more stable O species with a time constant of approximately 700 ps. In cyclohexane, Spears et al (118) calculated the rate constants for formation of $W(CO)_5$(cyclohexane) in both the TBP and SP geometries. They observed that $W(CO)_5$(cyclohexane) (TBP) is formed approximately 2.3 times faster than $W(CO)_5$(cyclohexane) (SP).

Qualitative observation of $W(CO)_6$ in methanol, butanol or octanol illustrates that between 0 and 100 ps there is very little growth of the transient signal. The bands are narrower and blue-shifted compared to those observed for this complex in cyclohexane. If the behavior of $W(CO)_6$ in the alcohols is similar to that observed for $Cr(CO)_6$ in the alcohols, the possibility exists that under singlet LF irradiation both hydroxyl and alkyl transients are initially present. This is especially true for the alcohols which have substantial alkyl chains. Observation of the behavior of $W(CO)_6$ between 100 ps and 10 ns shows that for butanol and octanol, the transient absorbance drops to about half of that observed at 100 ps. This behavior is also seen for $W(CO)_6$ in 1-hexene. This suggests rearrangement from the alkyl to the

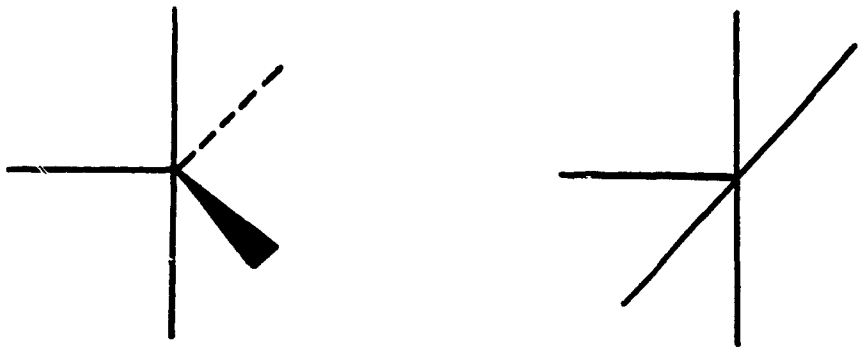

(A) TBP **(B) SP**

Figure 4.10. (a) trigonal bipyramid (TBP) structure with D_{3h} symmetry, and (b) square pyramid (SP) structure with C_{4V} structure.

more stable hydroxyl or alkene species is occurring. The time constant calculated for the 1-hexene case is approximately 600 ps. The behavior in butanol and octanol is the same suggesting the same time frame for rearrangement is reasonable. The time for rearrangement which we have observed for $W(CO)_5S$ is comparable to the 700 ps observed by Spears et al (116) for rearrangement of the $Cr(CO)_5S$ intermediate from a C-H-bonded to O-bonded species in THF.

In our picosecond experiments, 355 nm irradiation of $W(CO)_6$ populates primarily a LF triplet state. Previous steady state studies have shown that the singlet state relaxes to the triplet. For $W(CO)_5L$, 355 nm irradiation populates a LF singlet state. According to Spears et al (116), the TBP species is non-discriminate in its preference to bind to a C--H group or an O atom whereas the SP species prefers to bind to an O atom. In cyclohexane, where the only binding site available is a C--H group, the TBP species binds 2.3 times faster than the SP species. With our picosecond results, it is possible to use Hollebone's rules to analyze the dissociative step (111). According to Hollebone's rules (111), a $^3T_1(P)$ <--- $^1A_1(D)$ transition leads to decay along the t_{1u} vibrational mode referred to as an asymmetric stretch. This mode may simulate the SP geometry in which there is a substantial extension along one specific axis. The W atom and the four equatorial CO molecules remain in the same plane. In this geometry, the W atom is not highly exposed to solvent molecules and the extent of solvent coordination may depend on proper orientation of the solvent as well as dissociation of the ligand. This is the case which is expected upon 355 nm irradiation of $W(CO)_6$. 355 nm excitation of $W(CO)_5L$ (L = py, pip) results in a transition from a singlet ground state to a singlet excited state. This results in decay along a t_{1u} vibrational mode referred to as the "buckle". This mode may simulate the TBP geometry in which the W atom is highly exposed to the surrounding solvent molecules on the four

octahedral faces above the x,y plane. This permits access to the metal by the surrounding solvent without necessary prior release of the unique ligand. Since the metal is highly exposed to the surrounding solvent, it can be indiscriminate in its coordination to either an alkyl or a hydroxyl portion of the solvent chain available. This can account for the presence of both species. In an asymmetric stretch mode, the percentage of alkyl transients would be expected to be lower than for a buckle mode. For the three solvents which we calculated quantitative values, the alkyl percentages for $W(CO)_6$ are lower than the alkyl percencentages for $W(CO)_5L$. This is consistent with our interpretation. In cyclohexane, both the TBP and SP geometries will bind to a C--H group. It is possible that from the asymmetric mode of $W(CO)_6$, the formation of $W(CO)_5$(cyclohexane) would be slower than from the buckle mode of $W(CO)_5L$. This may account for the growth of the transient from 0 to 50 ps for $W(CO)_6$ in cyclohexane compared to the prompt formation within 20 ps of $W(CO)_5L$ in cyclohexane.

The information obtained from the transient spectra can not adequately account for differences in the overall quantum yields observed for these complexes in various solvents. It is probable, therefore, that the overall yields are determined by processes which occur between 0 and 20 ps, a time frame which is inaccessible with the system available to us.

Conclusion

Some interesting observations have been made from the experimental results obtained in this study of the photochemical substitution reactions of $W(CO)_5L$ (L = CO, pyr, pip). First, for L = pyr, pip, there are two distinct photochemical pathways for substitution of the unique ligand, a singlet LF pathway which is the most efficient and a triplet LF pathway. Of the two LF singlet states, ^1A and ^1E, the ^1E state which possesses greater dz^2 than $dx^2 - y^2$ character appears to be the state responsible for unique ligand substitution. This contrasts with the behavior observed for the $M(CO)_6$ (M = Cr, W) complexes in which all substitution reactions occur from the triplet LF state. Second, dissociation of L (L = CO, pyr, pip) occurs on a very fast time scale (<< 50 ps) as observed from picosecond experiments, and is faster for the pyr or pip complexes compared to the parent hexacarbonyl. Third, the W ---> π^*(pyridine) MLCT state is not reactive. Substitution upon irradiation into this MLCT state is due to efficient internal conversion to the reactive LF states. This behavior confirms earlier studies which have concluded that MLCT states in these types of complexes are unreactive toward substitution. Fourth, the solvent dependence observed for the photosubstitution quantum yields may be due to different rates of vibrational energy transfer between reactant and solvent molecules which lead to different rates of vibrational relaxation to the ground state. No other solvent parameter has satisfactorily explained the observed results.

These observations lead to two obvious areas for further research. The first area of interest would be to examine the transient behavior of these complexes on a faster time scale since picosecond lasers with pulse widths of 30 ps are too slow to adequately examine the primary events occurring in these complexes. A pulse width in the femtosecond range would be ideal as this would provide an excellent

opportunity to examine in detail both the process of dissociation and the process of solvent coordination. The use of IR detection systems, if available on systems using femtosecond pulses, may provide additional structural information not available from UV-Vis detection systems. The second area of interest would be to extend the solvent dependent studies by examining the simpler of the two C_{4v} complexes, $W(CO)_5pip$, in a variety of solvents using femtosecond spectroscopy. If, as in the I_2 experiments, transient spectroscopy records only the ground state intermediates, it would be interesting to determine if times for the appearance of the transient differ depending on the solvent. A greater understanding of the process of solute-solvent interaction and a possible insight into the contribution of vibrational relaxation to overall quantum efficiency in these systems may result.

References

1. J.S. Thayer, Adv. Organomet. Chem., (1974), 13,1.
2. L. Mond, J. Chem. Soc., (1890), 57, 749.
3. L. Mond, F. Quinke, J. Chem. Soc., (1891), 59, 604.
4. M. Berthelot, C.R. Acad. Soc., (1891), 112, 1343.
5. J. Dewar, H.O. Jones, Proc. Roy. Soc. (London) A, (1905), 76, 558.
6. L.H. Jones, J. Chem. Phys. (1962), 36, 2375.
7. L.O. Brockway, R.V.G. Ewens, M.W. Lister, Trans. Farad. Soc.,(1938), 34, 1350.
8. F.A. Cotton, C.S. Kraihanzel; J. Am. Chem. Soc., (1962), 84, 4432.
9. L. Tutt, J.I. Zink, J. Am. Chem. Soc., (1986), 108, 5830.
10. L.H. Jones, Spectrochim. Acta., (1963), 19, 329.
11. R.A. Brown, G.R. Dobson, Inorg. Chim. Acta., (1972), 6, 65.
12. M. Wrighton, G.S. Hammond, H.B. Gray, Inorg. Chem., (1972), 11, 3122.
13. M. Wrighton, G.S. Hammond, H.B. Gray, J. Am. Chem. Soc., (1971), 93, 4336.
14. M. Wrighton, H.B. Abramson, D.L. Morse, J. Am. Chem.Soc., (1976), 98, 4105.
15. A.J. Lees, A.W. Adamson, J. Am. Chem. Soc., (1982), 104, 3804.
16. J. Nasielski, P. Kirsch, L. Wilputte-Steinert, J. Organomet. Chem.(1971), 29, 269.
17. R. Bonneau, J.M. Kelly; J. Am. Chem. Soc., (1980), 102, 1220.
18. A.J. Lees, A.W. Adamson, Inorg. Chem. (1981), 20, 4381.
19. W.H. Breckenridge, G.M. Stewart, J. Am. Chem. Soc. (1986), 108, 364.
20. R.N. Perutz, J.J. Turner, J. Am. Chem. Soc. (1975), 97, 4791.
21. D.R. Tyler, D.P. Petrylak, J. Organomet. Chem. (1981), 212, 389.
22. R.N. Perutz, J.J. Turner, J. Am. Chem. Soc. (1975), 97, 4800.
23. J.M. Kelly, H. Hermann, E.K. von Gustorf, J. Chem. Soc. Chem. Commun.

(1973), 105.

24. J.M. Kelly, C. Long, R. Bonneau, J. Phys. Chem. (1983), 87, 3345.

25. L. Flamigni, Radiat. Phys. Chem. (1979), 13, 133.

26. J.K. Burdett, M.A. Graham, R.N. Perutz, M. Poliakoff, A.J. Rest, J.J. Turner, R.F. Turner, J. Am. Chem. Soc. (1975), 97, 4805.

27. H. Hermann, F.W. Grevels, A. Henna, K. Schaffner, J. Phys. Chem. (1982), 86, 5151.

28. G.R. Dobson, P.M. Hodges, M.A. Heely, M. Poliakiff, J.J. Turner, S. Firth, K.J. Asali, J. Am. Chem. Soc. (1987), 109, 4218.

29. J.D. Black, P.S. Braterman, J. Organomet. Chem, (1973), 63, c19.

30. J.A. Welch, K.S. Peters, V. Vaida, J. Phys. Chem. (1982), 86, 1941.

31. J.D. Simon, X. Xie, J. Phys. Chem. (1986), 90, 6751.

32. W. Kaim, S. Kohlman, Inorg. Chem. (1986), 25, 3306.

33. R.W. Balk, D.J. Stufkens, A. Oskam, Inorg. Chim. Acta. (1978), 28, 133.

34. D.M. Manuta, A.J. Lees, Inorg. Chem. (1986), 25, 1354.

35. A.J. Lees, A.W. Adamson, J. Am. Chem. Soc. (1982), 104, 3804.

36. D.M. Manuta, A.J. Lees, Inorg. Chem. (1986), 25, 3212.

37. T.R. Miller, J.G. Dance, J. Am. Chem. Soc. (1973), 65, 6970.

38. S. Ernst, Y. Kurth, W. Kaim, J. Organomet. Chem. (1986), 302, 211.

39. M.J. Boylan, P.S. Braterman, A. Fullerton, J. Organomet. Chem. (1985), 24, 418.

40. S.P. Church, F. Grevels, H. Hermann, K. Schaffner, Inorg. Chem.(1985), 24, 418.

41. J. Nasielski, A. Colas, J. Organomet. Chem (1975), 101, 215.

42. J. Nasielski, A. Colas, Inorg. Chem. (1978), 17, 237.

43. W.H. Breckenridge, N.Sinai, J. Phys. Chem. (1981), 85, 3557.

44. W. Strohmeier, K. Gerlach, Chem. Ber. (1961), 94, 398.

45. M. Wrighton, G.S. Hammond, H.B. Gray, J. Organomet. Chem.(1974),70, 283.

46. R.M. Dahlgren, J.I. Zink, Inorg. Chem. (1977), 16, 3154.

47. M. Wrighton, G.S. Hammond, H.B. Gray, Mol. Photochem. (1973), 5, 179.

48. M. Wrighton, Inorg. Chem. (1974), 13, 905.

49. M. Wrighton, K.R. Pope, Inorg. Chem. (1985), 24, 2792.

50. D.J. Darensbourg, M.Y. Darensbourg, R.J. Dennenberg, J.Am.Chem.Soc. (1971), 93, 2807.

51. G.Schwerzer, M.Y. Darensbourg, D.J. Darensbourg, Inorg. Chem. (1972), 11, 1967.

52. P.C. Ford, D. Wink, J. Dibenedetto, Prog. Inorg. Chem. (1983), 30,213.

53. H. H. Schmidtke, Inorg. Chem. (1966), 5, 1682.

54. V.F. Manfrin, G. Vareni, L. Moggi, V. Balzani, Mol. Photochem. (1969), 1, 387.

55. J. D. Petersen, P.C. Ford, J. Phys. Chem. (1974), 78, 1144.

56. M. Talebinasab-Sarvari, A. Zanelli, P.C. Ford, Inorg. Chem. (1980), 19, 1835.

57. C.H. Langford, C.P. Vuik, J. Am. Chem. Soc. (1976), 98, 5410.

58. C.H. Langford, A.Y.S. Malkasian, J. Am. Chem. Soc. (1987), 109, 2683.

59. D.A. Chaisson, R.E. Hintze, D.H. Stuermer, J.D. Petersen, D.P. McDonald, P.C. Ford, J. Am. Chem. Soc. (1972), 94, 6665.

60. C. Malouf, P.C. Ford, J. Am. Chem. Soc. (1977), 99, 7213.

61. C. Malouf, P.C. Ford, J. Am. Chem. Soc. (1974), 96, 601.

62. M.S. Wrighton, D.L. Morse, J. Organomet. Chem. (1975), 97, 405.

63. D.V. Stynes, X. Chen, Inorg. Chem. (1987), 26, 3145.

64. J. Franck, E. Rabinowitch, Trans. Farad. Soc. (1934), 30, 120.

65. P. Debye, Trans. Electrochem. Soc. (1942), 81, 265.

66. J. Zimmerman, R.M. Noyes, J. Chem. Phys. (1950), 18, 658.

67. F.W. Lampa, R.M. Noyes, J. Am. Chem. Soc. (1954), 76, 2140.

68. T.J. Chuang, G.W. Hoffman, L.B. Eisenthal, Chem. Phys. Lett. (1974), 25, 201.

69. D.L. Bunker, B.S. Jacobsen, J. Am. Chem. Soc. (1972), 94, 1843.

70. J.N. Murrell, A.J. Stace, R. Dammel, J. Chem. Soc. Farad. Trans. (1978), 274, 1532.

71. D.J. Nesbitt, J.T. Hynes, J. Chem. Phys. (1982), 77, 2130.

72. P. Bado, P.H. Berens, K.R. Wilson, Proc. Soc. Photo-optic Instrum. Eng. (1982), 322, 230.

73. P. Bado, P.H. Berens, J.P. Bergsma, M.H. Coladonato, C.G. Edelsten, P.M. Kahn, J.D. Wilson, R.K. Wilson in Photochemistry and Photobiology, Ed. A. Zewail, 1983, 1, 615.

74. A.L. Harris, M. Berg, C.B. Harris, J. Chem. Phys. (1988), 84, 788.

75. J.K. Brown, C.B. Harris, J.C. Tully, J. Chem. Phys. (1988), 89, 6687.

76. J.D. Simon, Acc. Chem. Res. (1988), 21, 128.

77. J.T. Hynes, Ann. Rev. Phys. Chem. (1985), 36, 573.

78. D. Kwelson, P.A. Madden, Ann. Rev. Chem. Phys. (1980), 31, 523.

79. M. Davies, Dielectric Properties and Molecular Behavior, N.E. Hill, W.E. Vaughan, A.H. Price, M. Davies ed. Van Nostrand, London, 1969.

80. S.K. Garg and C.P. Smyth, J. Phys. Chem. (1965), 69, 1294.

81. E.M. Kosower, D. Huppert, Ann. Rev. Phys. Chem. (1986), 37, 127.

82. H. Sumi, R.A. Marcus, J. Chem. Phys. (1986), 84, 4272.

83. S.G. Su, J.D. Simon, J. Phys. Chem. (1987), 91, 2693.

84. J.D. Simon, X. Xie, J. Phys. Chem. (1987)m 91, 5538.

85. V. Gutmann, Coordination Chemistry in Non-aqueous Solutions, Springer -Verlag, New York, 1968.

86. V. Gutmann, The Donor-Acceptor Approach to Molecular Interactions, Plenum, New York, 1978.

87. U. Mayer, V. Gutmann, W. Gerger, Mh. Chem. (1975), 106, 1235.

88. V. Gutmann, Electrochim. Acta. (1976), 21, 661.

89. E.S. Amis, J.F. Hinton, Solvent Effects on Chemical Phenomena, Vol. 1, Academic Press, New York, 1973.

90. C. Reichardt, Angew. Chem. Int. Ed. (1979), 18, 98.

91. K. Dimroth, C. Reichardt, T. Siepmann, F. Bohlmann, J. Liebys, Ann. Chem. (1963), 1, 661.

92. D.M. Manuta, A.J. Lees, Inorg. Chem. (1983), 22, 3825.

93. J.N. Demas, J.F. Turner, G.A. Crosby, Inorg. Chem. (1969), 8, 674.

94. D.M. Manuta, A.J. Lees, Inorg. Chem. (1986), 25, 3212.

95. P.M. Gidney, R.D. Gillard, B.T. Heaton, J. Chem. Soc. Dalt. Trans.(1973), 132.

96. H. Bock, H. tom Dieck, Angew. Chem. Int. Ed. Engl. (1966), 5, 520.

97. J.G. Calvert, J.N. Pitts, Photochemistry, J. Wiley & Sons Ltd, New York, 1966.

98. C.G. Hatchard, C.A. Parker, Proc. R. Soc. London, Ser. A. (1956), 235, 518.

99. J.N. Demas, W.D. Bowman, E.F. Zalewski, R.A. Velapoldi, J. Phys. Chem. (1981), 85, 2766.

100. C. Arbour, PhD Thesis, Concordia University, 1988.

101. T.F. Belliveau, PhD. Thesis, McGill University, 1988

102. D.W. Marquardt, J. Soc. Ind. Appl. Math II, (1963), 431.

103. N.A. Beach, H.B. Gray, J. Am. Chem. Soc. (1968), 90, 5713.

104. H.B. Gray, N.A. Beach, J. Am. Chem. Soc. (1963), 85, 2922.

105. G.L. Geoffroy, M. Wrighton, G.S. Hammond, H.B. Gray, Inorg. Chem.(1974), 13, 430.

106. F.A. Cotton, Chemical Applications of Group Theory, Interscience, New York, 1963.

107. A.W. Adamson, J. Phys. Chem. (1967), 71, 798.

108. M. Wrighton, H.B. Gray, G.S. Hammond, Mol. Photochem. (1973) 5, 165.

109. L.G. Vanquickenborne, A. Ceulemens, J. Am. Chem. Soc., 1977, 99, 2208.

110. J.I. Zink, J. Am. Chem. Soc., (1974), 96, 4464.

111. B.R. Hollebone, C.H. Langford, N. Serpone, Coord. Chem. Rev., (1981), 39, 181.

112. B.R. Hollebone, M.J. Stillman, J. Chem. Soc. Farad. Trans., (1978), 2, 2107.

113. E.J. Heller, Acc. Chem. Res. (1981), 14, 368.

114. P. Ford, DeF.P. Rudd, R. Gaunder, H. Taube, J. Am. Chem. Soc. (1968), 90,

1187.

115. J.F. Endicott, G.J. Ferraudi, J. Am. Chem. Soc. (1974), 96, 3681.

116. L. Wang, X. Zhu, K.G. Spears, J. Phys. Chem. 1989, 93, 2.

117. P. J. Hay, J. Am. Chem. Soc., (1978), 100, 2411.

118. F.R. Dollish, W.G. Fataley, F.F. Bentley, Characteristic Raman Frequencies of Organic Compounds, J. Wiley & Sons, New York, 1974.

Appendix A

A1. Table of Infrared and Raman Frequencies for $W(CO)_5$pyr.

		Assignment[abc]	
	$W(CO)_5$pyr	IR	R
R	2075		
Ir	2073	υ(CO)w(A_1^2)	
R	1973		
R	1953		
R,Ir	1934	υ(CO)vs(E)	
Ir	1921	υ(CO)m(A_1^1)	
R	1890		
R	1651		
R	1607		
R	1489		
R	1223		
R	1073		
R	1012		
R	636		
Ir	627		δ(W-CO)
R	602		
Ir	600		δ(WCO)vs
Ir	588		δ(WCO)vs
Ir	547		δ(WCO)vs
R	470		υ(W-C)
Ir	468		
R	462		υ(W-C)
R	434		υ(W-C)
Ir	428		υ(WC)vw(A^8)
R	427		υ(W-C)
Ir	403		υ(WC)vw(A^1)
Ir	368.5	υ(WC)vs(E)	
R	195		υ(W-N)

a) Ir = infrared, R = Raman

b) Ir frequencies are from reference 11, Raman frequencies are from ref 10

c) w = weak, vs = very strong, m = medium, vw = very weak

A2. Table of Raman frequencies and assignments for various solvents

MEOH	PrOH	BUOH
3330 υ(OH)	3340 υ(OH)	3340 υ(OH)
1363 twist	1275 twist	1250 twist
1033 +υ(CCO)	1100 1058 -υ(CCO) 971 +υ(CCO)	1100 1070 -υ(CCO) 965 +υ(CCO)
480 δ(CCO)	460 δ(CCO)	450 δ(CCO)

CH_2Cl_2	$CHCl_3$	CCl_4
742 vw -υ(C-X)	761 s υ(C-X)deg	790 m υ(C-X)deg
703 vs +υ(C-X)	668 s +υ(C-X)	459 vs +υ(C-X)
	366 s +υ(C-X) deform	314 vs C-X deg deform
285 s C-X scissor	262 vs C-X deg deform	217 C-X deg deform

A3. Table of Infrared and Raman frequencies for $W(CO)_5pip$

		Assignment[abc]	
	$W(CO)_5pip$	Ir	R
R	2950		
R	2930		
Ir	2072.5	$\upsilon(CO)w(A_1^2)$	
R	2069		
R	1982		
R	1970		
Ir	1930	$\upsilon(CO)vs(E)$	
R,Ir	1919	$\upsilon(CO)m(A_1^1)$	
R	1905		
R	1860		
R	1837		
R	1030		
R	810		
Ir	601		
R	596		$\delta(WCO)$
Ir	584		
Ir	547		
R	484		
R	433	$\upsilon(WC)$	
Ir	429	$\upsilon(WC)w(A_1)$	
R	426	$\upsilon(WC)$	
R	414	$\upsilon(WC)$	
Ir	403	$\upsilon(WC)w(A_1)$	
R	377		
Ir	371	$\upsilon(WC)vs(E)$	
R	256		

a) Ir = Infrared, R = Raman

b) Ir frequencies are from reference 11, Raman frequencies are from ref 10

c) w = weak, vs = very strong, m = medium

Table A4. Table of Infrared frequencies for $W(CO)_6$ (ref 10).

Representation & Designation	Frequency cm^{-1}	Assignment
A_{1g}	2124	υ(CO)
	420	
E_g	2019	υ(CO)
	363	
T_{1g}	484	
T_{1u}	1998	υ(CO)
	585	δ(MCO)
	374	υ(MC)
	81	
T_{2g}	83	
T_{2u}	520	

Appendix B.

B1. TABLE OF FINAL POSITIONAL PARAMETERS X,Y,Z AND BISO[a].

	X	Y	Z	BISO
W	0.160139(22)	0.156233(24)	0.825398(20)	2.971(10)
C1	0.1182(8)	0.0014(6)	0.9120(6)	3.9(3)
C2	0.1994(7)	0.3177(7)	0.7458(7)	4.3(3)
C3	0.0954(6)	0.2751(6)	0.9170(5)	3.52(23)
C4	-0.0208(7)	0.1399(6)	0.7067(7)	3.71 (25)
C5	0.3359(8)	0.1628(7)	0.9518(7)	4.5(3)
O1	0.0943(7)	-0.0821(6)	0.9620(6)	6.0(3)
O2	0.2200(6)	0.4133(5)	0.7062(6)	6.1(3)
O3	0.0568(6)	0.3462(5)	0.9711(5)	4.97 (23)
O4	-0.1248(6)	0.1294(5)	0.6429(6)	5.59(24)
O5	0.4324(6)	0.1655(7)	1.0270(6)	7.0(3)
N	0.2352(5)	0.0236(5)	0.7094(4)	3.15 (18)
C6	0.3569(8)	0.0711(8)	0.6961(7)	4.8(3)
C7	0.3918(9)	-0.0084(8)	0.6049(8)	5.5(4)
C8	0.4141(11)	-0.1503(9)	0.6449(10)	7.2(5)
C9	0.2905(11)	-0.2064(10)	0.6613(8)	6.1(4)
C10	0.2554(8)	-0.1162(7)	0.7488(7)	4.5(3)

a) BISO IS THE ARITHMETIC MEAN OF THE PRINCIPAL AXES OF THE THERMAL ELLIPSOID. THE ESTIMATED STANDARD DEVIATIONS IN PARENTHESES ARE RIGHT JUSTIFIED TO THE LEAST SIGNIFICANT DIGITS OF THE FRACTIONAL COORDINATES.

B2. TABLE OF FINAL THERMAL PARAMETERS: U(I,J) OR U VALUES *100[a].

	U_{11}(U)	U_{22}	U_{33}	U_{12}	U_{13}	U_{23}
W	4.423(16)	4.296(16)	3.494(16)	0.041(10)	1.317(13)	0.012(10)
C1	6.4(4)	4.7(4)	4.7(4)	0.7(3)	1.6(4)	0.3(3)
C2	5.5(4)	6.2(4)	6.2(5)	0.7(3)	2.4(4)	0.9(4)
C3	5.1(3)	4.9(4)	4.4(4)	-0.7(3)	1.3(3)	-0.3(3)
C4	4.2(4)	4.1(3)	6.5(5)	0.1(3)	1.1(3)	-0.3(3)
C5	5.8(5)	7.7(5)	4.6(4)	-0.2(3)	1.5(4)	-0.3(3)
O1	11.8(5)	6.0(3)	9.3(4)	-0.7(3)	6.0(4)	1.2(3)
O2	10.7(5)	5.5(3)	10.3(5)	-0.8(3)	4.8(4)	1.8(3)
O3	7.3(4)	7.0(4)	7.1(4)	-0.00(24)	3.6(3)	-1.4(3)
O4	6.2(3)	8.0(4)	7.5(4)	-0.4(3)	0.8(3)	-0.4(3)
O5	5.4(4)	14.4(6)	5.9(4)	-0.3(3)	0.2(3)	-1.2(3)
N	4.8(3)	4.3(3)	3.9(3)	0.31(23)	1.55(24)	-0.22(24)
C6	7.6(5)	5.5(5)	9.0(6)	-1.2(4)	5.5(5)	-1.7(4)
C7	9.1(6)	7.8(6)	7.5(6)	0.1(4)	5.0(5)	-1.7(4)
C8	10.0(8)	12.1(9)	8.4(7)	4.7(6)	4.4(7)	-0.0(5)
C9	11.0(7)	6.5(5)	9.5(7)	1.6(6)	5.3(6)	-1.7(5)
C10	8.9(6)	4.0(4)	6.2(5)	1.4(4)	3.0(4)	1.0(3)

a) THE ANISOTROPIC PARAMETERS ARE APPLIED IN THE EXPRESSION $EXP[-2\pi^2(h^2a^{*2}U_{11} + ... + 2hka^*b^*U_{12} + ...)]$. THE NUMBERS IN PARENTHESES ARE THE ESTIMATED STANDARD DEVIATIONS IN THE LEAST SIGNIFICANT DIGITS.

Appendix C.

Method for calculating transient alkyl percentages from picosecond spectra measurements .

1. $A_{alkyl} + A_{1\text{-hexene}} = A_{trans}$ C1

where A_{alkyl} = absorbance of the alkyl transient = W(CO)(cyclohexane)

$A_{1\text{-hexene}}$ = absorbance of $W(CO)_5$(1-hexene) product

A_{trans} = total absorbance of transient

2. $A_{alkyl} = \varepsilon_{alkyl} \times b \times [W(CO)_5(cyclohexane)]$ C2

$A_{1\text{-hexene}} = \varepsilon_{1\text{-hexene}} \times b \times [W(CO)_5(1\text{-hexene})]$ C3

$A_{trans} = \Delta A + A_{gr}$ C4

where ε_{alkyl} = molar extinction coefficient of $W(CO)_5$(cyclohexane) calculated from from picosecond spectra

$\varepsilon_{1\text{-hexene}}$ = molar extinction coefficient of $W(CO)_5$(1-hexene) calculated from steady state photolysis

ΔA and A_{gr} have same meaning as described in eq. 2.12 and 2.13

b = path length of cell (.2 cm)

3. $(\varepsilon_{alkyl})bX + \varepsilon_{1\text{-hexene}}b[W(CO)_5L - X] = A_{trans}$ C5

$(\varepsilon_{alkyl})bX - (\varepsilon_{1\text{-hexene}})bX = A_{trans} - (\varepsilon_{1\text{-hexene}})b[W(CO)_5L]$ C6

$$X = \frac{A_{trans} - (\varepsilon_{1\text{-hexene}})b([W(CO)_5L]}{(\varepsilon_{alkyl} - \varepsilon_{1\text{-hexene}})b} \qquad C7$$

$$\% \text{ of alkyl transient} = \frac{X}{[W(CO)_5L]} \times 100 \qquad C8$$

where X = concentration of alkyl transient

$[W(CO)_5L]$ = total concentration of transient

This method assumes only monosubstituted alkyl and hexene intermediates are formed.

Appendix D

D1. Band Maxima for transitions in $W(CO)_5pyr$ determined from deconvolution of spectral bands.

Solvent	Band Maxima (± 2 nm)			
	MLCT	^1A	^1E	^3E
isooctane	352	388	404	448
iso/hex (2:1 v/v)	352	388	404	448
1-hexene	354	386	405	448
CCl_4/hex (2:1 v/v)	354	386	405	446
C_6H_6/hex (2:1 v/v)	344	382	402	446
$CHCl_3$/hex (2:1 v/v)	336	384	404	440
CH_2Cl_2/hex (2:1 v/v)	336	380	400	440
n-octanol	340	382	402	440
n-butanol	334	380	400	440
n-propanol	332	378	400	436
methanol	322	378	400	436

D2. Band Maxima for transitions of $W(CO)_5$pip determined from deconvolution of spectral bands.

Solvent	Band Maxima (± 2 nm)		
	^1A	^1E	^3E
isooctane	388	410	448
iso/hex (2:1 v/v)	388	409	448
1-hexene	388	409	448
CCl_4/hex (2:1 v/v)	389	410	448
C_6H_6/hex (2:1 v/v)	385	408	440
$CHCl_3$/hex (2:1 v/v)	389	407	448
CH_2Cl_2/hex (2:1 v/v)	386	406	444
n-octanol	386	406	440
n-butanol	385	405	440
n-propanol	385	404	440
methanol	384	404	440